8-2023

Aspects of Topological Quantum Computation

Elias Kokkas
ikokkas@vols.utk.edu

To the Graduate Council:

I am submitting herewith a dissertation written by Elias Kokkas entitled "Aspects of Topological Quantum Computation." I have examined the final electronic copy of this dissertation for form and content and recommend that it be accepted in partial fulfillment of the requirements for the degree of Doctor of Philosophy, with a major in Physics.

George Siopsis, Major Professor

We have read this dissertation and recommend its acceptance:

Steven Johnston, Joon Sue Lee, Ahmedullah Aziz

Accepted for the Council:

Dixie L. Thompson

Vice Provost and Dean of the Graduate School

(Original signatures are on file with official student records.)

Aspects of Topological Quantum Computation

A Dissertation Presented for the

Doctor of Philosophy

Degree

The University of Tennessee, Knoxville

Elias Kokkas

August 2023

To my family

Acknowledgements

I am grateful to the many people who helped me throughout my journey in physics. First and foremost, I am grateful to my advisor Prof. George Siopsis for his constant guidance and mentoring. I would like to thank my Ph.D. committee Profs. Steven Johnston, Joon Sue Lee, and Ahmedullah Aziz, for reviewing my dissertation and providing valuable feedback. I am also grateful to my collaborators Aaron Bagheri, Dr. Zhenghan Wang, Nora Bauer, and Victor Ale. Additionally, I would like to express my gratitude to Profs. Marianne Breinig and Norman Mannella for their guidance and the many helpful physics-related discussion during the first year of my studies. Moreover, I would like to thank the staff of the physics department for constantly helping me with the bureaucratic tasks. I am also thankful to Profs. Nicholas Vlachos and Anastasios Petkou for their guidance and inspiration in the early stages of my career back in Greece.

Of course, I could not forget to mention a few of my closest friends that I have met along the way. I will always cherish the discussions and fun times we had. From Knoxville: Vikram, Rahul, Chinmay, Shikha, Anjali, Igor, Jinu, and Kostas. From Thessaloniki: Dimitrios, Evangelos, and Stergios. From Larissa: Ilias, Alexandros, Chrysanthos, Rafael, Dimitris, Lefteris, Giannis, and Ioannis.

Finally, I want to thank my mother, Dimitra, and my father, Nikolaos, who passed away before my passion for physics was ignited for their sacrifices in order to secure my education and well-being, as well as my brother, George, and my sister Maria for believing in me and constantly supporting me.

‘‘ Όσοι σέρνονται τις νύχτες πέφτουνε σε μαύρες τρύπες. ’’ Θ. Παπακωνσταντίνου

Abstract

Topological quantum computation is a promising scheme leading towards fault-tolerant quantum computation. This can be achieved by harnessing systems in topological phases of matter and, specifically, the non-Abelian anyons' exotic exchange (braiding) statistics. By doing so, quantum information gets encoded and processed in a robust way against small local perturbations. This is guaranteed by the existence of an energy gap and the topology depended nature of the "braiding" gates. However, to this day, experimental observation of non-Abelian anyons remains elusive and a major bottleneck. The most prominent candidate for realizing Ising (non-Abelian) anyons is the fractional quantum Hall effect at $\nu = \frac{5}{2}$. A wavefunction to describe this state, exhibiting Ising statistics, was proposed by Moore and Read via the Ising Minimal Model $\mathcal{M}(4,3) = SU(2)_1^{\otimes 2}/SU(2)_2$. In this thesis, we build a "family" of such wavefunctions based on the coset $SU(2)_1^{\otimes k}/SU(2)_k$ CFT. Unlike, Minimal Models with $k > 2$, this gives gapped wavefunctions with generalized quasi-hole or quasi-particle statistics. Specifically, for $k = 3$, we obtain the Fibonacci braid group, which, together with the $k \geq 5$ theories, offer universal fault-tolerant quantum computation. We find the four and six-anyon wavefunctions and their braiding matrices and discuss the generalization to an arbitrary number of anyons. The coset wavefunction construction offers new directions for experimental observation of non-Abelian anyons in fractional quantum Hall effect and fast-rotating cold atoms. An alternative approach in searching for non-Abelian anyons is by working with lattice models and quantum error correcting codes (e.g., toric code, honeycomb model). Recently, experimental evidence for realizing Abelian anyons with $\mathbb{Z}_2$ topological order was discovered by employing Rydberg atoms in

a Ruby lattice. However, Abelian braiding statistics cannot lead to non-trivial quantum computation schemes. Here, we provide numerical results that support the emergence of non-Abelian statistics in these systems by adding mixed-boundary punctures and ancillary qubits. Specifically, we realize the Ising braiding and fusion matrices which can be used to construct several quantum gates, such as the Hadamard, Pauli, and CNOT gates.

Table of Contents

Chapter 1

Introduction

1.1 Quantum Computation

According to Moore's Law, the number of transistors in electronic chips doubles every two years, enhancing the performance of our computers by a factor of two in the same time period [1]. This empirical law has held true ever since its observation in the mid-1960s. Nonetheless, it is widely accepted within the scientific community that it will eventually cease to be valid. Eventually, the size of these chips, which are the basic hardware components of a computer, will be so small that quantum mechanical effects might no longer be negligible [2]. This motivates the idea of utilizing quantum effects in order to build a more powerful type of computer, a quantum computer.

The benefits of quantum computers for addressing non-trivial research problems, particularly in the field of quantum many-body physics, rapidly became evident. Feynman [3] was the first to suggest that quantum computers could simulate quantum systems exponentially faster compared to classical computers. However, the advantages of quantum computers are not limited to the physics community. By harnessing the principles of quantum superposition and entanglement, scientists were able to present theoretical quantum advantages in numerous scientific fields using certain quantum algorithms. More specifically, Deutsch [4] demonstrated the power of quantum parallelism, Shor [5] achieved an exponential

speedup for factoring large numbers into prime factors, and Grover [6] a quadratic speedup for searching unstructured databases. In recent years, significant progress has been accomplished in a variety of fields, such as cryptography [7] and the drug development industry [8].

In a quantum computer, the basic unit of information is referred to as a qubit (quantum bit). Compared to a classical bit, which can be either in the state "0" or "1", a qubit may be in any superposition

$$|\psi\rangle = a\,|0\rangle + b\,|1\rangle \tag{1.1}$$

where a and b are complex numbers satisfying the normalization condition $|a|^2+|b|^2 = 1$. The process of quantum computation requires a quantum state initialization, scalability, long-decoherence times (compared to the gate operation time), a universal set of quantum gates, and a quantum measurement device. The requirements for the physical implementation of a quantum computer were first introduced by DiVincenzo [9]. In quantum computers, quantum information gets processed by applying quantum gates to the qubits. To obey the rules of quantum mechanics, these quantum gates have to be unitary operators. To perform any arbitrary computation, a universal set of quantum gates is necessary. A conventional choice of quantum gates consists of the Hadamard, CNOT, S-phase, and T-phase gates. More details about the matrix representation of these quantum gates and the fundamentals of quantum computation are discussed in Appendix A.

Following the requirements highlighted in Ref. [9], numerous approaches for the physical realization of quantum computers have been proposed. Within the field of quantum information and computation, no consensus has been reached on a preferred qubit construction. Generally, any two-level quantum system can be considered a qubit. As a result, the implementation of quantum gates depends on the particular architecture of each quantum computer [10]. Some of the most promising technologies for realizing qubits include superconducting circuits, trapped ions, neutral atoms, and topological qubits.

Despite the plethora of different architectures, developing an ideal quantum computer has proven to be a rather challenging task. An ideal quantum computer has to be scalable to a sufficiently large number of qubits and fault-tolerant. Alas, our quantum computers are

not perfectly isolated; interactions with the environment during a quantum computation can corrupt the information, thereby leading to errors. In general, errors can be distinguished into random or systematic. The first is caused by the interaction of the quantum computer with the environment, which results in quantum decoherence. The latter is due to the imperfect fidelity of quantum gates. While such errors can also occur in classical computers, modern classical devices are typically fault-tolerant due to the application of classical error-correcting techniques [11]. Classically in order to protect a message, you have to clone it, then measure all the copies and use the majority rule to track and correct the error. Clearly, quantum mechanics forbids us from correcting errors in the same way as in classical computers. Quantum mechanics doesn't allow cloning [12], and on top of that, measuring would destroy the quantum information (coined by the term collapse of the wavefunction) [13]. Nevertheless, Shor [14] developed the first quantum error correcting code, which protects us against a bit flip or a phase flip, or both.

Today's quantum computers, often called Noisy Intermediate Scale Quantum (NISQ) devices [15], are not yet fault-tolerant. To achieve fault tolerance, the error associated with each quantum gate has to be below a certain threshold [16]. Furthermore, implementing quantum error-correcting codes significantly increase the size of quantum algorithms and the number of required qubits. For example, Shor's code requires 8 ancilla qubits to protect a single qubit from error. A promising alternative, known by the name Topological Quantum Computation (TQC), was first proposed by Kitaev [17, 18] and further studied in [19, 20, 21, 22]. Quantum information is encoded and processed by employing quasi-particles with anyonic quantum statistics. This approach offers fault tolerance, as the quantum hardware is resistant to local perturbations by design. A more comprehensive review on the topic can be found in [23, 24].

1.2 Topological Quantum Computation

Anyons, which are the fundamental building blocks of TQC, are exotic particles that exist in two spatial dimensions. We can distinguish them into two different types: Abelian and

non-Abelian anyons. Abelian anyons are associated with the one-dimensional representation of the braid group and were first studied in Ref. [25]. They acquire a global phase when two identical particles are exchanged. On the other hand, non-Abelian anyons have their quantum state changed via a unitary matrix when two of them are exchanged. Another important difference between Abelian and non-Abelian anyons regards their fusion rules. Abelian anyons fuse into a single Abelian anyon, whereas non-Abelian anyons have multiple fusion channels. We can store and process information using the fusion rules and braiding statistics of these anyons, respectively. However, only non-Abelian anyons can be used to implement non-trivial quantum gates. Ising [18, 26] and Fibonacci [26, 27] anyons are the most celebrated candidates for TQC, but only the latter offers a universal set of topologically protected quantum gates. Nonetheless, Abelian anyons are still useful for quantum computation tasks, such as storing quantum information (quantum memory). In this quantum computation scheme, we achieve fault tolerance by encoding information non-locally and processing it using braidings that depend only on the topology of anyons. Anyons emerge as localized excitations in a topological phase of matter, provided there exists an energy gap and a ground state topological degeneracy, which is robust against external interactions [28, 29].

Despite the enormous theoretical success of anyons and their implications for TQC, their physical realization is, to this day, a challenge. Superconductor-semiconductor nanowires are promising candidates for Majorana zero modes [30, 31], which are quasi-particles that obey the same fusion and braiding rules as the Ising anyons. Different approaches involve studies of lattice models [17, 18] and in systems with Fractional Quantum Hall Effect (FQHE). Experimental data [32, 33] suggest the emergence of Abelian anyonic excitations at the quantum Hall effect for filling fraction $\nu = \frac{1}{3}$. Additionally, there is some evidence that Ising anyons can be found at filling $\nu = \frac{5}{2}$ quantum Hall state [34, 35] and Fibonacci anyons exist in the $\nu = \frac{12}{5}$ quantum Hall state [36].

1.3 Fractional Quantum Hall Effect

The Fractional Quantum Hall Effect was experimentally discovered by Ref. [37] in 1982. These results demonstrated that by placing a system of two-dimensional electron gas under a strong perpendicular magnetic field, the Hall resistivity becomes quantized $\rho_{xy} = \frac{2\pi\hbar}{e^2}\frac{1}{\nu}$ and takes values at plateaux with non-integer values of filling fractions $\nu \in \mathbb{Q}$. In contrast to the Integer Quantum Hall Effect, first discovered in [38], the theoretical description of the FQHE is more challenging as it cannot be understood using free electrons. Coulomb interactions appear to be essential prerequisites for obtaining the plateaux at non-integer values of filling fractions. By including these interactions, the Hamiltonian governing these systems becomes

$$H_{FQHE} = \frac{1}{2m_e}\sum_j (-i\hbar\nabla_j + eA_j)^2 + \frac{k_e}{2}\sum_{i\neq j}\frac{e^2}{|\boldsymbol{r}_i - \boldsymbol{r}_j|} \tag{1.2}$$

where m_e is the mass of the electron, e is the charge of the electron, k_e is Coulomb's constant, and $A_j = A(\boldsymbol{r}_j)$ is the vector potential of the magnetic field evaluated at the point $\boldsymbol{r}_j$. Of course, finding exact analytic solutions of Eq. (1.2) is impossible, as we would have to diagonalize a many-body interactive Hamiltonian. Nevertheless, finding approximate solutions using trial wavefunctions has become a successful alternative. This was pioneered by Laughlin [39] who proposed

$$\Psi_L(\boldsymbol{z}) = \prod_{i<j}(z_i - z_j)^\Lambda \, e^{-\sum_i \frac{|z_i|^2}{4l_B^2}} \tag{1.3}$$

as a trial ground state wavefunction at filling fraction $\nu = \frac{1}{\Lambda}$. Here, $\boldsymbol{z} = (z_1, z_2, \dots)$ refers to a vector of the holomorphic coordinates $z = x + iy$ of all different electrons in the 2-dimensional plane and $l_B = \sqrt{\frac{\hbar}{eB}}$ the magnetic length. The Laughlin wavefunction is anti-symmetric and corresponds to a system of electrons for odd Λ, whereas it's symmetric and represents a bosonic system for even Λ. The trial wavefunction for quasi-particle and quasi-hole excitations of Eq. (1.3) can be found in [40]. After a brief inspection, one finds that the quasi-particles and quasi-holes describe Abelian anyons.

Following Laughlin's work, further trial wavefunctions were discovered. A major breakthrough was the idea to build these trial wavefunctions using conformal blocks from certain Conformal Field Theories (CFTs). The motivation behind this is two-fold. Primarily, it was known that the quantum Hall effect could be described by effective field theory description via the $2+1$ dimensional Chern-Simons (CS) theories [41, 42]. Secondly, a duality between Topological Quantum Field Theories (TQFTs) in $2+1$ dimensions and CFTs in $1+1$ dimensions was discovered by Witten [43]. A more pedagogical introduction to FQHE and its connection to CS and CFT theories can be found in [40].

It turns out that one can construct the Laughlin wavefunction using a free boson CFT. Additionally, Moore and Read [44] constructed the Pfaffian Moore-Read wavefunction, with excitations obeying non-Abelian Ising statistics, using the critical Ising CFT Minimal Model $\mathcal{M}(4,3)$ to describe the $\nu = \frac{5}{2}$ FQHE.

$$\Psi_{MR}(\boldsymbol{z}) = Pf\left(\frac{1}{z_i - z_j}\right)\prod_{i<j}(z_i - z_j)^{\Lambda}\, e^{-\sum_i \frac{|z_i|^2}{4l_B^2}} \tag{1.4}$$

where the Pfaffian $Pf\left(\frac{1}{z_i - z_j}\right) = \mathcal{A}\left(\frac{1}{z_1 - z_2}\frac{1}{z_3 - z_4}\cdots\right)$ is the antisymmetrized product over all electron pairs. More details about this subject can be found in [45, 46]. Alternative proposals suggest that the $\nu = \frac{5}{2}$ state is described by the anti-Pfaffian state [47, 48]. Likewise, the Read-Rezayi wavefunction [49] can be constructed using a $\mathbb{Z}_k$ parafermionic field theory. The parafermionic theory with $k = 3$ has excitations that exhibit Fibonacci braiding statistics, hence offering the possibility of universal topological quantum computation. The Read-Rezayi state is seen as a generalization of the Moore-Read as the former allows the clustering of electrons into groups of k-electrons. Its derivation involves symmetrization over all possible clustering configurations, as illustrated below

$$\Psi_{RR}(\boldsymbol{z}) = \mathcal{S}\left(\prod_{i_1<j_1}(z_{i1} - z_{j1})^2 \cdots \prod_{i_k<j_k}(z_{ik} - z_{jk})^2\right)\prod_{i<j}(z_i - z_j)^{\Lambda-1}\, e^{-\sum_i \frac{|z_i|^2}{4l_B^2}} \tag{1.5}$$

It is worth mentioning that all three wavefunctions that we introduced here represent spin-polarized states. The proposal for spin-singlet states in FQHE was discussed in [50] (Halperin state) and further studied in [51, 52]. In particular, the Non-Abelian Spin-Singlet (NASS) states introduced in [51] generalize the Moore-Read, thus yielding Fibonacci statistics. The physical realization of the NASS states has been studied in fast-rotating cold atoms [53] and in two-dimensional coupled wires [54].

1.4 Lattice Models

Lattice models are prime candidates for realizing topological systems that might be applicable in the field of quantum computing. Several examples hint at the existence of Abelian anyons in these systems. These systems can also be understood as quantum error-correcting codes. Kitaev's toric code [17] serves as an example of $\mathbb{Z}_2$ topological order emerging by placing a square lattice spin system on a torus. Later, it was realized that toroidal geometry was not necessary, leading to generalizations such as the surface or planar code [55, 56]. Here, $\mathbb{Z}_2$ topological order implies that this is an Abelian anyon model described by the vacuum $\mathbb{I}$ and the excitations e, m, and f, where e and m are bosons, and their composition $f = e \otimes m$ is a fermion. The four-fold degenerate ground state of the toric code Hamiltonian defines the code-space, and the anyonic excitations correspond to errors. Error detection is performed with vertex and plaquette stabilizer operators, defined as products of four Pauli operators. Lately, neutral Rydberg atoms placed on Kagome and Ruby lattices were proposed as candidates for quantum computing and quantum memory [57, 58] with topological properties. Numerical and experimental results [59, 60] claim the realization of a topological spin liquid using neutral atoms and the mechanism of Rydberg blockade [61, 62]. These results suggest the emergence of the $\mathbb{Z}_2$ topological order of the toric code using Rydberg atoms.

Numerous theoretical results predict the emergence of non-Abelian anyons within lattice models. Kitaev first found Ising anyons in Ref. [18] from a spin system in a honeycomb lattice interacting with an external magnetic field. The extensive study of non-Abelian statistics

emerging from Abelian anyons has been conducted through either the introduction of lattice twists [63, 64, 65, 66] or punctures [67, 68].

In more recent years, significant progress has been made by numerically simulating Abelian and non-Abelian anyons in NISQ devices. In Ref. [69], the Abelian topological order of the toric code was realized using superconducting qubits. Followed by observing non-Abelian topological order on the same quantum hardware in [70]. Similar results were found using a quantum processor based on traped-ions [71].

1.5 New Schemes for Topological Quantum Computation

This dissertation aims towards developing new tools and schemes for realizing non-Abelian anyons, which are the fundamental components of topological quantum computers. More specifically, we construct a coset CFT wavefunction that generalizes the anyonic statistics of the Moore-Read wavefunction. The Moore-Read state has been proposed to describe systems in fractional quantum Hall effect and exhibit excitations with non-Abelian (Ising) anyonic statistics [44]. Nonetheless, the experimental results for the observation of the Ising anyons and the Moore-Read state in FQHE with filling factor $\nu = \frac{5}{2}$ are to this day non-conclusive. Experimentally, the particular non-Abelian signature of the quantum Hall state is observed by measuring the longitudinal resistance or conductance. The coset wavefunction construction, which we introduce in Chapter 5, suggests that a family of Moore-Read type of wavefunctions could be realized and utilized for universal topological quantum computation. These new coset wavefunctions are expected to have different experimental signatures, depending on their quantum statistics, and could be observed in FQHE.

Apart from FQHE systems, we investigate the possible realization of non-Abelian anyons in Rydberg atoms placed on Ruby lattices. This was motivated by the observation of a $\mathbb{Z}_2$ topological order, with Abelian anyonic statistics, in these lattice models [59]. Here, we propose that Ising (non-Abelian) anyons can be realized in these systems by introducing

punctures with mixed boundary conditions, as described in [68]. In order to experimentally define the topological qubit and perform the braiding, we introduce two ancillary qubits. These ancilla qubits are atoms different than Rubidium (e.g., ^{23}Na) that form the Ruby lattice. This scheme could be feasible in the near future, using current devices, and could improve the efforts for fault-tolerant quantum computation.

1.6 Outline

This thesis is organized as follows. In Chapter 2, we provide a literature review of anyons with particular emphasis on Non-Abelian anyons and their implications for quantum computation. We introduce the basic properties that systems in topological phases of matter ought to have. Next, we introduce the Ising and Fibonacci anyon models and we demonstrate how to use them to construct quantum gates and perform quantum computation. In Chapter 3, we briefly introduce Conformal Field Theories in $d \geq 3$ and $d = 2$ spacetime dimensions. In particular, we discuss fundamental concepts such as Virasoro algebra and primary fields. Next, we review a special family of CFTs known as Minimal Models using the Coulomb-Gas formalism. In Chapter 4, we calculate the braiding matrices from conformal blocks of CFT Minimal Models. In particular, we provide explicit calculations for four-point and six-point amplitudes and illustrate the strategy for higher-order amplitudes. In Chapter 5, we introduce a wavefunction construction based on the coset CFT $SU(2)_1^{\otimes k}/SU(2)_k$. We demonstrate the requirements to obtain a well-defined wavefunction that can describe a gapped state. Then, we find certain properties of these wavefunctions, such as the braiding statistics and their clustering properties. In Chapter 6, we review Rydberg atoms and the Rydberg blockade mechanism. Next, we perform numerical simulations on a system of Rydberg atoms placed on a Ruby lattice with mixed-boundary punctures and verify the $\mathbb{Z}_2$ topological order. Finally, we consider a system of four punctures, coupled with four ancillary qubits, in order to realize the Ising braid group for quantum computation.

Chapter 2

Quantum Computation using Non-Abelian Anyons

2.1 Anyons

All fundamental quantum mechanical particles are either bosons or fermions, depending on their quantum statistics. This restriction arises from the topological properties of the rotation group $SO(3)$ describing our four-dimensional spacetime. To illustrate this property, let us consider two identical particles. Performing a complete rotation of one particle around the second is equivalent to a double exchange of the two particles. In a three-dimensional space, such a trajectory can always be deformed to the trivial path, where a trivial path implies no rotation at all. Therefore, the operator that generates the double exchange of these two particles is equal to the identity and its possible eigenvalues are $+1$ for bosons and -1 for fermions. In two spatial dimensions, the previous topological property is no longer valid. As we try to deform the path of a complete rotation into smaller paths, we eventually come across the second particle and further deformations into smaller paths are no longer possible. As a result, we observe a new family of "particles" with peculiar quantum statistics, known as anyons [25].

Based on their braiding and fusion properties, anyons can be categorized into two distinct types: Abelian anyons and non-Abelian anyons. For Abelian anyons, the exchange or braid of two of them introduces a global phase into the quantum state

$$|a,b\rangle \to e^{i\theta}\,|a,b\rangle \tag{2.1}$$

where θ is an arbitrary phase. Evidently, bosons and fermions are nothing but special cases of Abelian anyons for $\theta = 0$ and $\theta = \pi$. On the other hand, the exchange of two non-Abelian anyons changes the quantum state via a unitary matrix

$$|a,b\rangle_\mu \to U_{\mu\nu}(a,b)\,|a,b\rangle_\nu \tag{2.2}$$

A key distinction between Abelian and non-Abelian quantum states is the degeneracy of the latter. We label this degeneracy by the parameter $\mu = 1, 2, \ldots, g$, where g defines the total number of degenerate states. Hence, the state $|a,b\rangle_\mu$ is a column vector of dimension g, and the unitary matrix $U_{\mu\nu}(a,b)$ is $g \times g$ dimensional.

Within a system of N anyons, the possible exchanges of anyons are elements of the braid group $\mathcal{B}_N$ [72]. While Abelian anyons are related to the one-dimensional representation of the braid group, non-Abelian anyons are associated with higher-dimensional representations. The generators of the braid group b_i , for $1 \leq i \leq N-1$, represent a counter clockwise exchange of the i^{th} and $(i+1)^{th}$ anyons, whereas the b_i^{-1} represent a clockwise exchange of them. These generators obey the following consistency relations

$$b_i b_j = b_j b_i \quad \text{for} \quad |i-j| \geq 2 \tag{2.3}$$

$$b_i b_{i+1} b_i = b_{i+1} b_i b_{i+1} \quad \text{for} \quad 1 \leq i \leq N-1 \tag{2.4}$$

The first equation indicates that non-neighboring braid generators commute, and the second is the Yang-Baxter equation. Both equations can be understood diagrammatically from Figure 2.1.

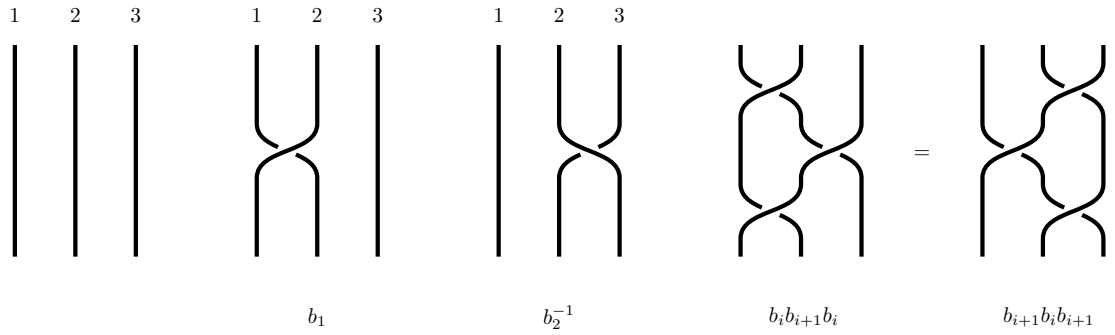

Figure 2.1: Example of the braid group. Notice that for the b_i braiding, we move the second under the first, while for b_i^{-1}, we move the first under the second.

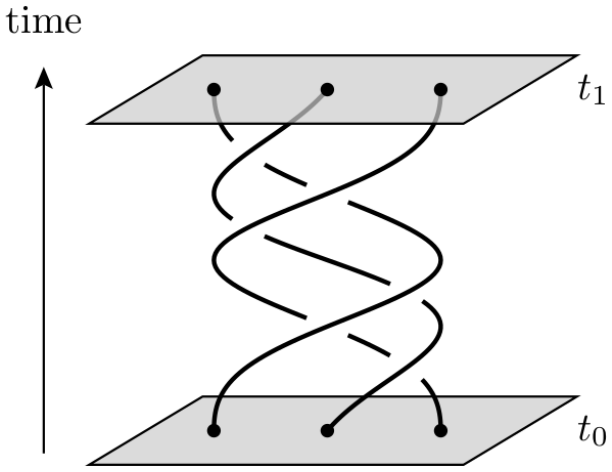

Figure 2.2: Example of anyonic braiding. A counter-clockwise exchange of two anyons in the two-dimensional spatial plane translates into braiding in the three-dimensional spacetime.

In addition to their braiding statistics, anyons have rich fusion properties. By bringing two anyons very close together, they can annihilate and create new anyons. This procedure is algebraically defined by the fusion rules

$$\alpha \otimes \beta = \sum_{\gamma} N_{\alpha\beta}^{\gamma} \gamma \tag{2.5}$$

The different outcomes of this process are called fusion channels. We can observe that if a type α anyon and a type β anyon are fused, the result can be either a single anyon or many different depending on $N_{\alpha\beta}^{\gamma}$. By definition, Abelian anyons are associated with a single fusion channel and one-dimensional Hilbert spaces, whereas non-Abelian anyons have multiple channels and higher-dimensional Hilbert spaces. Clearly, the existence of multiple channels is crucial as it creates degenerate states.

Non-Abelian anyons are promising candidates for quantum computation, known as topological quantum computation, due to their braiding and fusion rules [73]. We can encode quantum information into a logical qubit using the two fusion channels of non-Abelian anyons. A greater number of channels leads to Hilbert spaces with dimensions larger than two and generalizations known as qudits, where a qudit is a d-dimensional unit of quantum information. Quantum gates can be implemented by considering braiding matrices or products of them, as illustrated in Figure 2.2. These are associated with the two or higher-dimensional representations of the braid group as we are dealing with non-Abelian anyons. These non-commuting matrices provide enough non-triviality to construct useful quantum gates.

2.2 Topological Phases of Matter

While anyon-based quantum computation has achieved significant theoretical progress, its physical realization remains elusive. Unlike different architectures (superconducting, trapped ions, cold atoms, etc.), there is no hardware for TQC. One of the major difficulties is the experimental observation of anyons that can be utilized for quantum computation.

As we discussed in the previous sections, anyons exist in two spatial dimensions. Yet, our world has at least three spatial dimensions. It turns out that anyons emerge as quasi-particles or quasi-holes in systems with fermionic or bosonic degrees of freedom by restricting their motion into a two-dimensional plane. Such systems, with anyonic excitations, are said to be in a topological phase and are characterized by the following three properties

1. Degenerate ground state
2. An energy gap between the ground and excited states
3. Anyonic quasi-particles or quasi-holes excitations

Topological phases of matter are peculiar phases of matter which cannot be explained by the Ginzburg-Landau theory [74, 75], as there is no local order parameter to distinguish between different phases. It was proposed in [76] that these systems are described by topological order, which is characterized by long-range entanglement.

Both experimental and theoretical results in the literature suggest that topologically ordered states might appear in the following systems. In fractional quantum Hall effect systems [39] where anyons emerge from fermionic degrees of freedom (electrons) in the presence of an external magnetic field, which breaks the time-reversal symmetry. Unlike, the integer quantum Hall effect in the case of the fractional the Coulomb interactions between electrons are crucial. Kitaev's original work proposed lattice spin models [17, 18] for topologically ordered systems. Lastly, the most recent findings show evidence of quantum spin liquid phase in neutral cold atoms [59, 60].

Searching for topological matter is extremely important in the quantum computing community, as it protects against errors and offers a scheme for fault-tolerant quantum computation. Quantum information is stored in the Hilbert space of the degenerate ground states, which is separated from the excited states by an energy gap. Assuming low temperature the external interactions can cause local perturbations but they are not enough to excite the system due to the energy gap. The system will always remain in the degenerate subspace and can go from one of these states to another through braiding [28, 29].

Unitary gates are implemented through braiding the anyonic excitations; however, when we braid anyons we only care about the topology of the trajectories, small perturbations on the trajectories result in the same gate.

Nevertheless, there are still a few caveats we need to address, as pointed out in [77]. Firstly, these anyonic quasi-particles or quasi-holes must be well separated to avoid interactions that might destroy the degeneracy. Thermal quasiparticles-quasiholes might be created, which might cause unintentional braiding. To avoid these problems, we require low temperatures, lower than the energy gap.

2.3 Ising Anyon Model

One of the simplest and most extensively studied anyon models in the literature for potential applications in topological quantum computation is the Ising model [18]. A more comprehensive review of Ising anyons, discussing their fusion and braiding properties, can be found in [26, 77]. This model has three degrees of freedom: a non-Abelian anyon σ, a Majorana fermion ψ, and finally, the vacuum $\mathbb{I}$. The non-trivial fusion rules of these "particles" follow a closed algebra

$$\psi \otimes \psi = \mathbb{I} \ , \ \ \psi \otimes \sigma = \sigma \ , \ \ \sigma \otimes \sigma = \mathbb{I} \oplus \psi \tag{2.6}$$

A logical qubit can be constructed using the Ising anyon model as follows. To begin, consider three Ising anyons σ_1, σ_2, σ_3 and let them fuse. From the previous set of fusion rules, we get $\sigma \otimes \sigma \otimes \sigma = 2\sigma$. The final outcome of the fusion is a new Ising anyon σ_4, multiplied by a factor of 2, indicating two independent ways of fusing the three Ising anyons. The first way is to fuse σ_1 and σ_2 into the vacuum, followed by fusing the vacuum with σ_3. The second method involves fusing σ_1 and σ_2 into a fermion, followed by a fusion of a fermion with the σ_3. These two fusion channels form the qubit states $|0\rangle$ and $|1\rangle$, respectively. However, this is not the entire story since we could have started by fusing σ_2 with σ_3 and then fuse their outcome with σ_1. In this case, we get yet again two independent channels

that form the qubit states $|0'\rangle$ and $|1'\rangle$. The order of the fusion matters, as they can be two different but linearly dependent basis sets for the qubit, as shown in Figure 2.3. The primed and unprimed basis are related via the F (fusion) matrix, which is defined in Figure 2.4. Additionally, the exchange of two anyons, whose worlds lines fuse in the past, is given by the diagonal R matrix as shown in Figure 2.4. In order to obtain more complicated exchange matrices involving anyons whose world lines don't intersect, we need first to change the basis via the F matrix, perform the exchange using the diagonal R matrix and then change the basis again.

The F and R matrices can be obtained by applying the pentagon and hexagon identities as instructed in [73]. Using the unprimed basis, so that the exchange of σ_1 and σ_2 is diagonal, we find the following matrix representations

$$\mathrm{F} = \frac{1}{\sqrt{2}} \begin{pmatrix} 1 & 1 \\ 1 & -1 \end{pmatrix} \tag{2.7}$$

$$\mathrm{R} = e^{-i\frac{\pi}{8}} \begin{pmatrix} 1 & 0 \\ 0 & i \end{pmatrix} \tag{2.8}$$

The braiding of σ_1 and σ_2 is defined by the matrix

$$b_1 = \mathrm{R} = e^{-i\frac{\pi}{8}} \begin{pmatrix} 1 & 0 \\ 0 & i \end{pmatrix} \tag{2.9}$$

Furthermore, we can consider the braining of σ_2 and σ_3, which is implemented by b_2. As previously described, finding b_2 is more complicated. First, we have to switch to the primed basis using the F matrix, then carry out the exchange of σ_2 and σ_3 in the new basis, and finally, return to the unprimed basis

$$b_2 = \mathrm{F}^{-1} \cdot \mathrm{R} \cdot \mathrm{F} = \frac{e^{i\frac{\pi}{8}}}{\sqrt{2}} \begin{pmatrix} 1 & -i \\ -i & 1 \end{pmatrix} \tag{2.10}$$

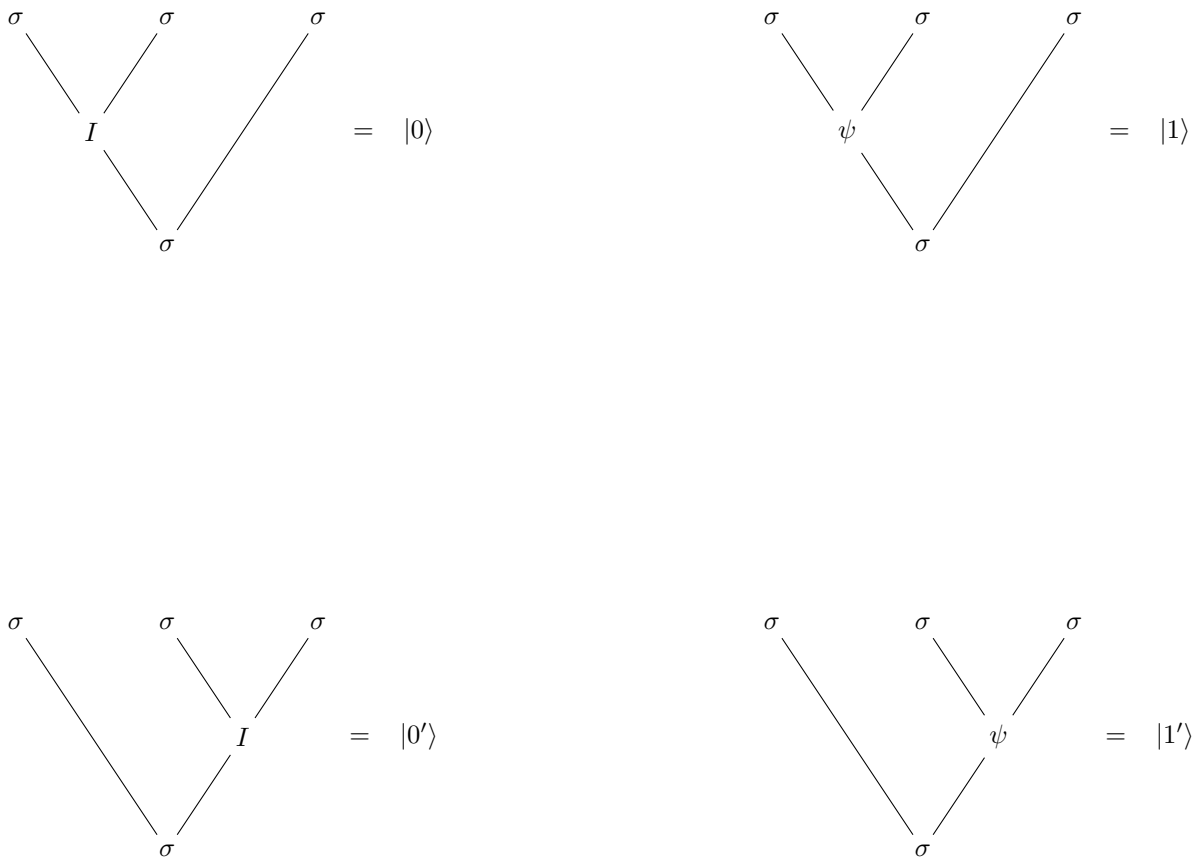

Figure 2.3: A qubit construction using Ising anyons. Starting from three anyons, after fusion, there are two different channels to obtain another Ising anyon on both the primed and unprimed basis.

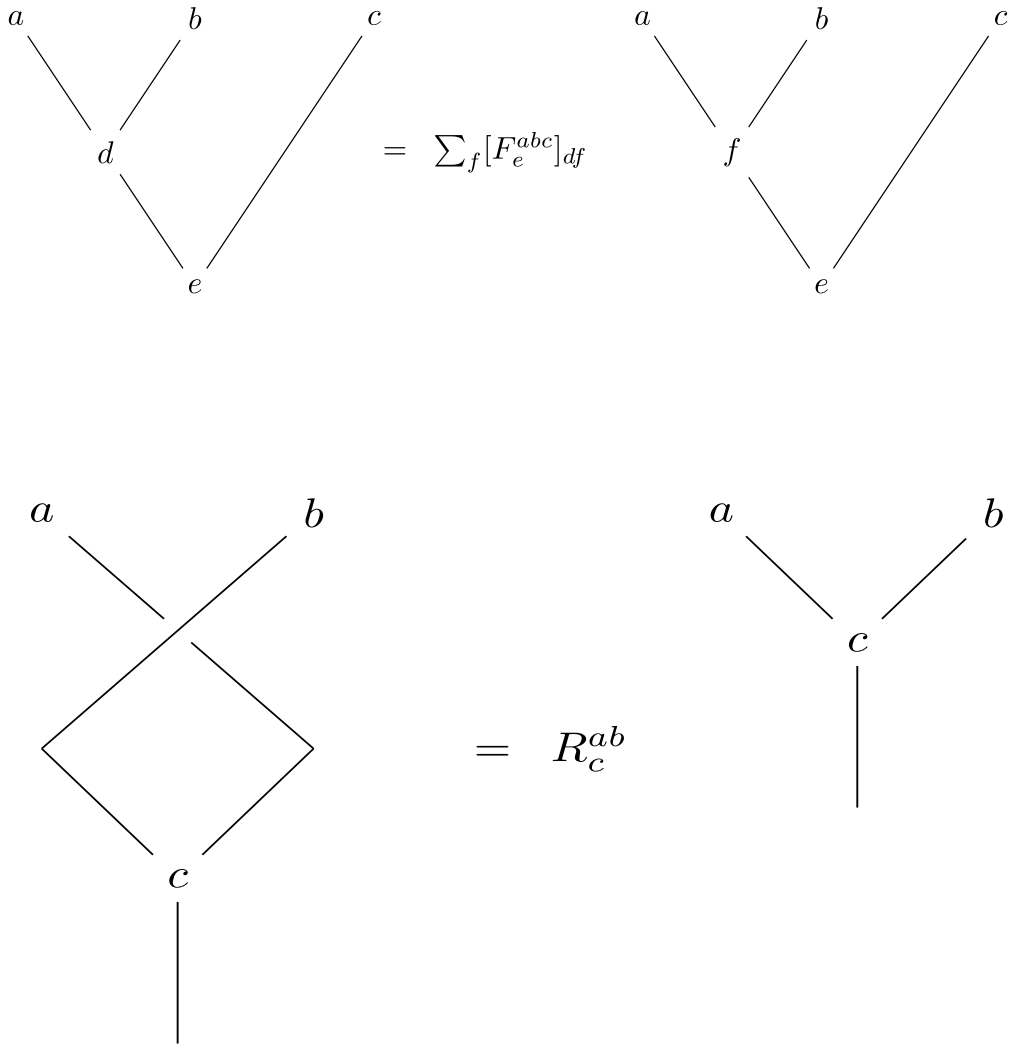

Figure 2.4: Top: The algebraic definition F (fusion) matrix. Bottom: The definition R (exchange) matrix. These matrices are valid for all anyon models.

As discussed in [78, 79], we can construct several logical quantum gates simply through the braiding generators. Notice that the fusion matrix F matches the Hadamard gate, and the exchange matrix R is the same as the S-phase gate up to a global phase. Furthermore, we can construct all Pauli matrices by combining products of b_1 and b_2 matrices as follows

$$\mathrm{X} = b_1 \cdot b_2 \cdot b_2 \cdot b_1 \tag{2.11}$$

$$\mathrm{Y} = b_1^{-1} \cdot b_1^{-1} \cdot b_2 \cdot b_2 \tag{2.12}$$

$$\mathrm{Z} = e^{i\frac{\pi}{4}}\, b_1 \cdot b_1 \tag{2.13}$$

Of course, these are all single qubit gates. In order to study more complex problems involving interacting qubits we need to introduce entangling 2 qubit gates such as the CNOT and CZ gates. It turns out these can be constructed by considering the fusion of five Ising anyons

$$\mathrm{CNOT} = e^{i\frac{3\pi}{8}}\, b_3^{-1} \cdot b_4 \cdot b_3 \cdot b_1 \cdot b_5 \cdot b_4 \cdot b_3^{-1} \tag{2.14}$$

$$\mathrm{CZ} = e^{i\frac{\pi}{8}}\, b_1 \cdot b_5^{-1} \cdot b_3 \tag{2.15}$$

In the previous definition of CNOT and CZ gates, the generators of the braid group involved are no longer 2×2 matrices. Instead, they are 4×4 matrices since the 5 Ising anyons span a four-dimensional Hilbert space. The matrix representations of the four-dimensional braid group will be discussed later in Chapter 4. In fact, we observe that N anyons, including anyons that appear at the end as fusion products, create a 2^{N-1} dimensional Hilbert space. Unfortunately, b_1 and b_2 don't generate a universal set of quantum gates since we can't get the T-phase gate using braiding. This means that we cannot have a universal topological quantum computer using Ising anyons [79]. We are forced to implement the T-phase gate through a non-topologically protected method, not braiding, which spoils fault tolerance.

2.4 Fibonacci Anyon Model

The second non-Abelian anyon model under discussion is the Fibonacci model [27]. This model has two degrees of freedom the vacuum, represented by I, and the non-Abelian anyon, denoted by τ, which obey the non-trivial fusion rule

$$\tau \otimes \tau = I \oplus \tau \tag{2.16}$$

To define a logical qubit, we need to fuse three Fibonacci anyons, which gives $\tau \otimes \tau \otimes \tau = I \oplus 2\tau$, and restrict to the sector with the outcome of a Fibonacci anyon. Yet again, the order of the fusion matters[†] and gives rise to two different qubit basis as can be seen from Figure 2.5. The two bases are related by the fusion matrix

$$\mathrm{F} = \begin{pmatrix} \gamma^{-1} & \gamma^{-\frac{1}{2}} \\ \gamma^{-\frac{1}{2}} & -\gamma^{-1} \end{pmatrix} \tag{2.17}$$

where $\gamma = \frac{1+\sqrt{5}}{2}$ is the golden ratio.

Similarly to the previous section, we get the exchange matrix R or b_1 which represents the braiding of τ_1 and τ_2. On the unprimed basis, we find

$$b_1 = \mathrm{R} = \begin{pmatrix} e^{i\frac{4\pi}{5}} & 0 \\ 0 & e^{-i\frac{3\pi}{5}} \end{pmatrix} \tag{2.18}$$

The b_2 braiding matrix which corresponds to the exchange of τ_2 and τ_3 is obtained by changing basis via the F matrix as follows

$$b_2 = \mathrm{F}^{-1} \cdot \mathrm{R} \cdot \mathrm{F} = \begin{pmatrix} \gamma^{-1} e^{i\frac{4\pi}{5}} & \gamma^{-\frac{1}{2}} e^{-i\frac{3\pi}{5}} \\ \gamma^{-\frac{1}{2}} e^{-i\frac{3\pi}{5}} & -\gamma^{-1} \end{pmatrix} \tag{2.19}$$

[†]The order of the fusion doesn't matter only when the fusion outcome of the 3 Fibonacci anyons is the vacuum.

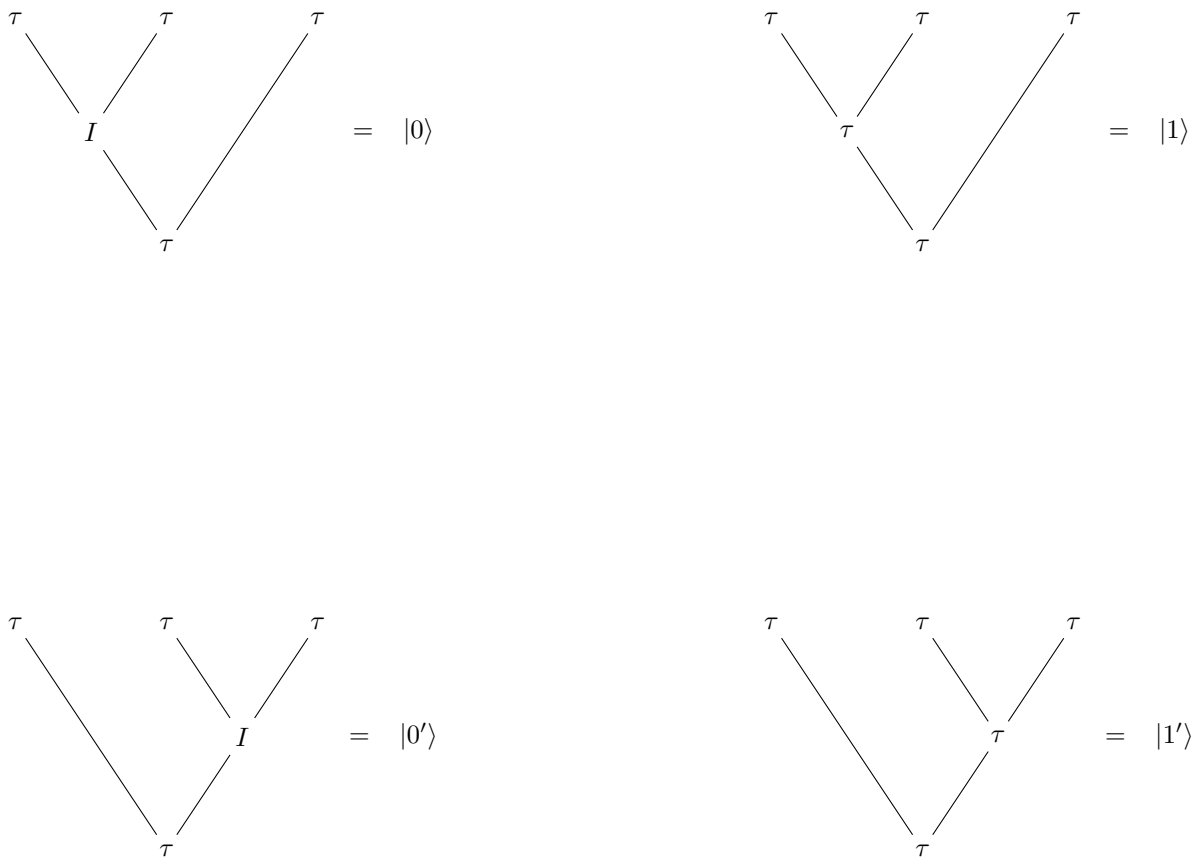

Figure 2.5: A qubit construction based on Fibonacci anyons. Starting from three anyons, after fusion, there are two different channels to obtain another Fibonacci anyon on both the primed and unprimed basis.

Contrary to the Ising model, Fibonacci offers universal quantum computation [80] since the braid group generated by b_1 and b_2 is dense in $SU(2)$. This is a result of the Solovay–Kitaev theorem, which states that given a set of single-qubit gates that form a dense subset of $SU(2)$, we approximate any arbitrary quantum gate, as explained in [81]. However, constructing logical quantum gates requires a large number of braidings in a specific order, which is complicated even for simple gates. Single qubit gates such as the Pauli and the Hadamard gates were implemented by applying more than 30 braiding matrices in a specific order in [80, 82, 83]. Product combinations of b_1 and b_2 that approximate two-qubit gates, such as the CNOT, were also found in [82, 84].

Another important distinction between Ising and Fibonacci anyons regards the scaling of the Hilbert space. In the case of the latter, the dimension grows according to the Fibonacci sequence as we add more anyons.

2.5 Experimental Approaches to Topological Quantum Computation

In order to utilize these theoretical anyon models for topological quantum computation their experimental detection is required. Various experimental setups have been proposed for the observation of exotic quasi-particles following anyonic quantum statistics. As discussed in Chapter 1, two of the most prominent experimental approaches involve studies of the fractional quantum Hall effect. Despite these efforts, the direct experimental observation of Abelian anyons and their statistics has been observed only recently [32, 33], whereas non-Abelian anyons remain elusive.

It was proposed that the anyonic braiding statistics could be probed in fractional quantum Hall systems via Fabry-Perot interference experiments. The experimental setup, illustrated in Figure 2.6, consists of a two-dimensional electron gas, two quantum point contacts (QPCs), and an antidot that controls the number of quasi-particles localized between the two QPCs.

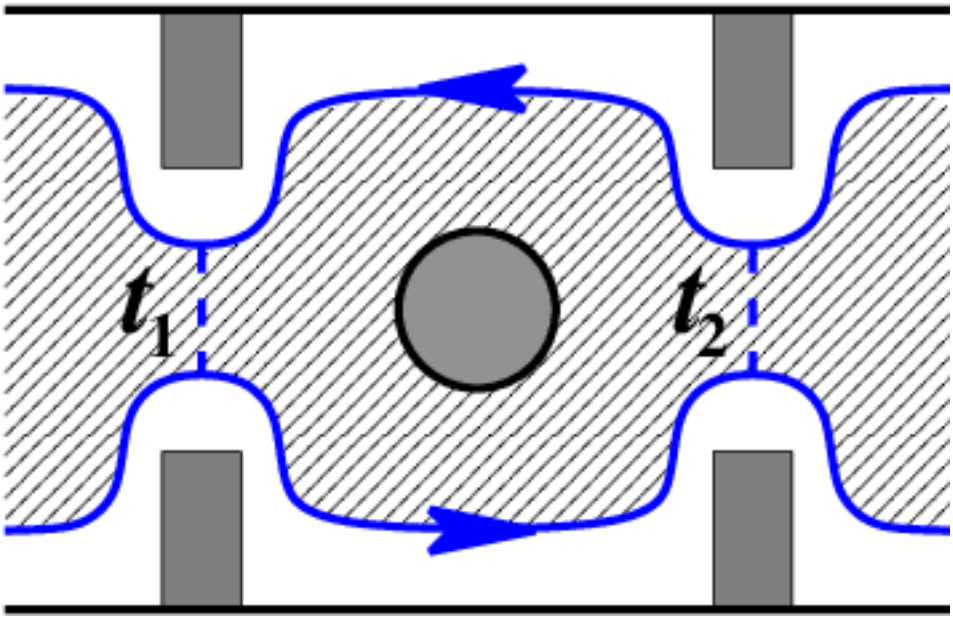

Figure 2.6: A two-point contact Fabry-Perot interference experiment designed to detect anyonic braiding statistics.

The presence of the two QPCs allows for the edge current to scatter resulting in the tunneling current amplitudes t_1 and t_2.[†] The first current tunnels before the antidot whereas the second tunnels right after the antidot. In the end, both currents will contribute to the total longitudinal conductivity. However, as the second tunneling current goes around the antidot, its quantum state changes since the anyons from the tunneling current wind around anyons in the antidot. Thus, resulting in non-trivial interference between the two currents. The signature for the experimental observation of Abelian anyons at filling $\nu = \frac{1}{3}$ through such interference experiments was proposed in [85] and studied in [86, 87, 88]. More recently, in Ref. [32] the authors were able to overcome previous experimental challenges, such as edge/bulk Coulomb interactions and Aharonov-Bohm phase dominating over the anyonic phase, and directly observe the Abelian braiding statistics of this state.

Similar proposals [89, 90, 91] can be found in the literature for non-Abelian anyons and the state at filling $\nu = \frac{5}{2}$. Finding the predicted oscillatory value of the longitudinal conductance is less straightforward since braiding non-Abelian anyons doesn't introduce a global phase but changes the state via a unitary matrix U. It can be found that

$$\sigma_{xx} \sim |t_1|^2 + |t_2|^2 + 2\mathrm{Re}(t_1 * t_2 e^{i\phi} \langle \xi_0 | U | \xi_0 \rangle) \tag{2.20}$$

where $|\xi_0\rangle$ corresponds to the current tunneling at the first QPC and $U|\xi_0\rangle$ at the second. Experimental results suggesting the emergence of non-Abelian anyons using Fabry-Perot interference can be found in [92, 93]. In the more recent work of Ref. [93], a different filling factor $\nu = \frac{7}{2}$ is been examined as a candidate for exhibiting non-Abelian anyons.

[†]In the weak backscattering regime, these tunneling currents are mainly due to quasiparticle excitations.

Chapter 3

Conformal Field Theories

In this chapter, we will provide a brief introduction to Conformal Field Theories (CFTs) following [94, 95]. These are Quantum Field Theories that are invariant under conformal transformations. The group of conformal transformations is an extension of the Poincare symmetry group (translations, spatial rotations, and boosts), which describes all relativistic field theories. The additional symmetries include dilations or scale transformations and special conformal transformations, which are a composition of inversion and translation transformations.

In particular, we will focus on CFTs in two spacetime dimensions, as they have an infinite dimensional algebra of conformal transformations. This mathematical structure allows us to find exact solutions for certain CFTs, such as the Minimal Models, Liouville theory, and WZW models. CFTs are powerful mathematical theories that can be used to describe numerous phenomena in different fields of physics. In two dimensions, they can be used to study condensed matter [96, 97, 98]. Specifically, they can be used to describe phase transition and critical points of two-dimensional systems. A few prominent examples that have been studied using CFT regard the description Ising model at criticality [99], the tricritical Ising model [100], and the 3-state Potts model in [101]. Conformal Fields Theories have contributed significantly to developments in string theory [102, 103, 104].

3.1 The Conformal Group in d Dimensions

Consider a flat d dimensional spacetime with the Minkowski metric tensor $g_{\mu\nu}$ using the gravitational sign convention $(-,+,\cdots,+)$. A conformal transformation is a coordinate transformation $x^\mu \to x'^\mu$, which preserves the metric tensor up to a scale factor

$$g'_{\mu\nu}(x') = \Lambda(x) g_{\mu\nu}(x) \tag{3.1}$$

To obtain the generators and the symmetries of the conformal group, we will study the infinitesimal transformations $x^\mu \to x'^\mu = x^\mu + \epsilon^\mu(x)$. One finds that, up to the first order, the metric changes according to

$$g_{\mu\nu} \to g'_{\mu\nu} = g_{\mu\nu} - (\partial_\mu \epsilon_\nu + \partial_\nu \epsilon_\mu) \tag{3.2}$$

The conformal factor $\Lambda(x)$ can also be expanded for infinitesimal transformations, up to first order, as follows

$$\Lambda(x) = 1 + \frac{2}{d}\partial_\kappa \epsilon^\kappa(x) \tag{3.3}$$

After some algebra, we find that in $d \geq 3$ spacetime dimensions, the infinitesimal change in the coordinates can be at most quadratic in terms of the x coordinate. The most generic transformation is given by

$$\epsilon_\mu = a_\mu + b_{\mu\nu} x^\nu + c_{\mu\nu\rho} x^\nu x^\rho \tag{3.4}$$

From Eq. (3.4), we observe that the zeroth term (i.e., $\epsilon_\mu = a_\mu$) corresponds to spacetime translations. Similarly, we find that the linear term (i.e., $\epsilon_\mu = b_{\mu\nu} x^\nu$) results in dilations, spatial rotations, and boosts. Finally, the quadratic term corresponds to the special conformal transformations. Hence, the conformal group is a generalization of the Poincare group, which includes dilations and special conformal transformations.

Finally, the number of free parameters can be deduced in the following way. We notice that a_μ is an arbitrary vector and the rest parameters are constrained by

$$b_{\mu\nu} = \alpha g_{\mu\nu} + m_{\mu\nu} \tag{3.5}$$

$$c_{\mu\nu\rho} = g_{\mu\rho} b_\nu + g_{\mu\nu} b_\rho - g_{\nu\rho} b_\mu \tag{3.6}$$

$$b_\mu = \frac{1}{d} c^\kappa_{\kappa\mu} \tag{3.7}$$

where $m_{\mu\nu}$ is an antisymmetric tensor. To summarize, there are in total $\frac{(d+2)(d+1)}{2}$ free parameters for the conformal group accounting for one scalar α, two vectors a_μ and b_μ, and a rank 2 tensor $m_{\mu\nu}$. Overall, this is equal to the number of parameters of the group $SO(d,2)$. By exponentiating these infinitesimal transformations, we obtain the finite transformations presented in Table 3.1 along with their generators. More details about conformal field theories in $d \geq 3$ dimensions can be found in the fourth chapter of [94].

3.2 Conformal Field Theories in Two Dimensions

The Conformal Group in Two Dimensions

Most of the previously discussed results regard the conformal group and CFTs in $d \geq 3$ dimensions. The case of CFTs in two dimensions requires separate discussion as the conformal group has an infinite number of generators [99]. This is due to the existence of infinitely many coordinate transformations[†] that preserve the conformal symmetry. For the remainder of this chapter, our consideration will shift to a two-dimensional Euclidean metric, a positive signature metric tensor, which is related to the Minkowski metric by a Wick rotation $x^0 \to -ix^0$. One finds that the infinitesimal transformations ϵ satisfy the Cauchy-Riemann equations

$$\partial_0 \epsilon^0 = \partial_1 \epsilon^1 \quad , \quad \partial_0 \epsilon^1 = -\partial_1 \epsilon^0 \tag{3.8}$$

[†]These transformations are not necessarily well-defined everywhere.

Table 3.1: Generators and finite transformations of the conformal group.

Transformation	Finite Transformation	Generator
Translation	$x'^{\mu} = x^{\mu} + a^{\mu}$	$P_{\mu} = -i\partial_{\mu}$
Dilation	$x'^{\mu} = \alpha x^{\mu}$	$D = -ix^{\mu}\partial_{\mu}$
Rotation	$x'^{\mu} = M^{\mu}_{\nu} x^{\nu}$	$L_{\mu\nu} = i(x^{\mu}\partial_{\nu} - x_{\nu}\partial_{\mu})$
SCT	$x'^{\mu} = \frac{x^{\mu} - b^{\mu}x^2}{1 - 2b\cdot x + b^2 x^2}$	$K_{\mu} = -i(x_{\mu}x^{\nu}\partial_{\nu} - x^2\partial_{\mu})$

The study of two-dimensional conformal field theories becomes more convenient by adopting a new set of holomorphic and anti-holomorphic complex coordinates. These are defined by

$$z = x^0 + ix^1 \quad , \quad \bar{z} = x^0 - ix^1 \tag{3.9}$$

$$\epsilon = \epsilon^0 + i\epsilon^1 \quad , \quad \bar{\epsilon} = \epsilon^0 - i\epsilon^1 \tag{3.10}$$

$$\partial_z = \frac{1}{2}\left(\partial_0 - i\partial_1\right) \quad , \quad \partial_{\bar{z}} = \frac{1}{2}\left(\partial_0 - i\partial_1\right) \tag{3.11}$$

Upon solving the Cauchy-Riemann Eq. (3.8) with the complexified coordinates z and $\bar{z}$, we obtain a holomorphic $z \to f(z)$ and an anti-holomorphic $\bar{z} \to \bar{f}(\bar{z})$. Thus, the local conformal group in two dimensions is defined by the infinite set of all analytic functions $f(z)$, representing the conformal transformations. However, it's worth noting that this isn't precisely a group, as it includes functions that aren't always invertible or well-defined. Nonetheless, we can define a subset of analytic functions that satisfy all necessary requirements and form the global conformal group by

$$f(z) = \frac{a\, z + b}{c\, z + d} \tag{3.12}$$

where the parameters $(a, b, c, d) \in \mathbb{C}$ satisfy the constraint equation $a\, d - b\, c = 1$. It can be proved all transformations described in Table 3.1 can be generated from the global conformal group.

In order to identify the generators of the local conformal group, we take into consideration the infinitesimal transformation $z \to z' = z + \epsilon(z)$ and assume a Laurent expansion around $z = 0$

$$\epsilon(z) = \sum_{n=-\infty}^{\infty} c_n z^{n+1} \tag{3.13}$$

It follows that the generators of these transformations can be separated into holomorphic and anti-holomorphic components as follows

$$l_n = -z^{n+1}\partial_z \quad , \quad \bar{l}_n = -\bar{z}^{n+1}\partial_{\bar{z}} \tag{3.14}$$

obeying the Witt algebra

$$[l_n, l_m] = (n-m)l_{n+m} \tag{3.15}$$

$$[\bar{l}_n, \bar{l}_m] = (n-m)\bar{l}_{n+m} \tag{3.16}$$

$$[l_n, \bar{l}_m] = 0 \tag{3.17}$$

Clearly, there is an infinite number of generators, one corresponding to each value of n. Furthermore, we notice that generators L_{-1}, L_0 and L_1, which satisfy a finite subalgebra, generate the global conformal group. It turns out, the Witt algebra admits an extension, known as Virasoro algebra [105, 106]

$$[L_n, L_m] = (n-m)L_{n+m} + \frac{c}{12}n^2(n-1)\delta_{n+m,0} \tag{3.18}$$

$$[\bar{L}_n, \bar{L}_m] = (n-m)\bar{L}_{n+m} + \frac{c}{12}n^2(n-1)\delta_{n+m,0} \tag{3.19}$$

$$[L_n, \bar{L}_m] = 0 \tag{3.20}$$

where the constant c is called central charge. This central charge is related to the c-theorem of the renormalization group (RG) flow in quantum field theories as it corresponds to the value of the c function at fixed critical points [107].

Primary Fields

Let us now consider a field $\phi(z, \bar{z})$ with scaling dimension Δ and planar spin s. We define the holomorphic and anti-holomorphic conformal dimensions as

$$h = \frac{1}{2}(\Delta + s) \quad , \quad \bar{h} = \frac{1}{2}(\Delta - s) \tag{3.21}$$

A field $\phi(z,\bar{z})$ is a primary field if under any local conformal transformation $z \to w(z)$ and $\bar{z} \to \bar{w}(\bar{z})$ it follows the rule

$$\phi'(w,\bar{w}) = \left(\frac{dw}{dz}\right)^{-h} \left(\frac{d\bar{w}}{d\bar{z}}\right)^{-h} \phi(z,\bar{z}) \tag{3.22}$$

Any field that only transforms according to Eq. (3.22) for the global conformal transformations is called quasi-primary. The remaining fields will be referred to as secondary.

Under a local conformal transformation, correlation functions involving N primary fields $\phi_i(z)$ follow the equation

$$\langle \phi_1(w_1,\bar{w}_1)\cdots\phi_N(w_N,\bar{w}_N)\rangle = \prod_{i=1}^{N} \left(\frac{dw}{dz}\right)^{-h_i}_{w=w_i} \left(\frac{d\bar{w}}{d\bar{z}}\right)^{-h_i}_{\bar{w}=\bar{w}_i} \langle \phi_1(z_1,\bar{z_1})\cdots\phi_N(z_N,\bar{z}_N)\rangle \tag{3.20}$$

Due to this transformation rule, the two-point and three-point functions are completely fixed, whereas the four-point functions depend only on a single variable, the anharmonic ratio $x = \frac{(z_1-z_2)(z_3-z_4)}{(z_1-z_3)(z_2-z_4)}$. Three points can be fixed by appropriately choosing the free parameters in the global conformal transformation Eq. (3.12).

3.3 Minimal Models

In this section, we review a special class of two-dimensional conformal field theories, the rational conformal field theories (RCFTs), which are characterized by a finite number of primary fields[†]. In particular, within the families of all RCFTs, we will consider the so-called Minimal Models. Following the work in [108, 109, 110], these can be classified into unitary representations with $c \geq 1$, unitary representations with $c < 1$, and non-unitary representations[‡]. Here we will focus on the $c < 1$ unitary Minimal Models, most commonly in the literature labeled by $\mathcal{M}(k+2,k+1)$, where $k \geq 1$ is an integer number. In particular, they will be studied using the Coulomb-Gas formalism introduced in [111, 112, 113]. Similar

[†]Equivalently, RCFTs have a finite number of representations of the Virasoro algebra.
[‡]A non-unitary Minimal Model has primary fields with negative conformal dimensions.

results have been obtained using the BRST formalism as studied in [114]. We consider a massless scalar field φ in two spacetime dimensions coupled to the scalar curvature R. The action of this theory becomes

$$S = \frac{1}{8\pi} \int d^2x \sqrt{g} \left(\partial_\mu \varphi \partial^\mu \varphi + 2\gamma \varphi R \right) \tag{3.23}$$

with an imaginary coupling constant $\gamma = i\sqrt{2}\alpha_0$. By adding a background charge α_0 at infinity the central charge gets shifted to $c = 1 - 24\alpha_0^2$.[†]

The primary fields of the CFT, defined by Eq. (3.23), are expressed as vertex operators, including both a holomorphic and an anti-holomorphic part

$$\Phi_\alpha(z, \bar{z}) = e^{i\sqrt{2}\alpha\varphi(z,\bar{z})} \tag{3.24}$$

where each primary field has charge α and conformal dimension

$$h_\alpha = \alpha^2 - 2\alpha_0\alpha \tag{3.25}$$

For each primary field, there is a conjugate field $\tilde{\Phi}_\alpha \equiv \Phi_{2\alpha_0-\alpha}$, which has the same conformal dimension as Φ_α but different charge. Furthermore, each primary field $\Phi_\alpha(z, \bar{z})$ can be decomposed into a holomorphic and anti-holomorphic vertex operator as [‡]

$$\Phi_\alpha(z) \otimes \bar{\Phi}_\alpha(\bar{z}) = e^{i\sqrt{2}\alpha\varphi(z)} \otimes e^{i\sqrt{2}\alpha\bar{\varphi}(\bar{z})} \tag{3.26}$$

This decomposition introduces the chiral primary fields $\Phi_\alpha(z)$ and $\Phi_\alpha(\bar{z})$, which have only holomorphic or anti-holomorphic dependence. By considering only the holomorphic or anti-holomorphic sector of the primary fields we can study chiral CFTs.

[†]The free massless boson theory has a central charge $c = 1$.

[‡]This decomposition is not entirely valid as it doesn't correctly account for the zero-mode of φ, which is neither holomorphic nor anti-holomorphic. Nevertheless, it's useful and yields correct results for correlation functions and amplitudes.

Studying the properties of primary fields is highly important as they represent physical observables, such as the energy density and spin, of the underlying physical system. This is most often achieved by calculating correlators or amplitudes. For example, let's consider the correlator function of N primary fields

$$\langle \Phi_{\alpha_1}(z,\bar{z})\Phi_{\alpha_2}(z,\bar{z})\cdots\Phi_{\alpha_N}(z,\bar{z})\rangle = \prod_{i<j}|z_i - z_j|^{4\alpha_i\alpha_j} \tag{3.27}$$

which can be reduced into the chiral correlator

$$\langle \Phi_{\alpha_1}(z)\Phi_{\alpha_2}(z)\cdots\Phi_{\alpha_N}(z)\rangle = \prod_{i<j}(z_i - z_j)^{2\alpha_i\alpha_j} \tag{3.28}$$

It turns out these correlators are further constrained by the internal symmetry of the massless boson field. In particular, the action defined by the Eq. (3.23) is invariant under the transformation $\varphi \to \varphi + a$. Therefore, the correlators in Eqs. (3.27) and (3.28) must also be invariant, giving rise to the charge neutrality condition

$$\sum_{i=1}^{N}\alpha_i = 2\alpha_0 \tag{3.29}$$

Correlators that don't satisfy the charge neutrality condition are identically equal to zero. At this point, the choice for an imaginary coupling constant γ becomes clear, as otherwise, the right-hand side of the Eq. (3.29) would become imaginary. Of course, that would mean that the charge neutrality condition couldn't be satisfied for any primary field. In order to successfully define non-vanishing correlators, one may have to replace a primary with its conjugate. Both fields having the same conformal dimension represent the same physical observable. Additionally, we can also include in the correlator the $Q_\pm$ screening charges. These are operators with zero conformal dimension and charge $\alpha_\pm = \pm 1$, defined as

$$Q_\pm = \int d^2w \Phi_\pm(w)\bar{\Phi}_\pm(\bar{w}) \quad , \quad \Phi_\pm(w) = e^{i\sqrt{2}\alpha_\pm\varphi(w)} \tag{3.30}$$

To obtain the Minimal Models $\mathcal{M}(k+2,k+1)$, we introduce a cutoff on the number of possible charges α by requiring the ratio $\frac{\alpha_+}{\alpha_-}$ to be rational. It's convenient to choose

$$\alpha_+ = \sqrt{\frac{k+2}{k+1}} \ , \ \ \alpha_- = -\sqrt{\frac{k+1}{k+2}} \tag{3.31}$$

We find that $\mathcal{M}(k+2,k+1)$ possesses a finite number of primary fields, each labeled by a pair of integers (r,s), where $r = 1,\ldots,k$, and $s = 1,\ldots,k+1$. The charge and conformal dimension of the primary field $\Phi_{(r,s)}$ are given, respectively, by

$$\alpha_{(r,s)} = \frac{(1-r)(k+2)-(1-s)(k+1)}{2\sqrt{(k+1)(k+2)}} \tag{3.32}$$

$$h_{(r,s)} = \frac{[r(k+2)-s(k+1)]^2-1}{4(k+1)(k+2)} \tag{3.33}$$

It follows that the conjugate field becomes $\tilde{\Phi}_{(r,s)} = \Phi_{(k+1-r,k+2-s)}$ and the background charge can be written as

$$\alpha_0 = \frac{1}{2\sqrt{(k+1)(k+2)}} \tag{3.34}$$

By bringing these primary fields very close together, we can fuse them. The outcome of a fusion is in general a linear combination of new primary fields. It was shown by Verlinde [115] that the primaries of $\mathcal{M}(k+2,k+1)$ satisfy the following fusion rules

$$\Phi_{(r,s)} \otimes \Phi_{(r',s')} = \sum_{r''\overset{2}{=}|r'-r|+1}^{\min(r+r'-1,2q-1-r-r')} \ \sum_{s''\overset{2}{=}|s'-s|+1}^{\min(s+s'-1,2p-1-s-s')} \Phi_{(r'',s'')} \tag{3.35}$$

Of particular importance are the primary fields with $r = 1$, which form a closed algebra thanks to the fusion rules

$$\Phi_{(1,s)} \otimes \Phi_{(1,s')} = \sum_{s''\overset{2}{=}|s'-s|+1}^{\min(s+s'-1,2k+3-s-s')} \Phi_{(1,s'')} \tag{3.36}$$

where $\overset{2}{=}$ denotes incrementing the summation variable by 2.

The Minimal Model with $k = 1$ corresponds to a trivial CFT, with only two primaries, $\Phi_{(1,1)}$ and $\Phi_{(1,2)}$, and thus won't be studied. For $k \geq 2$, the charge and dimension of these primary fields are summarized in Table 3.2. For convenience, we will denote the holomorphic part of the primary field $\Phi_{(1,2)}$ by $\sigma(z)$ and it's conjugate by $\tilde{\sigma}(z)$. Finally, the anti-holomorphic part of $\Phi_{(1,2)}$ will be expressed by $\bar{\sigma}(z)$. Hence, we can represent the non-chiral primary field $\Phi_{(1,2)}(z, \bar{z}) = \sigma(z)\bar{\sigma}(\bar{z})$. We can adopt a similar notation for the primaries with $s = 3, 4, \ldots$ via the operators $\epsilon, \epsilon', \ldots$ as indicated in Table 3.2.

In the context of quantum computation applications, we are primarily interested in the chiral correlator of $2N$ primary fields $\Phi_{(1,2)}$. The Hilbert space of our qubits, or more generally qudits, will be spanned by these correlators. To define them, we start with the non-chiral correlation function

$$G^{(2N)}(\boldsymbol{z}, \bar{\boldsymbol{z}}) = \left\langle \boldsymbol{\sigma}_1 \cdots \boldsymbol{\sigma}_{2N-1} \tilde{\boldsymbol{\sigma}}_{2N} Q_-^{N-1} \right\rangle \tag{3.37}$$

where $\boldsymbol{z} = (z_1, \ldots, z_{2N})$, $\boldsymbol{\sigma} = \Phi_{(1,2)}$, and $\boldsymbol{\sigma}_j = \boldsymbol{\sigma}(z_j, \bar{z}_j)$. To define a non-vanishing correlator, we inserted $N-1$ screening operators Q_- and used the conjugate field for one of the primary fields. Without loss of generality, we replaced the last primary by it's conjugate.

According to the Ref. [116] the non-chiral correlator in Eq. (3.37) can be split into holomorphic and antiholomorphic parts as

$$G^{(2N)}(\boldsymbol{z}, \bar{\boldsymbol{z}}) = \sum_{\mu} |\mathcal{F}_{\mu}^{(2N)}(\boldsymbol{z})|^2 \tag{3.38}$$

where we sum over the conformal blocks of the chiral model labeled by μ. The chiral correlator, frequently referred to as the conformal block, is given by

$$\mathcal{F}_{\mu}^{(2N)}(\boldsymbol{z}) = \sqrt{N_\mu} \oint_{\mu} d^{N-1}\boldsymbol{w}\, \mathcal{I}^{(2N)}(\boldsymbol{z}, \boldsymbol{w}) \tag{3.39}$$

where

Table 3.2: Charge and conformal dimension of $r = 1$ primary fields in the Minimal Model $\mathcal{M}(k+2, k+1)$.

Primary Field	Symbol	Dimension	Charge
$\Phi_{(1,1)}$	$\mathbb{I}$	0	0
$\Phi_{(1,2)}$	σ	$\frac{k-1}{4(k+2)}$	$\frac{k+1}{2\sqrt{(k+1)(k+2)}}$
$\Phi_{(1,3)}$	ε	$\frac{k}{k+2}$	$\frac{k+1}{\sqrt{(k+1)(k+2)}}$
$\Phi_{(1,4)}$	ε'	$\frac{3(3k+1)}{4(k+2)}$	$\frac{3(k+1)}{2\sqrt{(k+1)(k+2)}}$
$\vdots$	$\vdots$	$\vdots$	$\vdots$
$\Phi_{(1,k+1)}$	N/A	$\frac{k(k-1)}{4}$	$\frac{k(k+1)}{2\sqrt{(k+1)(k+2)}}$

$$\mathcal{I}^{(2N)}(\boldsymbol{z},\boldsymbol{w}) = \left\langle \sigma_1 \cdots \sigma_{2N-1}\tilde{\sigma}_{2N} \prod_{j=1}^{N-1} \Phi_-(w_j) \right\rangle \tag{3.40}$$

where $\boldsymbol{w} = (w_1, \ldots, w_{N-1})$, $\sigma_j = \sigma(z_j)$, and N_μ are normalization constants determined by matching the expressions in Eqs. (3.37) and (3.38).

The conformal block Eq. (3.39) is obtained by performing $N-1$ contour integrals. One distinguishes between different conformal blocks by the position of the contours of integration; μ labels the collective choice.

Chapter 4

Quantum Computation using CFT Minimal Models

This chapter presents in detail the construction of qudits and braiding-based quantum gates from the Minimal Models $\mathcal{M}(k+2, k+1)$ for $k \geq 2$ that were discussed in [117].

4.1 Braiding and Fusion Matrices

As outlined in the previous section, chiral amplitudes are not single-valued functions, as they depend on the choice of the contours of integration. Conformal blocks form a basis for these amplitudes, the dimensionality of which depends on the number of primary fields and the integer k labeling the CFT. This basis is mapped onto the basis for the Hilbert space of qubits within quantum computation.

The number of independent conformal blocks can be deduced directly from the fusion rules of the CFT. The exchange of two primary fields σ at positions η_i and η_j is equivalent to a change of basis from $\mathcal{F}_\mu$ to $\mathcal{F}'_\mu$ via an exchange matrix,

$$\mathcal{F}'_\mu = \sum_\nu (R_{ij})_{\mu\nu} \mathcal{F}_\nu \tag{4.1}$$

These exchange matrices lead to braiding and fusion matrices [118, 119] that can be mapped onto quantum gates. We discuss how this is done in detail for four-point and six-point σ amplitudes.

4.2 Four-point Amplitudes

The simplest non-trivial amplitude of interest is the four-point correlation function, which involves four σ primary fields. The non-chiral four-point correlation function becomes non-vanishing by introducing one negative screening charge and by replacing one of the σ fields with its conjugate $\tilde{\sigma}$ as follows

$$G^{(4)}(\boldsymbol{\eta}, \bar{\boldsymbol{\eta}}) = \langle \sigma(\eta_1, \bar{\eta}_1)\sigma(\eta_2, \bar{\eta}_2)\sigma(\eta_3, \bar{\eta}_3)\tilde{\sigma}(\eta_4, \bar{\eta}_4)Q_- \rangle \tag{4.2}$$

with $\boldsymbol{\eta} = (\eta_1, \ldots, \eta_{2N})$. Or written in terms of the conformal blocks

$$G^{(4)}(\boldsymbol{\eta}, \bar{\boldsymbol{\eta}}) = |\mathcal{F}_1^{(4)}(\boldsymbol{\eta})|^2 + |\mathcal{F}_2^{(4)}(\boldsymbol{\eta})|^2 \tag{4.3}$$

There are two conformal blocks associated with this four-point function for all values of the integer k, as can be easily deduced from the fusion rules in Eq. (3.36). These two conformal blocks form a two-dimensional Hilbert space, corresponding to a single qubit. We can simplify the calculations using the conformal invariance of the theory, which allows one to fix: $\eta_1 \to 0$, $\eta_2 \to x$, $\eta_3 \to 1$, and $\eta_4 \to \infty$, where $x = \frac{\eta_{12}\eta_{34}}{\eta_{13}\eta_{24}}$ is the anharmonic ratio with $\eta_{ij} = \eta_i - \eta_j$. After a global conformal transformation the conformal blocks become

$$\mathcal{F}_\mu^{(4)}(x) = \sqrt{N_\mu} \oint_\mu dw\, \mathcal{I}^{(4)}(x, w) \tag{4.4}$$

where

$$\mathcal{I}^{(4)}(x, w) = \lim_{\eta_4 \to \infty} \left(\frac{\eta_{13}\eta_{24}}{\eta_{12}\eta_{23}\eta_{34}\eta_{41}} \right)^{2h_\sigma} \langle \sigma(0)\sigma(x)\sigma(1)\tilde{\sigma}(\eta_4)\Phi_-(w) \rangle \tag{4.5}$$

To evaluate the two conformal blocks, we need to carefully choose the contour of integration in order to avoid the branch points and singularities at $0, x, 1, \infty$. This can be done by choosing two branch cuts along the real axis; one that goes from 0 to x and another one from 1 to ∞. We obtain two different contours which encircle $(0, x)$ and $(1, \infty)$, as seen in Figure 4.1. After shrinking the contours and using the Eq. (3.28), the two conformal blocks are defined as

$$\mathcal{F}_1^{(4)}(x) = \sqrt{N_1}[x(1-x)]^{\frac{k+1}{2(k+2)}} \int_0^x dw\, [w(x-w)(1-w)]^{-\frac{k+1}{k+2}} \tag{4.6}$$

$$\mathcal{F}_2^{(4)}(x) = \sqrt{N_2}[x(1-x)]^{\frac{k+1}{2(k+2)}} \int_1^\infty dw\, [w(w-x)(w-1)]^{-\frac{k+1}{k+2}} \tag{4.7}$$

Upon integrating, we obtain these conformal blocks in terms of Hypergeometric functions

$$\mathcal{F}_1^{(4)}(x) = \sqrt{N_1}\frac{\Gamma^2(\frac{1}{k+2})}{\Gamma(\frac{2}{k+2})} x^{\frac{1-k}{2(k+2)}}(1-x)^{\frac{k+1}{2(k+2)}}\, {}_2F_1\left(\frac{k+1}{k+2}, \frac{1}{k+2}; \frac{2}{k+2}; x\right) \tag{4.8}$$

$$\mathcal{F}_2^{(4)}(z) = \sqrt{N_2}\frac{\Gamma(\frac{1}{k+2})\Gamma(\frac{2k+1}{k+2})}{\Gamma(\frac{2k+2}{k+2})}[x(1-x)]^{\frac{k+1}{2(k+2)}}\, {}_2F_1\left(\frac{k+1}{k+2}, \frac{2k+1}{k+2}; \frac{2(k+1)}{k+2}; x\right) \tag{4.9}$$

To understand the physical content of these conformal blocks, we should compare them with the operator product expansion (OPE). In the limit $x \to 0$, we observe that

$$\mathcal{F}_1^{(4)}(x) \sim x^{-\frac{k-1}{2(k+2)}}[1 + \mathcal{O}(x)] \quad , \quad \mathcal{F}_2^{(4)}(x) \sim x^{\frac{k+1}{2(k+2)}}[1 + \mathcal{O}(x)] \tag{4.10}$$

The OPE can be derived from the fusion rules of Eq. (3.36). Specifically, for the product $\sigma(x)\sigma(0)$, we get a linear combination of the $\mathbb{I}$ and ε fields, as defined in Table 3.2. The coefficients of each field in this expansion are fixed by the conformal invariance of the left and right-hand sides. Thus, we get

$$\sigma(x)\sigma(0) \sim x^{-\frac{k-1}{2(k+2)}}\mathbb{I} + x^{\frac{k+1}{2(k+2)}}\varepsilon(0) \tag{4.11}$$

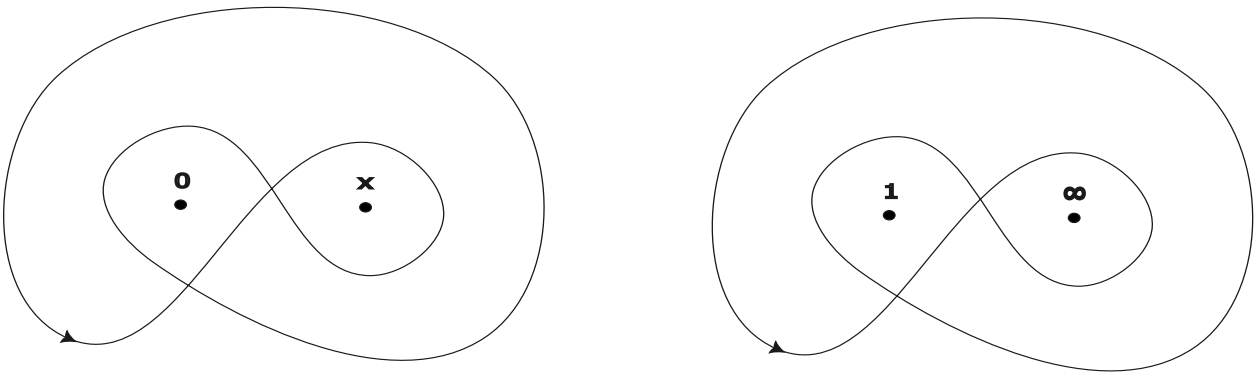

Figure 4.1: Two independent contour choices of the integral in Eq. (4.4). The first choice reduces to an integral from 0 to x, whereas the second geives the interval from 1 to ∞.

By comparing the Eqs. (4.10) and (4.11), we find that the conformal blocks $\mathcal{F}_1^{(4)}$ and $\mathcal{F}_2^{(4)}$ have intermediate states $\mathbb{I}$ and ε, respectively. Schematically, they are given by the two diagrams shown in Figure 4.2.

The normalization constants N_μ, for $\mu = 1, 2$, are determined by comparing the expressions in Eqs. (4.2) and (4.3) for the non-chiral amplitude $G^{(4)}$. Calculating the non-chiral amplitude can be avoided using an argument based on monodromy transformations around 0 and 1. As explained in the ninth chapter of [94], the monodromy transformation around 1 becomes diagonal if we change bases and evaluate the conformal blocks $\mathcal{F}_\mu^{(4)}(1-\boldsymbol{\eta})$. The conformal blocks in the new basis must provide a decomposition of the non-chiral amplitude similar to the Eq. (4.3). This leads to linear constraints that determine the normalization constants up to an overall multiplicative factor, which suffices for our application to quantum computation. After some algebra, we obtain

$$N_1 = \mathcal{N} \sin \frac{\pi}{k+2} \ , \quad N_2 = \mathcal{N} \sin \frac{3\pi}{k+2} \tag{4.12}$$

where $\mathcal{N}$ can be determined using Eq. (4.2), but is not needed for our purposes.

For the four-point chiral amplitude, we derive two braiding matrices, R_{12} and R_{23}, and a fusion matrix R_{13}, where R_{ij} corresponds to the exchange of positions $\eta_i \leftrightarrow \eta_j$. These matrices are defined diagrammatically in Figure 4.3.

The braiding matrix R_{12} is diagonal because the two fields we exchange fuse together. More specifically, the non-zero elements are the coefficients of the two channels, namely the $\mathbb{I}$ and ϵ, found previously. From the OPE (4.11), we deduce

$$R_{12}^{(4)} = \begin{pmatrix} e^{-i\pi \frac{k-1}{2(k+2)}} & 0 \\ 0 & e^{i\pi \frac{k+1}{2(k+2)}} \end{pmatrix} \tag{4.13}$$

The other two exchange matrices can be found using standard Hypergeometric and Gamma function identities. After some algebra, we obtain

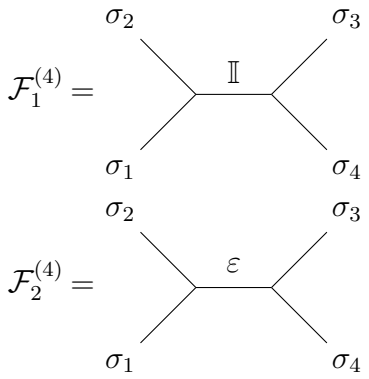

Figure 4.2: Two conformal blocks of the four-point function. The first block corresponds to an intermediate vacuum state while the second to ε.

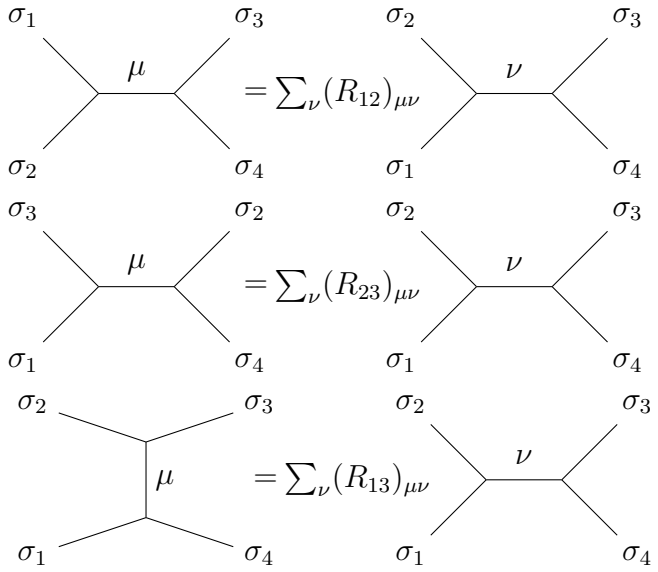

Figure 4.3: Exchange matrices of the four-point correlator.

$$R_{13}^{(4)} = \begin{pmatrix} \cos\theta_k & \sin\theta_k \\ \sin\theta_k & -\cos\theta_k \end{pmatrix} \tag{4.14}$$

where $\cos\theta_k = \frac{1}{2}\sec\frac{\pi}{k+2}$. The matrix R_{23} was deduced from

$$R_{23} = R_{13}R_{12}R_{13}^{-1} \tag{4.16}$$

$$R_{23}^{(4)} = \begin{pmatrix} e^{i\pi\frac{k-1}{2(k+2)}}\cos\theta_k & e^{-i\pi\frac{k+1}{2(k+2)}}\sin\theta_k \\ e^{-i\pi\frac{k+1}{2(k+2)}}\sin\theta_k & -e^{-i\pi\frac{3k+1}{2(k+2)}}\cos\theta_k \end{pmatrix} \tag{4.15}$$

Ising Statistics

As an example, consider the $k = 2$ case, which corresponds to the critical Ising model. In this case, the σ primary corresponds to the Ising anyon while the ϵ gives the Majorana fermion. The diagonal braiding matrix becomes the S-phase gate (up to a phase), while the fusion matrix reduces to the Hadamard gate, matching the Eqs. (2.7) and (2.8)

$$R_{12}^{(4)} = e^{-i\frac{\pi}{8}}\begin{pmatrix} 1 & 0 \\ 0 & i \end{pmatrix} \quad , \quad R_{13}^{(4)} = \frac{1}{\sqrt{2}}\begin{pmatrix} 1 & 1 \\ 1 & -1 \end{pmatrix} \tag{4.17}$$

As discussed in Chapter 2, these matrices can be used to implement quantum gates [78, 79] but are not enough to achieve universal quantum computation [79] because we have no way to construct the T-phase gate by exchanging Ising anyons.

Fibonacci Statistics

Universal quantum computation can be achieved for $k = 3$, corresponding to the tri-critical Ising model $\mathcal{M}(5, 4)$. Up to a global phase, we obtain the matrices that appear in the Fibonacci anyon model in Eqs. (2.17) and (2.18)

$$R_{12}^{(4)} = \begin{pmatrix} e^{-i\frac{\pi}{5}} & 0 \\ 0 & e^{i\frac{2\pi}{5}} \end{pmatrix} \quad , \quad R_{13}^{(4)} = \begin{pmatrix} \gamma^{-1} & \gamma^{-\frac{1}{2}} \\ \gamma^{-\frac{1}{2}} & -\gamma^{-1} \end{pmatrix} \tag{4.18}$$

where $\gamma = \frac{\sqrt{5}+1}{2}$ is the golden ratio. The set in Eq. (4.18) is dense in $SU(2)$ [80], leading to universal quantum computation, as shown in [80, 82, 83]. However, the Minimal Model $\mathcal{M}(5,4)$ cannot be used as a foundation for fault-tolerant quantum computation due to the absence of a gapped state. This will be discussed in more detail in Chapter 5, where we will explore an alternative proposal using the coset CFT $SU(2)^{\otimes 3}/SU(2)_3$. This proposal leads to universal quantum computation based on the braiding matrices of the Eq. (4.18) as well as fault-tolerant quantum computation since $SU(2)^{\otimes 3}/SU(2)_3$ possesses a gapped state.

4.3 Five-point Amplitudes

Next, we consider the five-point chiral amplitude of four σ fields and one ε field. This is not an amplitude of the type as the Eq. (3.39), which we use for quantum computation. However, it is needed for the six-point chiral amplitude of σ fields.

The correlator needs a single negative screening charge and a conjugate ϵ field in order to obey the charge neutrality condition,

$$\mathcal{I}^{(5)}(\boldsymbol{\eta}, w) = \langle \sigma_1 \sigma_2 \sigma_3 \sigma_4 \tilde{\varepsilon}_5 \Phi_-(w) \rangle \tag{4.19}$$

From the fusion rules as specified in Eq. (3.36), we deduce that there are two (three) conformal blocks for $k = 2$ ($k \geq 3$), defined diagrammatically in Figure 4.4, and in terms of contour integrals by

$$\mathcal{F}^{(5)}_\mu(\boldsymbol{\eta}) = \sqrt{N_\mu} \oint_\mu dw \mathcal{I}^{(5)}(\boldsymbol{\eta}, w) \tag{4.20}$$

As before, the normalization constants N_μ are evaluated using a monodromy argument. In particular, we find

$$\begin{aligned} N_1 &= \mathcal{N} \sin^2 \frac{2\pi}{k+2} \quad , \quad N_2 = \mathcal{N} \sin^2 \frac{3\pi}{k+2} \quad , \\ N_3 &= 8\mathcal{N} \cos^2 \frac{\pi}{k+2} \cos \frac{2\pi}{k+2} \sin^2 \frac{3\pi}{k+2} \end{aligned} \tag{4.21}$$

up to an overall multiplicative constant $\mathcal{N}$, which is not needed for our purposes.

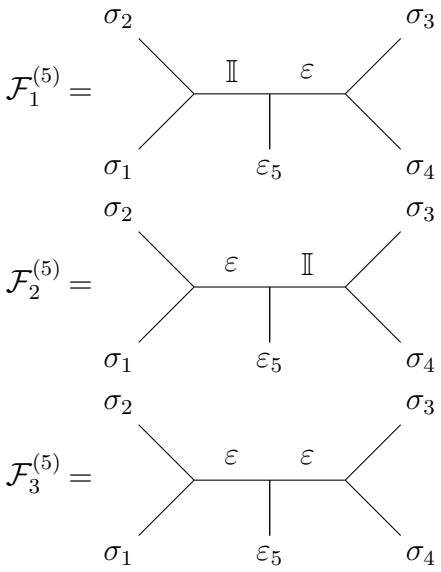

Figure 4.4: Conformal blocks of the five-point function. In the case of the critical Ising model ($k = 2$), the third conformal block vanishes since $\varepsilon \otimes \varepsilon = \mathbb{I}$.

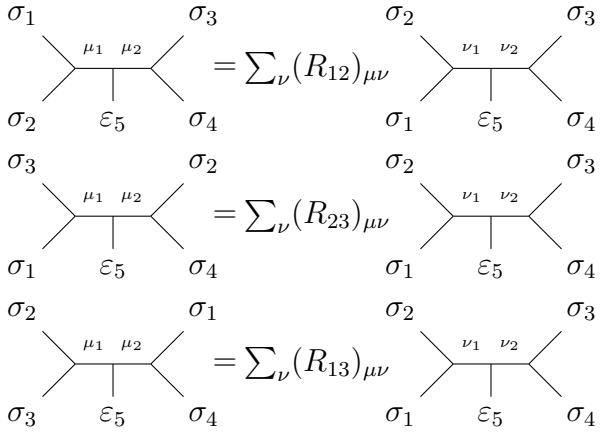

Figure 4.5: Exchange matrices of the five-point correlator. In our notation each channel μ is represented by a pair (μ_1, μ_2). For the first channel we have $(\mathbb{I}, \varepsilon)$, for the second $(\varepsilon, \mathbb{I})$, and the third $(\varepsilon, \varepsilon)$.

The conformal blocks of the five-point amplitude reduce to integrals that can no longer be calculated analytically. Nevertheless, we can still extract information about their braiding and fusion matrices. Here we are interested in the exchange matrices depicted in Figure 4.5. The braiding matrix R_{12} is easily obtained from the OPE (4.11)

$$R_{12}^{(5)} = e^{-i\pi\frac{k-1}{2(k+2)}} \begin{pmatrix} 1 & 0 & 0 \\ 0 & e^{i\pi\frac{k}{k+2}} & 0 \\ 0 & 0 & e^{i\pi\frac{k}{k+2}} \end{pmatrix} \tag{4.22}$$

The fusion matrix R_{13} is found by converting five-point functions into four-point functions, as explained in Appendix B in more detail. We obtain

$$R_{13}^{(5)} = \begin{pmatrix} c_k & c_k & -\sqrt{d_k} \\ c_k & \frac{d_k\omega_k - c_k^3}{s_k^2} & \frac{(\omega_k + c_k)\sqrt{d_k}}{s_k t_k} \\ -\sqrt{d_k} & \frac{(\omega_k + c_k)\sqrt{d_k}}{s_k t_k} & \frac{\omega_k c_k - d_k}{s_k t_k} \end{pmatrix} \tag{4.23}$$

where $c_k = \cos\theta_k$, $d_k = -\cos 2\theta_k$, $s_k = \sin\theta_k$, $t_k = \tan\theta_k$, and $\omega_k = e^{i\pi\frac{3(k+1)}{2(k+2)}}$. The braiding matrix R_{23} is deduced from the Eq. (4.16).

Fibonacci Statistics

For example, we can evaluate the exchange matrices for the tri-critical Ising model ($k = 3$). Specifically, we can find the braiding matrices, $R_{12}^{(5)}$ and $R_{23}^{(5)}$, and the fusion matrix $R_{13}^{(5)}$. By substituting $k = 3$, we obtain

$$R_{12}^{(5)} = \begin{pmatrix} e^{-i\frac{2\pi}{5}} & 0 & 0 \\ 0 & e^{i\frac{\pi}{5}} & 0 \\ 0 & 0 & e^{i\frac{\pi}{5}} \end{pmatrix} \tag{4.24}$$

$$R_{13}^{(5)} = \begin{pmatrix} \gamma^{-1} & \gamma^{-1} & -\gamma^{-3/2} \\ \gamma^{-1} & -\frac{\left(1+e^{i\frac{\pi}{5}}\right)}{\gamma^2} & -\gamma^{-5/2}e^{i\frac{2\pi}{5}} \\ -\gamma^{-3/2} & -\gamma^{-5/2}e^{i\frac{2\pi}{5}} & -\frac{\left(\gamma^{-1}+\gamma e^{i\frac{\pi}{5}}\right)}{\gamma^2} \end{pmatrix} \tag{4.25}$$

and

$$R_{23}^{(5)} = \begin{pmatrix} e^{i\frac{\pi}{5}}\gamma^{-1} & e^{-i\frac{2\pi}{5}}\gamma^{-1} & -e^{-i\frac{2\pi}{5}}\gamma^{-3/2} \\ e^{-i\frac{2\pi}{5}}\gamma^{-1} & e^{i\frac{\pi}{5}}\gamma^{-1} & -e^{-i\frac{2\pi}{5}}\gamma^{-3/2} \\ -e^{-i\frac{2\pi}{5}}\gamma^{-3/2} & -e^{-i\frac{2\pi}{5}}\gamma^{-3/2} & e^{i\frac{\pi}{5}} - \gamma^{-2} \end{pmatrix} \tag{4.26}$$

These expressions will not be used to construct braiding-based quantum gates but are needed to evaluate the exchange matrices for six-point amplitudes.

4.4 Six-point Amplitudes

Next, we consider the amplitude involving six σ fields. From Eq. (3.36), we know there are four conformal blocks for $k = 2$ and five conformal blocks for $k \geq 3$, as shown in Figure 4.6.

Using the OPE $\sigma(\eta_5)\sigma(\eta_6) \sim \eta_{56}^{-\frac{k-1}{2(k+2)}}\mathbb{I} + \eta_{56}^{\frac{k+1}{2(k+2)}}\varepsilon(\eta_5)$ to expand near $\eta_6 = \eta_5$, we notice two different subspaces, one for the $\frac{1-k}{2(k+2)}$ and one for the $\frac{k+1}{2(k+2)}$ powers of η_{56}. The first one contains $\mathcal{F}_1^{(6)}$ and $\mathcal{F}_2^{(6)}$ is similar to the four-point amplitude, whereas the second one contains $\mathcal{F}_3^{(6)}$, $\mathcal{F}_4^{(6)}$ and $\mathcal{F}_5^{(6)}$ and is similar to the five-point amplitude.

The exchange matrices corresponding to the exchanges $\eta_1 \leftrightarrow \eta_2$, $\eta_1 \leftrightarrow \eta_3$ and $\eta_2 \leftrightarrow \eta_3$ can be found using the four-point and five-point matrices,

$$R^{(6)} = \left(\begin{array}{c|c} R^{(4)} & \mathbf{0} \\ \hline \mathbf{0} & R^{(5)} \end{array}\right) \quad , \quad R \in \{R_{12}, R_{13}, R_{23}\} \tag{4.27}$$

For the critical Ising model ($k = 2$), the 4×4 exchange matrices have been studied in [78, 79]. Confirming these results, we observe that the last conformal block decouples and the remaining 2×2 blocks correspond to a system of two interacting qubits

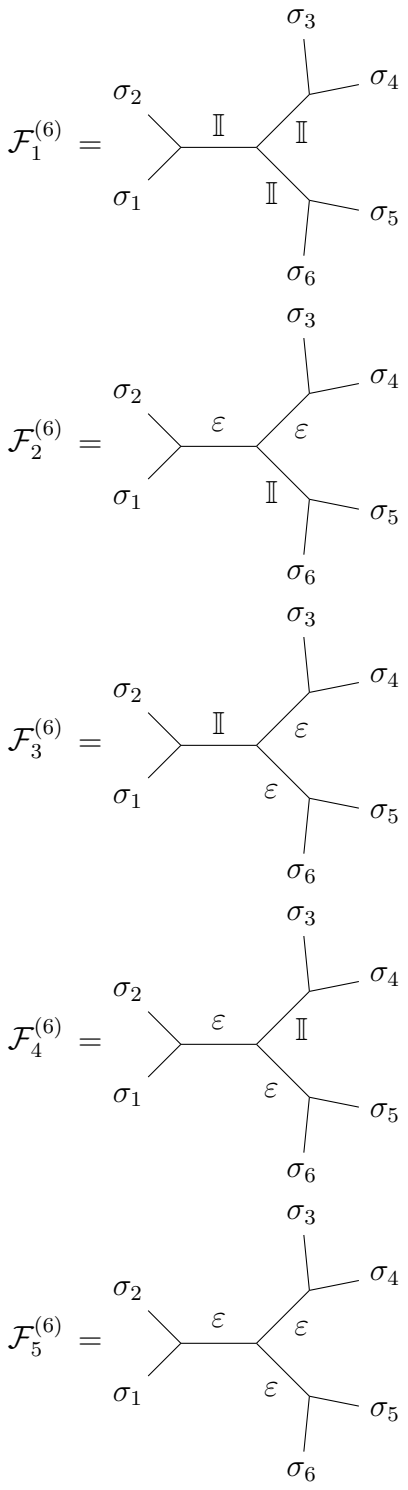

Figure 4.6: Conformal blocks of the six-point function. For $k = 2$ the last conformal block vanishes.

$$R^{(6)} = \left(\begin{array}{c|c|c} R^{(4)} & \mathbf{0} & 0 \\ \hline \mathbf{0} & R^{(4)} & 0 \\ \hline \mathbf{0} & \mathbf{0} & r \end{array}\right) \quad , \quad R \in \{R_{12}, R_{13}, R_{23}\} \tag{4.1}$$

where r is an irrelevant phase. These matrices are gates acting on two qubits; thus, we can construct entangling gates such as the CNOT and CZ gates. However, they do not lead to universal quantum computation [80]. Compared to the 4-dimensional representation of the braid group introduced in Chapter 2, we can have the identification $b_1 = R^{(6)}_{12}$, $b_2 = R^{(6)}_{23}$, etc.

For $k = 3$ and $k > 4$, the exchange matrices form a sufficient set of gates for universal quantum computation. The entangling quantum gates can be implemented based on the 5×5 exchange matrices.

Although we focused the discussion on exchange matrices R_{ij}, $i, j = 1, 2, 3$, the above method can be straightforwardly extended to include the point η_4. To obtain exchange matrices involving the points η_5 or η_6, we need to consider different limits that reduce the six-point amplitude to different four- and five-point amplitudes. For example, to calculate the exchange matrix R_{15} we can expand near $\eta_4 = \eta_3$ using the OPE $\sigma(\eta_4)\sigma(\eta_3) \sim \eta_{34}^{-\frac{k-1}{2(k+2)}}\mathbb{I} + \eta_{34}^{\frac{k+1}{2(k+2)}}\varepsilon(\eta_3)$. We obtain two distinct subspaces, one corresponding to the four-point results obtained earlier, but with conformal blocks $\mathcal{F}^{(6)}_1$ and $\mathcal{F}^{(6)}_4$, and the other corresponding to a five-point amplitude with conformal blocks $\mathcal{F}^{(6)}_2$, $\mathcal{F}^{(6)}_3$, and $\mathcal{F}^{(6)}_5$. All other exchange matrices are constructed similarly.

4.5 Higher-point amplitudes

The dimensionality of Hilbert space (number of conformal blocks) depends on both N and k. For the four-point amplitude ($N = 2$) we have two conformal blocks for all k, due to the fusion rule $\sigma \times \sigma \sim \varepsilon$ (Eq. (3.36) with $s = s' = 2$). For the six-point amplitude ($N = 3$), we have four conformal blocks for $k = 2$ and five conformal blocks for all other cases ($k \geq 3$). Using Eq. (3.36), we can find the number of conformal blocks for higher-point amplitudes. In particular, for $N = 4$, we have eight conformal blocks for $k = 2$, thirteen for $k = 3$, and

fourteen for all other cases ($k \geq 4$). For $k = 2$ (critical Ising model), the dimensionality of Hilbert space is 2^{N-1}, whereas for $k = 3$ (tricritical Ising model), it follows the Fibonacci sequence. General expressions for other $k \geq 4$ can be found using the fusion rules.

Although higher-point amplitudes cannot be explicitly calculated, we can still obtain the exchange matrices by following the procedure discussed above for the six-point amplitude. For example, to find the matrices R_{12}, R_{13} and R_{23} for the eight-point amplitude, we will work in the limit $\eta_8 \to \eta_7$ and $\eta_6 \to \eta_5$. We obtain the exchange matrix for the eight-point correlator as a block diagonal matrix, with each block corresponding to a four-point or five-point correlator. This procedure can be generalized to arbitrary N.

Chapter 5

Moore-Read Wavefunctions beyond Ising Statistics

This chapter presents, in detail, the construction of the Moore-Read wavefunction quantum statistics differing from the Ising model, using coset CFTs as discussed in [117].

5.1 Wavefunctions from Conformal Blocks

The conformal blocks we studied earlier compose the fundamental ingredient for constructing the qubits. However, by themselves, they don't correspond to physical states that can be realized in Nature. The issue becomes clear by recalling that any quantum mechanical system is generally described by a wavefunction or a density matrix, which is, in fact, an ensemble of different wavefunctions. These wavefunctions have to be well-defined and single-valued functions everywhere [120]. On the other hand, it's easy to observe that conformal blocks have pole singularities and are generally multi-valued functions as a result of the branch cuts that appear.

We overcome these problems in the following way. Let us consider the conformal blocks $\mathcal{F}_\mu(\boldsymbol{\eta})$ involving $2N$ primary fields $\sigma = \Phi_{(1,2)}$ at positions $\boldsymbol{\eta} = (\eta_1, \ldots, \eta_{2M})$. Next, we insert into the correlator $2M$ fields ψ that obey abelian fusion rules at positions $\boldsymbol{z} = (z_1, \ldots, z_{2M})$.

The amplitude $\mathcal{F}_\mu(\boldsymbol{\eta};\boldsymbol{z})$ corresponds to a single-valued function by demoting the positions $\boldsymbol{\eta}$ into parameters. The newly defined amplitude still has poles at $\boldsymbol{z}$ and $\boldsymbol{\eta}$. To eliminate them, we introduce the Jastrow factor $\mathcal{J}$ that has zeroes at the position of these poles canceling the singularities. Therefore, we are led to consider the wavefunction as the product of two chiral amplitudes

$$\Psi_{\mu;\boldsymbol{\eta}}(\boldsymbol{z}) \propto \mathcal{J}(\boldsymbol{\eta};\boldsymbol{z})\mathcal{F}_\mu(\boldsymbol{\eta};\boldsymbol{z}) \tag{5.1}$$

The first term is a chiral amplitude built from a free boson ϕ CFT. To its definition, we need to introduce the holomorphic vertex operators $\mathcal{V}$ at positions $\boldsymbol{\eta} = (\eta_1, \ldots, \eta_{2M})$ and $\mathcal{W}$ at positions $\boldsymbol{z} = (z_1, \ldots, z_{2M})$ and a screening charge $\mathcal{Q}$ to fix the charge neutrality condition. These are defined in terms of the free boson according to

$$\mathcal{V}_j = e^{i\frac{1}{2\sqrt{\Lambda}}\phi(\eta_j)} \quad , \quad \mathcal{W}_j = e^{i\sqrt{\Lambda}\phi(z_j)} \quad , \quad \mathcal{Q} = e^{-\frac{i}{\sqrt{\Lambda}}\int \frac{d^2w}{2\pi}\phi(w,\bar{w})} \tag{5.2}$$

The Jastrow factor is defined as an amplitude of $\mathcal{V}$ and $\mathcal{W}$ operators given by

$$\mathcal{J}^{(2N,2M)}(\boldsymbol{\eta};\boldsymbol{z}) = \langle \mathcal{V}_1 \ldots \mathcal{V}_{2N} \mathcal{W}_1 \ldots \mathcal{W}_{2M} \mathcal{Q} \rangle \tag{5.4}$$

Following the reference [46] one can write the Jastrow factor in an explicit form as

$$\mathcal{J}^{(2N,2M)}(\boldsymbol{\eta};\boldsymbol{z}) = \prod_{i<j}^{2M} z_{ij}^{\Lambda} \prod_{a<b}^{2N} \eta_{ab}^{\frac{1}{4\Lambda}} \prod_{a=1}^{2N}\prod_{i=1}^{2M} (\eta_a - z_i)^{\frac{1}{2}} e^{-\frac{1}{4}\sum_{i=1}^{2M}|z_i|^2} e^{-\frac{1}{8\Lambda}\sum_{a=1}^{2N}|\eta_a|^2} \tag{5.5}$$

where Λ is a positive integer that represents the inverse filling of FQHE. Similarly, the second term of (5.1) is defined as

$$\mathcal{F}_\mu^{(2N,2M)}(\boldsymbol{\eta};\boldsymbol{z}) = \langle \sigma_1 \cdots \sigma_{2N} \psi_1 \cdots \psi_{2M} \rangle \tag{5.6}$$

where $\sigma_j = \sigma(\eta_j)$ and $\psi_j = \psi(z_j)$ are primaries of a more complicated chiral CFT, such as the Minimal Model $\mathcal{M}(k+2, k+1)$. Notice that the amplitude in Eq. (5.6) might have to be modified by introducing conjugate fields and screening charges, as discussed in Chapter

3, in order to satisfy the charge neutrality condition. Calculations of amplitude with an arbitrary number of σ and ψ operators have been performed for the critical Ising model in [52, 121]. By mapping conformal blocks into wavefunctions, we map the braiding matrices into unitary quantum gates. These braiding matrices act as unitary transformations mixing the states $\Psi_{\mu;\boldsymbol{\eta}}$, as long as all conformal blocks yield states in the degenerate vacuum of the system. Moreover, as was emphasized in [122], for the braiding statistics of the wavefunction to match the monodromy around the branch points of the multi-valued part of the function, we need to ensure that the Berry holonomy vanishes. It was demonstrated in [46] using the plasma analogy that the Berry holonomy vanishes for the Moore-Read (MR) wavefunction.

The previously defined steps provide a way to construct wavefunctions from conformal blocks of an arbitrary CFT. Despite that, not every CFT is a good candidate for fault-tolerant quantum computation. An important last requirement is to construct wavefunctions with an energy gap. Only then is boundary CFT dual to a topological bulk that satisfies the three properties that characterize systems in a topological phase of matter defined in Chapter 2.

Following these instructions, we obtain the FQHE wavefunctions developed in [39, 44, 49]. In particular, in [44], the Moore-Read wavefunction was constructed using the critical Ising Minimal Model $\mathcal{M}(4,3)$. In this calculation, σ is the $\Phi_{(1,2)}$ primary field with conformal dimension $h_{(1,2)} = \frac{1}{16}$ and ψ is the $\Phi_{(1,3)}$ primary field with conformal dimension $h_{(1,3)} = \frac{1}{2}$. These fields acquire a nice physical meaning in the context of FQHE. We can interpret the product of ψ and $\mathcal{W}$ represents the electrons of the electron gas. Whereas the product of σ and $\mathcal{V}$ corresponds to the quasi-holes with Ising braiding statistics that are emerging in the fractional quantum Hall system. Unfortunately, braiding alone does not lead to universal quantum computation.

We are interested in finding different CFTs that can be used to construct energy-gapped wavefunctions which can offer universal topological quantum computation. An obvious choice would be to consider different Minimal Models $\mathcal{M}(k+2,k+1)$ for $k \geq 3$. This was motivated by observing Fibonacci statistics in the tri-critical Ising model $\mathcal{M}(5,4)$. As shown in [46] using the plasma analogy, to construct a gapped state that will lead to fault-tolerant quantum

computation, the dimension of ψ must be less than 1. In the critical Ising model $\mathcal{M}(4,3)$, this requirement is satisfied because ψ can be chosen as the primary field $\Phi_{(1,3)}$ which has conformal dimension $h_{(1,3)} = \frac{1}{2} < 1$. In the CFT Minimal Models $\mathcal{M}(k+2,k+1)$ with $k \geq 3$, we cannot identify ψ with any of their primary fields; therefore, we cannot construct a gapped wavefunction starting from the Eq. (5.1). Attempts to construct MR-like wavefunctions for Minimal Models $\mathcal{M}(k+2,k+1)$ with $k > 2$ were studied in [46].

5.2 Coset CFTs

The next step is to study various coset CFTs that might be able to support wavefunctions with an energy gap. Specifically, we propose an alternative construction of the MR wavefunction based on the coset $SU(2)_1^{\otimes k}/SU(2)_k$, where $SU(2)_k$ is the Wess-Zumino-Witten (WZW) model based on the gauge group $SU(2)$ at level k. For $k = 2$, it reduces to the MR wavefunction because the critical Ising model $\mathcal{M}(4,3)$ is isomorphic to the coset $SU(2)_1 \otimes SU(2)_1/SU(2)_2$. More generally, the entire family of the Minimal Models $\mathcal{M}(k+2,k+1)$ can be constructed from a similar coset $SU(2)_{k-1} \otimes SU(2)_1/SU(2)_k$ as explained in [123, 124, 125, 126] (GKO method). The choice of the coset CFT is motivated by observing that the two theories $SU(2)_1^{\otimes k}/SU(2)_k$ and $\mathcal{M}(k+2,k+1)$ share properties even for $k > 2$. In particular, we find that all primary fields $\Phi_{(1,s)}$ with $1 \leq s \leq k+1$ belonging to the Minimal Model $\mathcal{M}(k+2,k+1)$ are also primaries of the $SU(2)_1^{\otimes k}/SU(2)_k$ coset CFT. These primaries share the same conformal dimensions, fusion rules, and braiding statistics in both theories. The advantage of the coset CFT is having a new primary field of conformal dimension $\frac{1}{2}$ for all k, which is also present in the MR wavefunction. More details about coset construction can be found in [127, 128, 129]. Different approaches can be found in the literature, including from Chern-Simons theories [130], from functional integrals [131], and using the BRST formalism [132]. Cosets have also been studied for non-rational CFTs such as the Liouville theory [133] and parafermionic CFTs [134].

To construct the coset CFT, we start by reviewing the fundamental properties of the WZW theories that satisfy the affine Kac-Moody algebra $SU(2)_k$ (level $k : k \in \mathbb{Z}^+$). These

are rational conformal field theories that were first studied in [135]. A brief review of the Wess-Zumino-Witten theory can be found in Appendix C.

The Kac-Moody algebra is an infinite-dimensional generalization to the standard Lie algebra [136]. In particular, for $SU(2)_k$ the generators obey the algebra

$$[J^a_n, J^b_m] = if^{abc}J^c_{n+m} + ikn\delta^{ab}\delta_{n+m,0} \tag{5.7}$$

where f^{abc} is the structure constant of the $SU(2)$ Lie algebra and $n, m \in \mathbb{Z}$. The level k introduces a cut-off on the number of irreducible representations of $SU(2)_k$, which are defined by "spin" number $j = 0, \frac{1}{2}, \ldots, \frac{k}{2}$. The number of primary fields in these theories equals the number of "spin" representations. Each primary field has a conformal dimension given by

$$h_j = \frac{j(j+1)}{k+2} \tag{5.8}$$

It is instructive to first review the $SU(2)_{k-1} \otimes SU(2)_1 / SU(2)_k$ coset CFT and demonstrate how to obtain the Minimal Models using these three different WZW theories. We will denote the primary fields of these models as $\theta^{j_1}_{m_1}$ for the $SU(2)_{k-1}$ with $j_1 = 0, \frac{1}{2}, \ldots, \frac{k-1}{2}$, $\chi^{j_2}_{m_2}$ for the $SU(2)_1$ with $j_2 = 0, \frac{1}{2}$, and υ^j_m for the $SU(2)_k$ with $j = 0, \frac{1}{2}, \ldots, \frac{k}{2}$. Here, the number m takes values from $-j$ to j. The coset representations (primary fields) are identical to the Minimal models $\mathcal{M}(k+2, k+1)$; this can be seen by decomposing the $SU(2)_{k-1} \otimes SU(2)_1$ representations into a direct sum of $SU(2)_k \otimes \mathcal{M}(k+2, k+1)$ representations. The primary fields of the coset have conformal dimensions given by

$$h = \frac{j_1(j_1+1)}{k+1} + \frac{j_2(j_2+1)}{3} - \frac{j(j+1)}{k+2} + \omega \tag{5.9}$$

where $\omega = (j_1 - j)^2$ if $j_1 - j$ is an integer and $\omega = (j_1 - j)^2 - \frac{1}{4}$ if $j_1 - j$ is a half-integer number, as explained in [137, 138].

Here we are interested in the primary fields of the type $\Phi_{(1,s)}$, with $s = 1, 2, \ldots, k+1$. These can be constructed by choosing the "spin" representations according to [124]

$$(j_1 = 0)_{k-1} \otimes (j_2 = 0)_1 = (j = 0)_k \otimes \Phi_{(1,1)} \oplus (j = 1)_k \otimes \Phi_{(1,3)} \oplus \cdots \tag{5.10}$$

$$(j_1 = 0)_{k-1} \otimes (j_2 = \frac{1}{2})_1 = (j = \frac{1}{2})_k \otimes \Phi_{(1,2)} \oplus (j = \frac{3}{2})_k \otimes \Phi_{(1,4)} \oplus \cdots \tag{5.11}$$

where the $j = \frac{3}{2}$ component in the right-hand side of Eq. (5.10) vanishes for $k = 3$. Additional terms appear in the direct sum for $k > 3$, which can be found using the GKO method.

Next, we can proceed and study the $SU(2)_1^{\otimes k}/SU(2)_k$ coset. This CFT can be constructed from k copies of an $SU(2)_1$ and one $SU(2)_k$ WZW theory. The primary fields of each level 1 theory will be denoted by $\chi_{m_i}^{[i]j_i}$, where here the index $i = 1, 2, \ldots k$ labels the particular copy of the $SU(2)_1$ and the "spin" j_i can be either 0 or $\frac{1}{2}$. Similarly, the $SU(2)_k$ primaries are defined by υ_m^j, with $j = 0, \frac{1}{2}, \ldots, \frac{k}{2}$. The coset primary fields $\Phi_{(1,s)}$ can be obtained from Eqs. (5.10) and (5.11). In particular, we are interested in the explicit definition of the $\Phi_{(1,2)}$ field, as it's a main component of the wavefunction of Eq. (5.1). Though primaries with $s \geq 3$ participate in the wavefunction through fusion, their explicit definition is not necessary. For "spin"-$\frac{1}{2}$ Eq. (5.8) gives the conformal dimensions

$$h_\chi = \frac{1}{4} \quad , \quad h_\upsilon = \frac{3}{4(k+2)} \tag{5.12}$$

To simplify the notation, we will drop the index j and use $m = \pm$ to denote $m = \pm\frac{1}{2}$. Then, the primary field $\sigma = \Phi_{(1,2)}$ can be constructed in the following way

$$\sigma^{[i]} = \chi_+^{[i]}\bar{\tau}_+ + \chi_-^{[i]}\bar{\tau}_- \tag{5.13}$$

Evidently, this does not lead to a unique definition since we can consider any of the $SU(2)_1$ factors in the coset to construct σ. We will identify $\sigma \equiv \sigma^{[k]}$. Using Eq. (5.9), we obtain

its conformal weight $h_\sigma = h_\chi - h_\upsilon = \frac{k-1}{4(k+2)}$, in agreement with the minimal model result in Table 3.2.

Agreement with the minimal model $\mathcal{M}(k+2, k+1)$ is expected because the latter can be constructed from the coset $SU(2)_{k-1} \otimes SU(2)_1/SU(2)_k$. The field σ in the minimal model is also given by Eq. (5.13) with $\chi_\pm$ in the (single) $SU(2)_1$ factor in the coset $SU(2)_{k-1} \otimes SU(2)_1/SU(2)_k$.

5.3 Coset Amplitudes

Next, we aim to evaluate amplitudes using the coset definition. As demonstrated in [129, 131], an amplitude of the coset $SU(2)_1^{\otimes k}/SU(2)_k$ factorizes into a product of amplitudes of $SU(2)$ at levels 1 and $-(k+4)$ according to

$$\langle SU(2)_1^{\otimes k}/SU(2)_k \rangle = \langle SU(2)_1 \rangle \otimes \cdots \otimes \langle SU(2)_1 \rangle \otimes \langle SU(2)_{-k-4} \rangle \tag{5.14}$$

Following these definitions, the chiral conformal blocks for the 2N-point amplitude $\langle \sigma_1 \dots \sigma_{2N} \rangle$ are found from[†]

$$\mathcal{F}_\mu^{(4)}(\boldsymbol{\eta}) = \sqrt{N_\mu} \sum_{n_1 \dots n_{2N}} X^{[k]}_{n_1 \dots n_{2N}} Y_{\mu; n_1 \dots n_{2N}} \tag{5.15}$$

where each correlator is given by

$$X^{[k]}_{n_1 \dots n_{2N}} = \langle \chi^{[k]}_{n_1}(\eta_1) \cdots \chi^{[i]}_{n_{2N}}(\eta_{2N}) \rangle \tag{5.16}$$

$$Y_{\mu; n_1 \dots n_{2N}} = \langle \upsilon_{n_1}(\eta_1) \cdots \upsilon_{n_{2N}}(\eta_{2N}) \rangle \tag{5.17}$$

As discussed in [138], these correlators are solutions to the Knizhnik–Zamolodchikov (KZ) equation [139]. However, here we will use the free field representation of $SU(2)_k$ [140, 141] to evaluate them. The primary fields are defined in terms of a massless free boson $\tilde{\varphi}$ and a (β, γ) bosonic ghost system. Correlators are evaluated using the Coulomb gas formalism.

[†]Henceforth, we will associate the primary field σ to the index $n = \pm$ instead of $m = \pm$.

Charge neutrality is enforced using screening charges and conjugate fields as needed. Charge neutrality translates into the constraint $\sum_{i=1}^{2N} n_i = 0$.

As an example, we can find the four-point correlator involving four σ primary fields. The sum in Eq. (5.15) reduces to

$$\mathcal{F}_{\mu}^{(4)}(\boldsymbol{\eta}) = 2\sqrt{N_\mu}[X_{+--+}Y_{\mu;+--+} + X_{--++}Y_{\mu;--++} + X_{-+-+}Y_{\mu;-+-+}] \tag{5.18}$$

The factor of 2 comes from taking into account the symmetry between amplitudes $(++--)$ and $(--++)$, etc. As before, a global conformal transformation fixes three points: $\eta_1 \to 0$, $\eta_2 \to x$, $\eta_3 \to 1$ and $\eta_4 \to \infty$. A detailed calculation of $SU(2)_k$ correlators can be found in Appendix C. For $SU(2)_1$ we obtain the two linearly independent functions

$$X_{+--+} = \frac{4\pi^2}{\Gamma\left(\frac{1}{3}\right)^3}\sqrt{\frac{1-x}{x}} \quad , \quad X_{--++} = \frac{4\pi^2}{\Gamma\left(\frac{1}{3}\right)^3}\sqrt{\frac{x}{1-x}} \tag{5.19}$$

while the remaining one can be found from the constraint equation

$$X_{-+-+} = -X_{+--+} - X_{--++} \tag{5.20}$$

Similarly, we obtain the functions for the two $SU(2)_k$ conformal blocks by setting $k \to -k-4$ in the corresponding expressions (C.7) - (C.12)

$$Y_{1;+--+} = -\frac{\Gamma\left(\frac{1}{k+2}\right)\Gamma\left(\frac{k+3}{k+2}\right)}{\Gamma\left(\frac{k+4}{k+2}\right)}(1-x)^{-\frac{1}{2k+4}}x^{\frac{3}{2k+4}}\,{}_2F_1\left(-\frac{1}{k+2},\frac{1}{k+2};\frac{k+4}{k+2};x\right) \tag{5.21}$$

$$Y_{1;--++} = \frac{\Gamma\left(\frac{1}{k+2}\right)\Gamma\left(\frac{k+3}{k+2}\right)}{(k+4)\Gamma\left(\frac{k+4}{k+2}\right)}(1-x)^{-\frac{1}{2k+4}}x^{\frac{2k+7}{2k+4}}\,{}_2F_1\left(\frac{k+1}{k+2},\frac{k+3}{k+2};\frac{2(k+3)}{k+2};x\right) \tag{5.22}$$

$$Y_{2;+--+} = \frac{\Gamma\left(\frac{1}{k+2}\right)\Gamma\left(-\frac{3}{k+2}\right)}{2\Gamma\left(-\frac{2}{k+2}\right)}((1-x)x)^{-\frac{1}{2k+4}}\,{}_2F_1\left(-\frac{3}{k+2},-\frac{1}{k+2};\frac{k}{k+2};x\right) \tag{5.23}$$

$$Y_{2;--++} = -\frac{\Gamma\left(-\frac{3}{k+2}\right)\Gamma\left(\frac{1}{k+2}\right)}{\Gamma\left(-\frac{2}{k+2}\right)}((1-x)x)^{-\frac{1}{2k+4}}\,{}_2F_1\left(-\frac{3}{k+2},-\frac{1}{k+2};-\frac{2}{k+2};x\right) \tag{5.24}$$

with the constraint equation

$$Y_{\mu;-+-+} = -Y_{\mu;+--+} - Y_{\mu;--++} \quad , \quad \mu = 1, 2 \tag{5.25}$$

After some algebra involving Hypergeometric function identities, we arrive at compact explicit expressions for the conformal blocks given of Eq. (5.18)

$$\mathcal{F}_1^{(4)} = -\sqrt{N_1}\frac{32\pi^2\Gamma^2\left(\frac{1}{k+2}\right)}{\Gamma^3\left(\frac{1}{3}\right)\Gamma\left(\frac{2}{k+2}\right)} x^{\frac{1-k}{2k+4}}(1-x)^{\frac{k+1}{2k+4}}\,{}_2F_1\left(\frac{1}{k+2}, \frac{k+1}{k+2}; \frac{2}{k+2}; x\right) \tag{5.26}$$

$$\mathcal{F}_2^{(4)} = \sqrt{N_2}\frac{12\pi^2(1-k)\Gamma\left(-\frac{3}{k+2}\right)\Gamma\left(\frac{1}{k+2}\right)}{k\Gamma^3\left(\frac{1}{3}\right)\Gamma\left(-\frac{2}{k+2}\right)} x^{\frac{k+1}{2k+4}}\,(1-x)^{\frac{k+1}{2k+4}}_2F_1\left(\frac{k+1}{k+2}, \frac{2k+1}{k+2}; \frac{2(k+1)}{k+2}; x\right) \tag{5.27}$$

in agreement with our earlier result given by the Eqs. (4.8) and (4.9). It follows that the exchange matrices one obtains from the coset construction coincide with their counterparts in the corresponding minimal model.

For a sanity check, we should also confirm that we obtain correct exchange matrices for general correlators in the coset CFT $SU(2)_1^{\otimes k}/SU(2)_k$ by using the Eq. (5.18).

As a first example, under the transformation $\eta_1 \leftrightarrow \eta_3$ ($x \leftrightarrow 1-x$), it is easy to see that $X_{\boldsymbol{n}} \leftrightarrow X_{\boldsymbol{n}'}$ and $X_{\boldsymbol{n}''} \to X_{\boldsymbol{n}''}$, where $\boldsymbol{n} = +--+$, $\boldsymbol{n}' = --++$, and $\boldsymbol{n}'' = -+-+$. Also, using Hypergeometric identities, we obtain

$$\boldsymbol{Y}_{\boldsymbol{m}} \to R_{13}^{(4)}\boldsymbol{Y}_{\boldsymbol{m}'} \ , \ \boldsymbol{Y}_{\boldsymbol{m}'} \to R_{13}^{(4)}\boldsymbol{Y}_{\boldsymbol{m}} \ , \ \boldsymbol{Y}_{\boldsymbol{m}''} \to R_{13}^{(4)}\boldsymbol{Y}_{\boldsymbol{m}''} \tag{5.28}$$

where the two conformal blocks of the Y function are organized into a vector as

$$\boldsymbol{Y}_{\boldsymbol{m}} = \begin{pmatrix} \sqrt{N_1}Y_{1;\boldsymbol{m}} \\ \sqrt{N_2}Y_{2;\boldsymbol{m}} \end{pmatrix} \tag{5.29}$$

and $R_{13}^{(4)}$ is defined in Eq. (4.14). It follows from Eq. (5.18) that the conformal blocks transform under

$$\boldsymbol{\mathcal{F}}^{(4)} \to R_{13}^{(4)} \boldsymbol{\mathcal{F}}^{(4)} \quad , \quad \boldsymbol{\mathcal{F}}^{(4)} = \begin{pmatrix} \mathcal{F}_1^{(4)} \\ \mathcal{F}_2^{(4)} \end{pmatrix} \tag{5.30}$$

as expected. Similarly, we find that under the transformation $\eta_1 \leftrightarrow \eta_2$, we obtain

$$X_{\boldsymbol{m}} \boldsymbol{Y}_{\boldsymbol{m}} \to R_{12}^{(4)} X_{\boldsymbol{m}'} \boldsymbol{Y}_{\boldsymbol{m}'} \quad , \quad X_{\boldsymbol{m}'} \boldsymbol{Y}_{\boldsymbol{m}'} \to R_{12}^{(4)} X_{\boldsymbol{m}} \boldsymbol{Y}_{\boldsymbol{m}} \quad , \quad X_{\boldsymbol{m}''} \boldsymbol{Y}_{\boldsymbol{m}''} \to R_{12}^{(4)} X_{\boldsymbol{m}''} \boldsymbol{Y}_{\boldsymbol{m}''} \tag{5.31}$$

where $R_{12}^{(4)}$ is defined in Eq. (4.13). Then we find that the conformal blocks also transform via the $R_{12}^{(4)}$. By combining these two results, it's trivial to prove that the coset construction gives the correct exchange matrix even for the transformation $\eta_2 \leftrightarrow \eta_3$.

5.4 Coset Wavefunctions

In the CFT Minimal Models $\mathcal{M}(k+2, k+1)$ with $k \geq 3$, we cannot identify ψ ($h_\psi < 1$) with any of their primary fields; therefore, we cannot construct a gapped wavefunction defined by the Eq. (5.1).

A gapped wavefunction can be constructed from the coset CFT $SU(2)_1^{\otimes k}/SU(2)_k$ for all k, generalizing the Ising anyonic excitations of the MR wavefunction, to which it reduces for $k = 2$ [44]. Since the $\Phi_{(1,s)}$ primary fields with $1 \leq s \leq k+1$ in $\mathcal{M}(k+2, k+1)$ can be mapped onto primary fields in $SU(2)_1^{\otimes k}/SU(2)_k$ with the same fusion rules and conformal dimensions. The correlators of the field σ computed in $SU(2)_1^{\otimes k}/SU(2)_k$ are equivalent to those computed in the Minimal Model $\mathcal{M}(k+2, k+1)$. On the other hand, correlators involving the ψ field must be computed in $SU(2)_1^{\otimes k}/SU(2)_k$. We define the ψ field in the $SU(2)_1^{\otimes k}/SU(2)_k$ coset by

$$\psi^{[ij]} = \chi_+^{[i]} \chi_-^{[j]} + \chi_-^{[i]} \chi_+^{[j]} \tag{5.32}$$

Evidently, Eq. (5.32) does not lead to a unique definition of ψ since we can consider any pair of $SU(2)_1$ factors in the coset to construct ψ. The simplest generalization of the MR wavefunction requires one of the $SU(2)_1$ factors must be shared with the one in the definition

of σ (Eq. (5.13)). Since in the previous section we identified $\sigma \equiv \sigma^{[k]}$, here we will have to define $\psi \equiv \psi^{[1k]}$. We also identify the conjugate primary field $\tilde{\sigma} = \Phi_{(k,k)} \equiv \sigma^{[1]}$; thus generalizing the critical Ising model result. Following these definitions, we obtain the fusion rules

$$\sigma \otimes \psi \sim \tilde{\sigma} \quad , \quad \psi \otimes \psi \sim \mathbb{I} \tag{5.33}$$

for all k, which is the same as in the critical Ising model. It should be stressed here that the fusion rule for two σ primary fields (i.e., $\sigma \otimes \sigma$) does not involve ψ for $k > 2$; it follows the Eq. (3.36) and involves the fields $\mathbb{I}, \varepsilon, \varepsilon', \ldots$, which appear in the Table 3.2. The $k = 2$ is a special case, as we observe that $\psi = \varepsilon = \Phi_{(1,3)}$. From Eq. (5.9), we obtain its conformal weight $h_\psi = 2h_\chi = \frac{1}{2} < 1$, satisfying the requirement for a gapped wavefunction that leads to fault-tolerant quantum computing for $k = 3$ and $k > 4$.

Since ψ obeys Abelian fusion rules, the amplitudes $\langle \sigma_1 \cdots \sigma_{2N} \psi_1 \cdots \psi_{2M} \rangle$ and $\langle \sigma_1 \cdots \sigma_{2N} \rangle$ have the same number of conformal blocks. Diagrammatically, these are shown in Figure 5.1 for four σ fields ($N = 2$). Moving the ψ fields to different positions does not affect these conformal blocks.

Correlators of ψ are constructed as products of $SU(2)_1$ theories, similar to the factors of correlators of σ, as per Eq. (5.15). The $2M$-point ψ correlator is found to reproduce the Pfaffian wavefunction, as in the case of the critical Ising model

$$\langle \psi_1 \cdots \psi_{2M} \rangle = \sum_{\boldsymbol{m}} X^{[1]}_{\boldsymbol{m}} X^{[k]}_{\tilde{\boldsymbol{m}}} = \mathrm{Pf}\left(\frac{1}{z_i - z_j}\right) \tag{5.34}$$

where the two $SU(2)_1$ terms are defined as

$$X^{[1]}_{m_1 \ldots m_{2M}} = \langle \chi^{[1]}_{m_1}(z_1) \cdots \chi^{[1]}_{m_{2M}}(z_{2M}) \rangle \tag{5.35}$$

$$X^{[k]}_{\tilde{\boldsymbol{m}}_1 \ldots \tilde{\boldsymbol{m}}_{2M}} = \langle \chi^{[k]}_{-m_1}(z_1) \cdots \chi^{[k]}_{-m_{2M}}(z_{2M}) \rangle \tag{5.36}$$

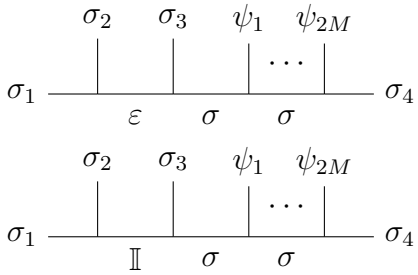

Figure 5.1: The two conformal blocks for $N = 2$ and arbitrary M. These correlators are independent of the location of the ψ operators.

Having defined a method to construct amplitudes that involve σ or ψ fields, we can now proceed to build more interesting states involving both fields simultaneously. More generally, we construct the correlator $\mathcal{F}_\mu(\boldsymbol{\eta};\boldsymbol{z})$ involving $2N$ σ and $2M$ ψ primary fields by

$$\mathcal{F}_\mu(\boldsymbol{\eta};\boldsymbol{z}) = \sqrt{N_\mu}\sum_{n,m} X^{[1]}_{\boldsymbol{m}} X^{[k]}_{\bar{\boldsymbol{m}},\boldsymbol{n}} Y_{\mu;\boldsymbol{n}} \tag{5.37}$$

where N_μ are the normalization constants defined in Chapter 4 and the three WZW factors are given by

$$X^{[1]}_{\boldsymbol{m}} = \langle \chi_{m_1}(z_1)\cdots\chi_{m_{2M}}(z_{2M})\rangle \tag{5.38}$$

$$X_{\bar{\boldsymbol{m}}^{[k]},\boldsymbol{n}} = \langle \chi_{n_1}(\eta_1)\cdots\chi_{n_{2N}}(\eta_{2N})\chi_{\bar{m}_1}(z_1)\cdots\chi_{\bar{m}_{2M}}(z_{2M})\rangle \tag{5.39}$$

$$Y_{\mu;\boldsymbol{n}} = \langle \upsilon_{n_1}(\eta_1)\cdots\upsilon_{n_{2N}}(\eta_{2N})\rangle \tag{5.40}$$

It is important to note that the multi-valued part of the conformal block appears in the last factor, as the fields in $SU(2)_1$ obey Abelian fusion rules. By combining Eqs. (5.5) and (5.34), we can derive a gapped wavefunction of the Eq. (5.1). To better understand the properties of these coset wavefunctions, i it would be instructive to study a few particular choices for the numbers N and M.

N=1 and M=1

For a state with two σ and two ψ operators, we obtain the wavefunction by setting $N=1$ and $M=1$. The factor $\langle\sigma\sigma\rangle$ gives a single conformal block; thus the $\mathcal{F}^{(2,2)}$ correlator becomes

$$\mathcal{F}^{(2,2)} = \sum_{m_1,m_2} X^{[1]}_{m_1m_2} X^{[k]}_{+-\bar{m}_1\bar{m}_2} Y_{+-} + \sum_{m_1,m_2} X^{[1]}_{m_1m_2} X^{[k]}_{-+\bar{m}_1\bar{m}_2} Y_{-+} \tag{5.41}$$

where $Y_{+-} = Y_{-+} = \eta_{12}^{\frac{3}{2(k+2)}}$, and similarly all the $SU(2)_1$ correlators are easily computed via the following equation

$$X_{m_1 \dots m_4} = \langle \chi_{m_1}(w_1) \cdots \chi_{m_{2M}}(w_{2M}) \rangle = \prod_{\boldsymbol{m}^\dagger} \prod_{i<j} (w_i - w_j)^{\frac{m_i m_j}{2}} \tag{5.42}$$

After some algebra, we find that

$$\mathcal{F}^{(2,2)} = 2 \frac{\eta_{12}^{\frac{1-k}{2k+4}}}{z_{12}} \frac{(\eta_1 - z_1)(\eta_2 - z_2) + (\eta_1 - z_2)(\eta_2 - z_1)}{\sqrt{(\eta_1 - z_1)(\eta_1 - z_2)(\eta_2 - z_1)(\eta_2 - z_2)}} \tag{5.43}$$

Notice that the exchange $\eta_1 \leftrightarrow \eta_2$ leads to the same factor as the one obtained for the propagator $\langle \sigma_1 \sigma_2 \rangle$. The corresponding Jastrow factor can be found in Eq. (5.5)

$$\mathcal{J}^{(2,2)} = \sqrt{(\eta_1 - z_1)(\eta_1 - z_2)(\eta_2 - z_1)(\eta_2 - z_2)} z_{12}^{\Lambda} \eta_{12}^{\frac{1}{4\Lambda}} e^{-\frac{|z_1|^2 + |z_2|^2}{4}} e^{-\frac{|\eta_1|^2 + |\eta_2|^2}{8\Lambda}} \tag{5.44}$$

Finally, the wavefunction becomes

$$\Psi_{\eta_1, \eta_2}(z_1, z_2) \propto \eta_{12}^{\frac{1}{4\Lambda} - \frac{k-1}{2(k+2)}} z_{12}^{\Lambda - 1} \xi e^{-\frac{|z_1|^2 + |z_2|^2}{4}} e^{-\frac{|\eta_1|^2 + |\eta_2|^2}{8\Lambda}} \tag{5.45}$$

where $\xi = (\eta_1 - z_1)(\eta_2 - z_2) + (\eta_1 - z_2)(\eta_2 - z_1)$ is a polynomial in (z_1, z_2). Thus, Ψ has no singularities in (z_1, z_2) for $\Lambda \geq 1$.

N=2 and M=1

In order to obtain a state with more interesting physics, we need to consider four σ and two ψ operators; thus, by setting $N = 2$ and $M = 1$. The factor $\langle \sigma\sigma\sigma\sigma \rangle$ gives two conformal blocks. Omitting overall normalization constants (*cf.* with Eq. (5.18)), after some algebra we obtain

$$\mathcal{F}_{\mu}^{(4,2)} = \frac{2}{z_{12}} \prod_{i=1}^{2} \prod_{a=1}^{4} (\eta_a - z_i)^{-\frac{1}{2}} \Xi \tag{5.46}$$

[†]The m index of the product is constraint so that $\sum_i m_i = 0$.

where Ξ is a polynomial in (z_1, z_2), defined as

$$\Xi = \xi_{(14)(23)} X_{+--+} Y_{\mu;+--+} + \xi_{(12)(34)} X_{--++} Y_{\mu;--++} + \xi_{(13)(24)} X_{-+-+} Y_{\mu;-+-+} \tag{5.47}$$

in terms of the polynomials

$$\xi_{(ab)(cd)} = (\eta_a - z_1)(\eta_b - z_1)(\eta_c - z_2)(\eta_d - z_2) + (z_1 \leftrightarrow z_2) \tag{5.48}$$

The corresponding Jastrow factor is found to be

$$\mathcal{J}^{(4,2)} = z_{12}^{\Lambda} \prod_{a<b}^{4} \eta_{ab}^{\frac{1}{4\Lambda}} \prod_{a=1}^{4} \prod_{i=1}^{2} (\eta_a - z_i)^{\frac{1}{2}} e^{-\frac{|z_1|^2+|z_2|^2}{4}} e^{-\frac{|\eta_1|^2+\cdots+|\eta_4|^2}{8\Lambda}} \tag{5.49}$$

and the wavefunctions for the two conformal blocks are

$$\Psi_{\mu;\boldsymbol{\eta}}(z_1, z_2) \propto \prod_{a<b}^{4} \eta_{ab}^{\frac{1}{4\Lambda}} z_{12}^{\Lambda-1} \Xi \, e^{-\frac{|z_1|^2+|z_2|^2}{4}} e^{-\frac{|\eta_1|^2+\cdots+|\eta_4|^2}{8\Lambda}} \tag{5.50}$$

These two wavefunctions are well-defined, with no singularities for $\Lambda \geq 1$. In the case of $k = 2$, they exactly match the MR wavefunctions, derived in Ref. [44], using the critical Ising model and exhibiting Ising anyonic excitations.

It is straightforward, albeit cumbersome, to generalize the above results to arbitrary numbers of σ and ψ fields.

Braiding Statistics

As a sanity check, we wish to demonstrate that the wavefunction, constructed from the coset $SU(2)_1^{\otimes k}/SU(2)_k$, reproduces the braiding statistics found in Chapter 4, using the Minimal models $\mathcal{M}(k+2, k+1)$ for every $k \geq 2$. Specifically, we will show the explicit calculations for four and six σ fields. Braiding statistics for wavefunctions with a higher number of σ operators can be easily generalized.

The simplest wavefunction with non-trivial braiding statistics, that we can define involves four σ and two ψ primaries. This is given by the product

$$\Psi_{\mu;\boldsymbol{\eta}}(z_1, z_2) = \mathcal{J}^{(4,2)} \mathcal{F}^{(4,2)}_{\mu;\boldsymbol{\eta}}(z_1, z_2) \tag{5.51}$$

Since the Jastrow factor doesn't contribute to the braiding statistics, we can neglect it and consider

$$\Psi_{\mu;\boldsymbol{\eta}} \propto \sqrt{N_\mu}[X_{--++}\xi_{(12)(34)}Y_{\mu;--++} + X_{-+-+}\xi_{(13)(24)}Y_{\mu;-+-+} + X_{+--+}\xi_{(14)(23)}Y_{\mu;+--+}] \tag{5.52}$$

The different channels of $\Psi_{\mu;\boldsymbol{\eta}}$ and the normalized conformal blocks $\sqrt{N_\mu}Y_{\mu;\boldsymbol{n}}$, are grouped into the column vectors $\boldsymbol{\Psi}_{\boldsymbol{\eta}}$ and $\boldsymbol{Y}_{\boldsymbol{n}}$. Then, we write

$$\boldsymbol{\Psi}_{\boldsymbol{\eta}} \propto X_{--++}\xi_{(12)(34)}\boldsymbol{Y}_{--++} + X_{-+-+}\xi_{(13)(24)}\boldsymbol{Y}_{-+-+} + X_{+--+}\xi_{(14)(23)}\boldsymbol{Y}_{+--+} \tag{5.53}$$

where $\boldsymbol{Y}_{\boldsymbol{n}}$ is given by Eq. (5.29) and the wavefunction vector is defined by

$$\boldsymbol{\Psi}_{\boldsymbol{\eta}} = \begin{pmatrix} \Psi_{1;\boldsymbol{\eta}} \\ \Psi_{2;\boldsymbol{\eta}} \end{pmatrix} \tag{5.54}$$

Let us now consider the exchange $\eta_1 \leftrightarrow \eta_3$. This transforms $\xi_{(12)(34)}$ into $\xi_{(14)(23)}$ and vice versa while keeping $\xi_{(13)(24)}$ the same. On the other hand, the X and $\boldsymbol{Y}$ terms transform according to Eq. (5.28). Thus, the wavefunction in Eq. (5.54) transforms according to

$$\Psi_{\boldsymbol{\eta}} \to R^{(4)}_{13}\Psi_{\boldsymbol{\eta}} \tag{5.55}$$

The rest of the exchange matrices are evaluated in a similar fashion, following the results discussed in the previous section.

Next, we consider the wavefunction of six σ fields. Once again, we can ignore the Jastrow factor in order to obtain the braidings. The wavefunction is defined as

$$\begin{aligned}\Psi_{\boldsymbol{\eta}} \propto & X_{+++---}\xi_{(123)(456)}\boldsymbol{Y}_{+++---} + X_{++-+--}\xi_{(124)(356)}\boldsymbol{Y}_{++-+--} \\ & + X_{++--+-}\xi_{(125)(346)}\boldsymbol{Y}_{++--+-} + X_{++---+}\xi_{(126)(345)}\boldsymbol{Y}_{++---+} \\ & + X_{+-++--}\xi_{(134)(256)}\boldsymbol{Y}_{+-++--} + X_{+-+-+-}\xi_{(135)(246)}\boldsymbol{Y}_{+-+-+-} \\ & + X_{+-+--+}\xi_{(136)(245)}\boldsymbol{Y}_{+-+--+} + X_{+--++-}\xi_{(145)(236)}\boldsymbol{Y}_{+--++-} \\ & + X_{+--+-+}\xi_{(146)(235)}\boldsymbol{Y}_{+--+-+} + X_{+---++}\xi_{(156)(234)}\boldsymbol{Y}_{+---++}\end{aligned} \tag{5.56}$$

Under the exchange $\eta_1 \leftrightarrow \eta_3$ and by considering and generalizing the transformation rules of the ξ, X, and $\boldsymbol{Y}$ terms we previously discussed, we get

$$\Psi_{\boldsymbol{\eta}} \to R_{13}^{(6)}\Psi_{\boldsymbol{\eta}} \tag{5.57}$$

where the dimension of the $R_{13}^{(6)}$ matrix and it's elements depend on the conformal blocks $\boldsymbol{Y}$. For $k = 2$, there are two conformal blocks that are related to the critical Ising CFT and support Ising anyonic statistics. In this case, we end up with a 4×4 dimensional matrix R_{13}. For $k > 2$, there are five conformal blocks that are related to Fibonacci anyonic statistics. In this case, we end up with a 5×5 dimensional matrix R_{13}. One way to simplify the calculations and obtain these braiding matrices is by working in the $\eta_6 \to \eta_5$ limit, as explained in Chapter 4. The study of the rest of the exchange matrices is similar.

Clustering Properties

The wavefunction we constructed based on the coset $SU(2)_1^{\otimes k}/SU(2)_k$ has a few important similarities with the Moore-Read (based on the minimal model $\mathcal{M}(4,3)$) [44] and the Read-Rezayi wavefunction (based on the parafermionic theory $\mathbb{Z}_3$) [49]. Firstly, we observe that for $k = 2$, the coset is equal to the critical Ising theory; hence the wavefunction matches the MR state. It's easy to check that for larger k, the ground state (zero quasi-hole and quasi-particle

excitations) coset wavefunctions are identical to the MR ground states, defined by Eq. (1.4). However, we observe that they differ in terms of the excitations. For $k = 3$, we find that the excitations of the coset wavefunction exhibit Fibonacci braiding statistics. Fibonacci anyons have also been found to emerge in the RR state. However, the coset wavefunction we propose here differs from the RR with regard to its clustering properties.

To understand the clustering properties of the coset wavefunctions (for $k \geq 2$), we consider 2M ψ and zero σ fields, which gives the MR Pfaffian ground state. This vanishes when more than two ψ fields come together at a single point. Therefore, we cannot have a clustering of more than two ψ fields. This property remains true even if we include 2N σ fields in the wavefunction. On the other hand, the $\mathbb{Z}_k$ RR state allows the clustering of k particles.

These wavefunctions are generally eigenstates of complicated many-body Hamiltonians. By inspecting the clustering properties of our wavefunctions, we can get insights and study specific toy model Hamiltonians. Indeed, the coset wavefunction based on $SU(2)_1^{\otimes k}/SU(2)_k$ corresponds to a Hamiltonian with three-body interactions, similar to the MR wavefunction. On the other hand, the RR wavefunction corresponds to $k+1-$ body interactions.

Energy Gap

To better understand the gap, let us couple our system (coset CFT) to a spinless fermionic field c in the state

$$|\Psi_c\rangle = \mathcal{N} \langle e^{i\sqrt{\lambda}\int d^2z \psi(z) c^\dagger(z,\bar{z})} \rangle |0_c\rangle \tag{5.58}$$

where $|0_c\rangle$ is the vacuum state annihilated by all fermionic operators $c(z,\bar{z})$, $\lambda \in \mathbb{C}$, and $\mathcal{N}$ is a normalization constant. The expectation value is taken with respect to the coset CFT and involves the ψ field. We may similarly include the Jastrow factor.

We recover the correlators (5.34) of the ψ field by projecting onto the basis states $|z_1, \ldots, z_{2M}\rangle \equiv c_1^\dagger \cdots c_{2M}^\dagger |0_c\rangle$, where $c_j \equiv c(z_j, \bar{z}_j)$

$$\langle z_1, \ldots, z_{2M} | \Psi_c \rangle = \mathcal{N} \lambda^M \langle \psi_1 \cdots \psi_{2M} \rangle \tag{5.59}$$

The normalization constant is easily computed

$$\mathcal{N} = \| \, |\Psi_c\rangle \, \|^{-1} \ , \quad \| \, |\Psi_c\rangle \, \|^2 = \langle e^{-i|\lambda| \int d^2z \psi(z) \bar{\psi}(\bar{z})} \rangle \tag{5.60}$$

Moreover, the two-point function in the fermionic system is easily expressed in terms of the CFT correlator as follows

$$\langle \Psi_c | c_1 c_2 | \Psi_c \rangle = -\lambda \frac{\langle \psi_1 \psi_2 e^{-i|\lambda| \int d^2z \psi(z) \bar{\psi}(\bar{z})} \rangle}{\langle e^{-i|\lambda| \int d^2z \psi(z) \bar{\psi}(\bar{z})} \rangle} \tag{5.61}$$

showing that it is a two-point function in the CFT perturbed by the operator $i\psi\bar{\psi}$, which is the energy operator in the Ising CFT. Since this operator has conformal dimensions $(h, \bar{h}) = (\frac{1}{2}, \frac{1}{2})$, the coupling constant λ has the dimension of mass. Since $h < 1$, this is a relevant perturbation and drives the system to a phase in which the two-point function decays exponentially and not as a power law. This behavior, short-range correlations, can be seen explicitly in the following way. Indeed, by taking Fourier transforms, we obtain

$$\langle \Psi_c | c_k c_{-k} | \Psi_c \rangle = \frac{\lambda \bar{k}}{|k|^2 + |\lambda|^2} \tag{5.62}$$

where $c_k \equiv c(k, \bar{k})$, which is a propagator for a massive particle of mass $|\lambda|$. It follows that in position space, the propagator decays exponentially

$$\langle \Psi_c | c_1 c_2 | \Psi_c \rangle \sim e^{-|\lambda||z_2 - z_1|} \tag{5.63}$$

This asymptotic behavior is intimately related to the existence of a gap in the system. This can be seen explicitly. Indeed, the state $|\Psi_c\rangle$ is the ground state of the "trial" Hamiltonian

$$H_c = \int \frac{d^2k}{(2\pi)^2} \begin{pmatrix} c_k^\dagger & c_{-k} \end{pmatrix} \begin{pmatrix} \frac{|k|^2 - |\lambda|^2}{2} & \lambda \bar{k} \\ \bar{\lambda} k & -\frac{|k|^2 - |\lambda|^2}{2} \end{pmatrix} \begin{pmatrix} c_k \\ c_{-k}^\dagger \end{pmatrix} \tag{5.63}$$

Finally, by diagonalizing H_c, we obtain a finite energy gap, for $|\lambda|^2 > 0$.

Chapter 6

Non-Abelian Statistics from Rydberg Atoms

In this chapter, we provide numerical results (using DMRG) for the observation of non-Abelian statistics in lattices with Rydberg atoms, from the work [142].

6.1 Rydberg Atoms

Neutral atoms have become promising candidates for large-scale quantum computers, either by using optical lattices [143, 144, 145] or via Rydberg atoms [146, 147, 148]. Rydberg atoms are atoms whose electrons are excited to high energy values, with the principal quantum number $n \gg 1$. Experimentally, the neutral atoms can be trapped in two-dimensional arrays of optical tweezers, as described in [149]. Progress in developing programmable quantum simulators based on neutral Rydberg atoms can be found in [148, 150]. Results that demonstrate high-fidelity quantum gates can be found in [151, 152]. In addition, they have applications in quantum error correcting codes [153, 154] and neural networks [155].

A key component of the Rydberg atoms, which appears in these paradigms, is the Rydberg blockade mechanism [61]. Loosely speaking, atoms excited in the Rydberg have very large dipole moments, as the positive and negative charge separation is proportional to

the large principal quantum number n. Bringing two such excited atoms close together leads to strong repulsive dipole forces. According to the blockade mechanism, if a particular atom is found in an excited Rydberg state, then neighboring atoms are energetically favorable to be in the ground state, as illustrated in Figure 6.1.

In more recent years, Rydberg atoms have also been suggested as potential platforms for realizing Kitaev's toric code [59] and, more generally, topological phases of matter [60]. In particular, the authors probed a Quantum Spin Liquid (QSL) phase by placing Rubidium-87 atoms on a Ruby (or Kagome) lattice and fine-tuning two free parameters: the Rabi frequency Ω of oscillation between the ground and Rydberg state, and the laser detuning Δ. Particularly, they observed $\mathbb{Z}_2$ topological order with emerging Abelian anyons e and m. Additionally, the authors found that by properly varying the detuning on the boundary of the lattice, the boundary changes from an e-condensate to an m-condensate and vice versa.

In this chapter, we follow the work in Refs. [59, 60], and introduce lattice punctures with mixed boundaries (where both e and m anyons condensate). By doing so, it's theoretically predicted to acquire non-Abelian statistics [67, 68]. We perform numerical simulations using the DMRG technique to verify the stabilization of a QSL phase with one, two, and four mixed boundary punctures.

6.2 Model

Hamiltonian

We consider ^{87}Rb neutral atoms placed on the sites of a Ruby lattice, with lattice spacing a, governed by the Hamiltonian

$$H = \frac{\Omega(t)}{2} \sum_j (e^{-i\vartheta(t)} b_j + e^{i\vartheta(t)} b_j^\dagger) - \sum_j \Delta_j(t) n_j + \frac{1}{2} \sum_{j,k} V(r_{jk}) n_j n_k \tag{6.1}$$

where each site j contains at most one atom. Equivalently, we can consider the atoms located on the links of a Kagome lattice, this duality is shown in Figure 6.2.

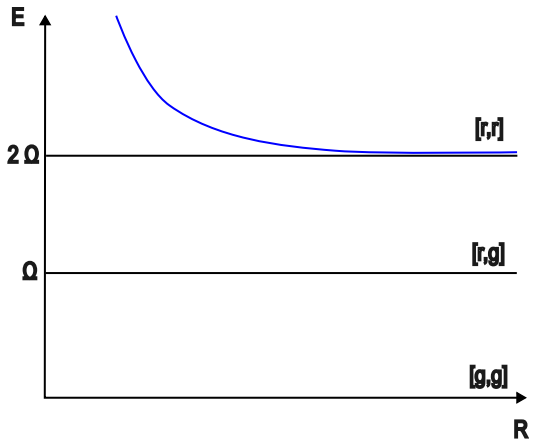

Figure 6.1: The energy graph of the Rydberg blockade mechanism for two interacting Rydberg atoms. The zero energy ground state requires both atoms to be in the ground state $|gg\rangle$. If either one atom is in the excited Rydberg ($|gr\rangle$ or $|rg\rangle$), then the system has energy Ω. On the other hand, the double excitation into $|rr\rangle$ has an energy that follows the "blue" line, with energy is much larger than 2Ω for distance less than the blockade distance R_b.

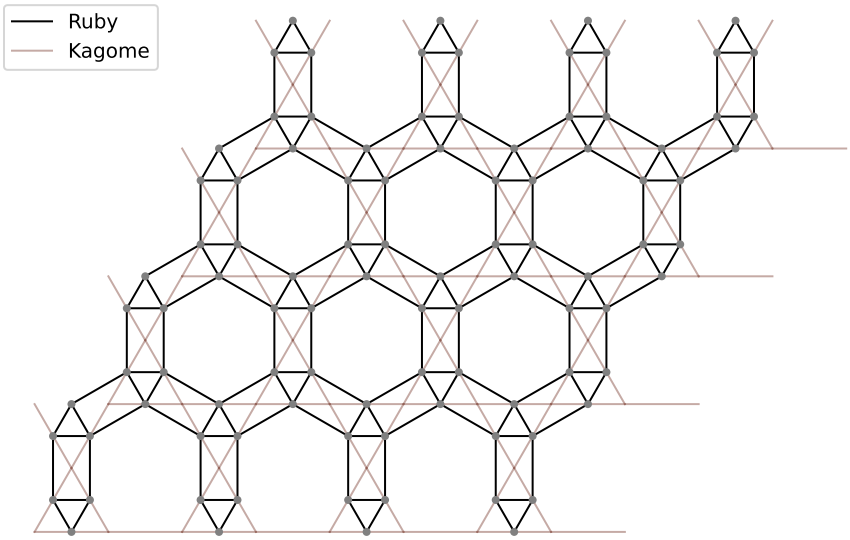

Figure 6.2: The equivalence between a Ruby and a Kagome lattice. For the former, the atoms are located on the sites of the lattice, whereas for the latter, they are on the links.

Each atom is effectively in a two-level quantum system and can be either in the ground state $|g\rangle_j$ or the Rydberg state $|r\rangle_j$. The two states are separated by a time-dependent Rabi frequency term $\Omega(t)$. Excitations from the ground state to the Rydberg state are driven by a laser with detuning $\Delta_j(t)$, which can be individually adjusted for each atom. The time-dependent parameter $\vartheta(t)$ that appears in Eq. (6.1) is the laser phase. The operators b_j and $b_j^\dagger$, which are introduced in the Rydberg Hamiltonian, are bosonic lowering and raising operators for the two-level quantum system $\{|g\rangle_j, |r\rangle_j\}$ at the site j and are defined as

$$b_j = |g\rangle_j \langle r| \quad , \quad b_j^\dagger = |r\rangle_j \langle g| \tag{6.2}$$

The "particle" number operator is defined as $n_j = b_j^\dagger b_j = |r\rangle_j \langle r|$ and determines whether the atom on the specific site is excited or not by projecting onto the Rydberg state. Furthermore, for every site j, we can define the local Pauli operators

$$X_j = b_j + b_j^\dagger = |g\rangle_j \langle r| + |r\rangle_j \langle g| \tag{6.3}$$

$$Y_j = i(b_j - b_j^\dagger) = i(|g\rangle_j \langle r| - |r\rangle_j \langle g|) \tag{6.4}$$

$$Z_j = b_j b_j^\dagger - b_j^\dagger b_j = |g\rangle_j \langle g| - |r\rangle_j \langle r| \tag{6.5}$$

The local Pauli Z_j operator can be written in terms of the "particle" number operator n_j as $Z_j = \mathbb{I} - 2n_j$. Finally, there is a strong repulsion due to the van der Waals potential $V(r_{ij}) = \Omega(R_b/r_{ij})^6$, where R_b is the Rydberg blockade radius. Hence, for every atom in the Rydberg state, there exists a barrier that blocks atoms inside a radius R_b from getting excited. In the subsequent numerical simulations, we will fine-tune the lattice spacing a and Rabi frequency Ω so that for each excited atom, its six closest neighbors are within the blockade radius.

String Operators

In order to study the different phases of matter that may emerge in this system and probe a potential topological phase, we have to introduce the non-local topological string operators

$$\boldsymbol{Z}_S = \prod_{j \in S} Z_j \quad , \quad \boldsymbol{X}_{S'} = \prod_{j \in S'} X_j \tag{6.6}$$

where the S string goes perpendicular to the links of the Kagome lattice, whereas the S' string is defined parallel to links. The non-local nature of the string operators makes them perfect tools for diagnosing topological order. These operators were introduced in [18] for an exactly solvable $\mathbb{Z}_2$ lattice gauge theory. In the context of gauge theories, the $\boldsymbol{X}_{S'}$ and $\boldsymbol{Z}_S$ string operators are the Wilson and 't Hooft lines, respectively. In terms of the Abelian anyons, an open $\boldsymbol{Z}$ string creates two m anyons at its endpoints, whereas an open $\boldsymbol{X}$ string operator creates two e anyons.

As observed in [59, 60], this Rydberg atom model has three distinct phases: a trivial phase for small Δ/Ω, a valence bond solid (VBS) phase for large Δ/Ω, and a quantum spin liquid (QSL) phase for intermediate values of Δ/Ω. We identify the phase of our system by measuring closed and open loops for both $\boldsymbol{X}$ and $\boldsymbol{Z}$ topological string operators, as shown in Figure 6.3. The expected values of the string operators that characterize each phase are summarized in Table 6.1.

Encoding Logical States

The boundaries of the Ruby lattice can either be periodic or open. The former choice results in the toric code [18], which has four-fold ground state degeneracy. The latter gives the planar or surface code [55, 56], which is experimentally more feasible. In the planar code, the boundaries can either be rough or smooth. The type of boundary is associated with the type of anyon condensation. Specifically, we will use the following notation: smooth boundaries have e-condenstation, and rough boundaries have m-condensation.

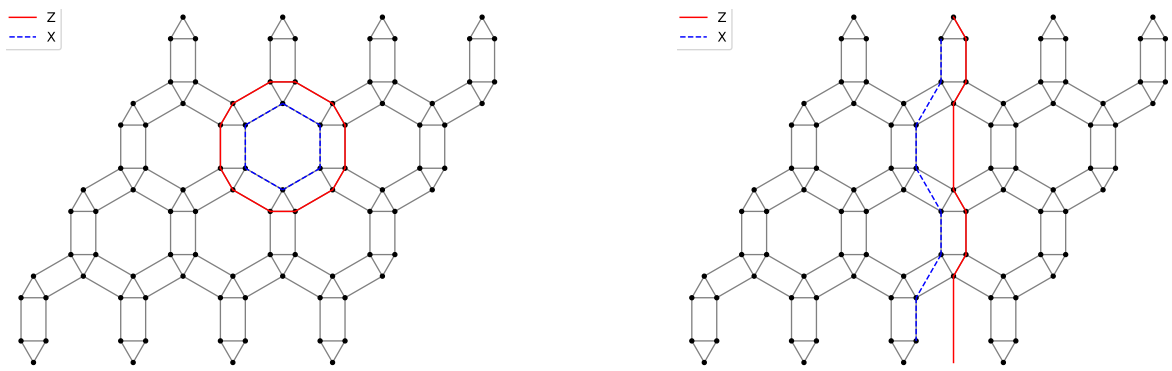

Figure 6.3: Left: A closed "hexagonal" Z and X string operator in a lattice with open boundary conditions. Right: A closed "top-bottom" Z and X string operator in a lattice with periodic boundary conditions on the top and bottom regions.

Table 6.1: Expectation values of Open and Closed string operators in the three different phases of matter.

Phase	Open $\boldsymbol{Z}$	Open $\boldsymbol{X}$	Closed $\boldsymbol{Z}$	Closed $\boldsymbol{X}$
Trivial	0	1	0	1
SQL	0	0	1	1
VBS	1	0	1	0

The planar code has Hilbert space dimensionality that depends on the boundaries and the genus of the plane. For a genus-0 plane, we need alternating boundaries in order to create a two-dimensional Hilbert space and encode a logical qubit. For a genus-1 plane, we can encode a qubit using uniform boundaries, as shown in Figure 6.4. Uniform rough boundaries, which correspond to an m-condensate, allow us to define two logical ground states: $|\mathbb{I}\rangle$ with no anyons (trivial state) and $|m\rangle$ containing m anyons in the puncture. Similarly, smooth boundaries, which correspond to an e-condensate, give two ground states: the trivial state $|\mathbb{I}\rangle$ and one that contains e anyons in the puncture, denoted by $|e\rangle$. To construct a four-dimensional Hilbert space spanned by states $(|\mathbb{I}\rangle, |e\rangle, |m\rangle, |f\rangle)$, where $|f\rangle = |e\rangle \otimes |m\rangle$, we require a puncture and mixed boundaries in both lattice and puncture.

An alternative construction of a four-dimensional space can be achieved by simply considering two mixed-boundary punctures while keeping a uniform lattice boundary. The four-degenerate ground states can be probed by measuring the four non-local string operators $\boldsymbol{Z}_C$, $\boldsymbol{X}_{C'}$, $\boldsymbol{Z}_S$, and $\boldsymbol{X}_{S'}$, as illustrated in Figure 6.5. The expected values of these operators for the four ground states are given in Table 6.2.

Before we discuss the mixed-boundary punctures further, it's instructive to consider the case of two punctures with uniform boundaries. Let's consider, for instance, a system with e-condensed boundaries. We can define the two logical operators $\boldsymbol{Z}_C$ and $\boldsymbol{X}_{S'}$, which we measure. The presence of an e anyon is verified by measuring $\langle \boldsymbol{Z}_C \rangle = -1$ otherwise we find $\langle \boldsymbol{Z}_C \rangle = 1$. The second logical operator, $\boldsymbol{X}_{S'}$, describes the overlap of the ground state with the state that results from adding an e anyon to each puncture. Similarly, we can work with m-condensed boundaries. We find that the presence of an m anyon within a puncture is verified by measuring $\langle \boldsymbol{X}_{C'} \rangle = -1$ or $\langle \boldsymbol{X}_{C'} \rangle = 1$ otherwise.

Following Ref. [68], an important ingredient for the observation of the Ising statistics is the creation of the superposition states via the two mixed boundary punctures, which we name p_1 and p_2

$$|\pm\rangle_{12} = \frac{|e\rangle_{12} \pm |m\rangle_{12}}{\sqrt{2}} \tag{6.7}$$

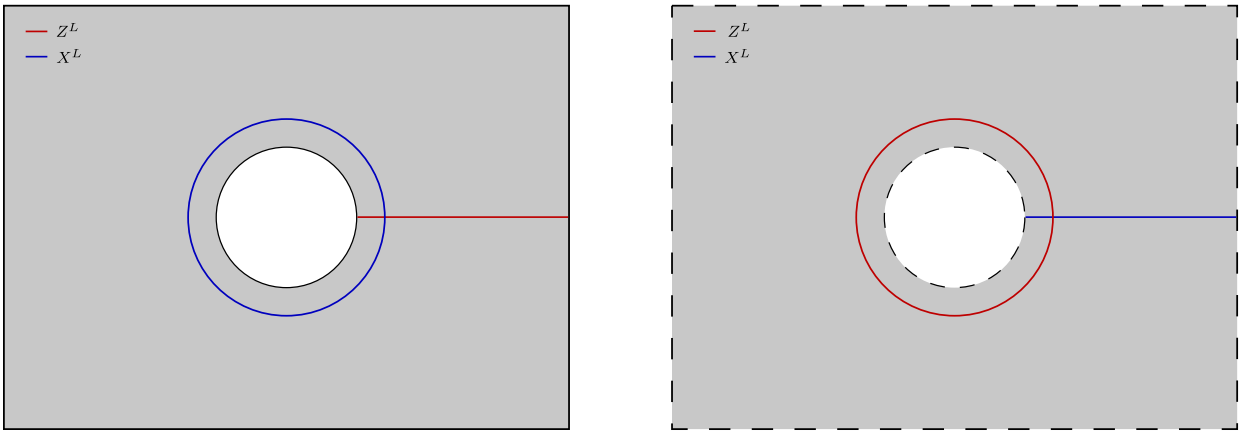

Figure 6.4: Left: A logical qubit is encoded in a planar code with rough boundaries and a puncture. Right: A logical qubit is encoded in a planar code with smooth boundaries and a puncture.

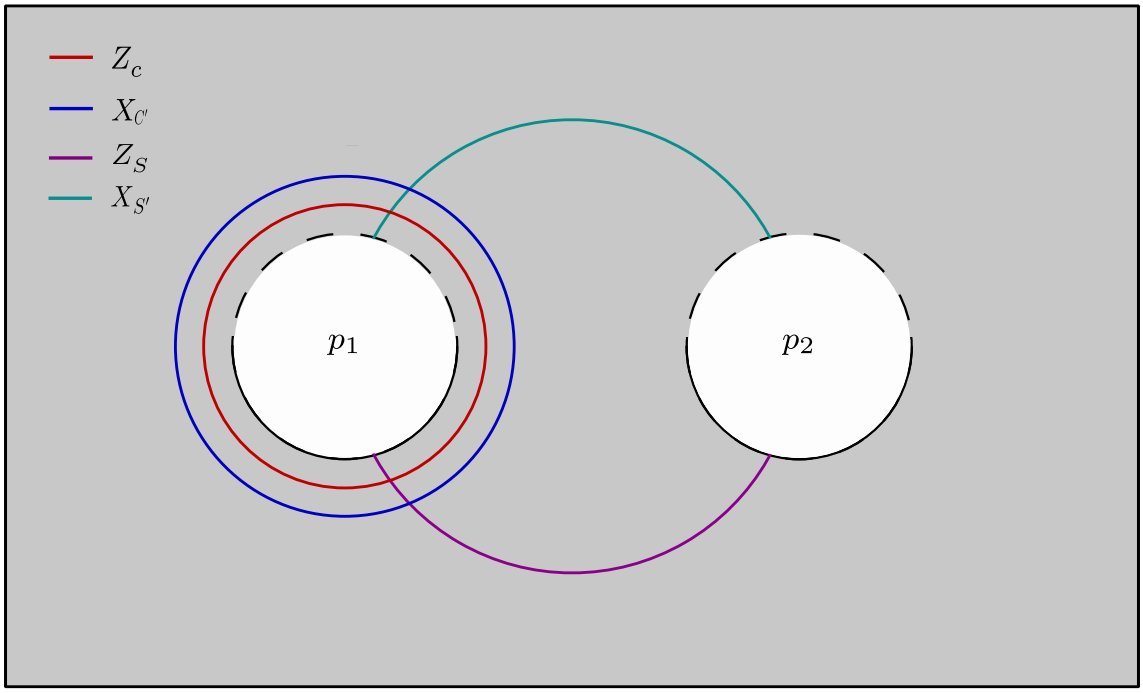

Figure 6.5: Two mixed boundary punctures on a non-periodic lattice. The closed logical string operators $\boldsymbol{Z}_C$ and $\boldsymbol{X}_{C'}$ with the loops C and C' are around puncture p_1 are introduced to measure the e and m anyons, respectively. Similarly, we define the logical $\boldsymbol{Z}_S$ and $\boldsymbol{X}_{S'}$ operators, where the S and S' are paths connecting the rough (m-condensate) and smooth (e-condensate) boundaries of the two punctures, respectivelly.

Table 6.2: Expectation values of string operators defined in Figure 6.5 for the four degenerate ground states $|\mathbb{I}\rangle$, $|e\rangle$, $|m\rangle$ and $|f\rangle$. In addition, we present the expectation values for the superposition states $|\pm\rangle$, introduced in Eq. (6.7).

State	$\boldsymbol{Z}_C$	$\boldsymbol{X}_{C'}$	$\boldsymbol{Z}_S$	$\boldsymbol{X}_{S'}$
$\|\mathbb{I}\rangle$	1	1	0	0
$\|e\rangle$	-1	1	0	0
$\|m\rangle$	1	-1	0	0
$\|f\rangle$	-1	-1	0	0
$\|+\rangle$	0	0	1	1
$\|-\rangle$	0	0	- 1	-1

For the numerical simulations to be discussed in the next section, the lattice will be placed in an infinite cylinder along the x-axis. Due to the periodicity across the boundaries in the y-direction, we can define the logical operators $\boldsymbol{Z}_C$ and $\boldsymbol{X}_{C'}$ in the following way. Instead of measuring the string that encloses the entire puncture, we measure two strings around the circumference of the cylinder: one before and one after the puncture. Thus, we can define the logical $\boldsymbol{Z}$ around the first puncture p_1 by taking the product of $\boldsymbol{Z}_{C_1}$ and $\boldsymbol{Z}_{C_2}$ or around the second puncture p_2 with the product of $\boldsymbol{Z}_{C_2}$ $\boldsymbol{Z}_{C_3}$. The same procedure can be repeated for $\boldsymbol{X}_{C'}$. The closed loops C_1, C_2, C_3 in the y-direction around the cylinder can be found in Figure 6.6.

Punctures

We introduce the punctures by removing unit cells of atoms on a Ruby lattice. In the QSL regime, a m-consdasate emerges in the boundaries of the punctures. This can be detected by measuring a finite $\langle \boldsymbol{Z} \rangle$ and a vanishing $\langle \boldsymbol{X} \rangle$ "open" string operator that starts and ends at the boundary. An e-condensation can be achieved by decreasing the detuning to $\Delta' < \Delta$. On the other hand, this is characterized by the vanishing $\langle \boldsymbol{Z} \rangle$ and finite $\langle \boldsymbol{X} \rangle$ operators. Here, we are interested in mixed-boundary punctures. These were created by only changing the detuning of the boundary sites on half of the boundary. Specifically, the detuning was reduced to $\Delta' = 0.48\Delta$ on highlighted sites shown in Figure 6.7.

6.3 Numerical Methods

We find the ground state $|\psi_0\rangle$ of the Rydberg Hamiltonian, defined in Eq. (6.1), by using the iDMRG algorithm of the TenPy library [156]. Since we are using the infinite-size Density Matrix Renormalization Group (iDMRG) method, we effectively place the Ruby lattice in an infinite cylinder. This cylinder will be periodic in the vertical direction and will have an infinite length on the horizontal axis.

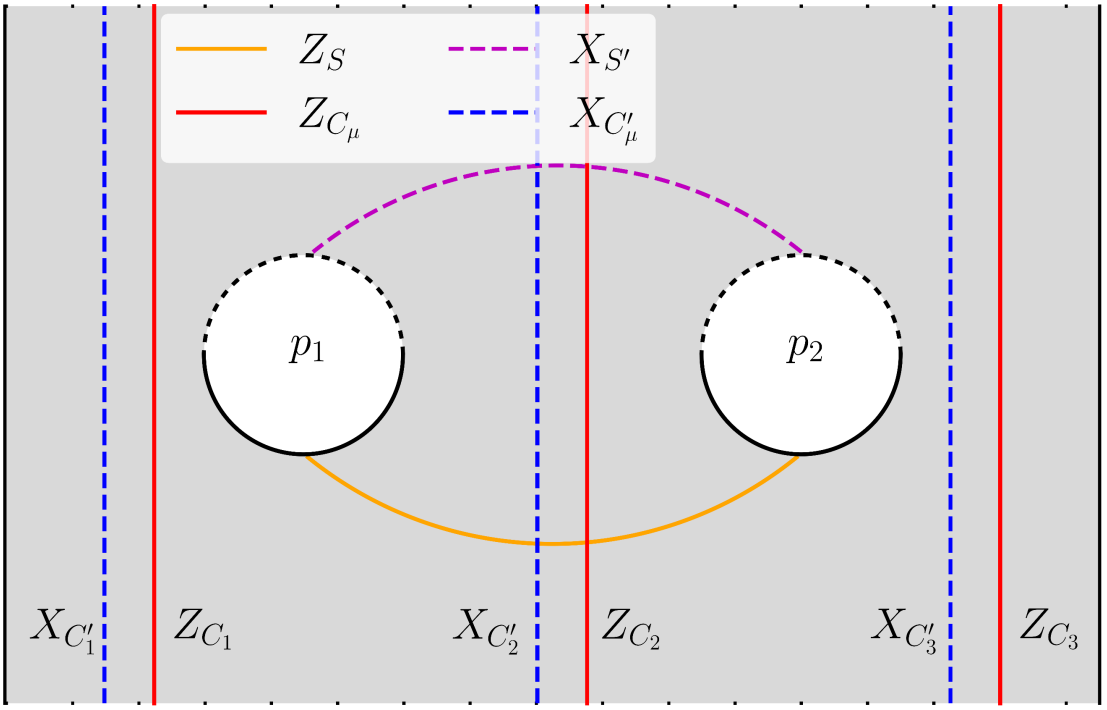

Figure 6.6: Two mixed boundary punctures on a lattice with periodic boundary conditions on the top and bottom.

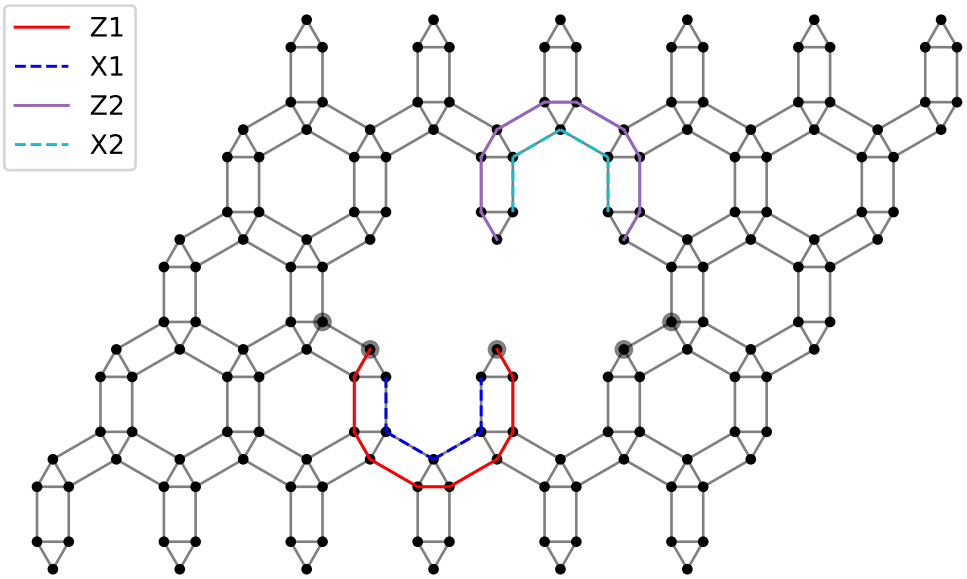

Figure 6.7: Mixed-boundary puncture on the Ruby lattice. Sites highlighted in gray have detuning $\Delta' = 0.48\Delta$. The boundary-boundary string operators are used to identify the type of condensation.

For the iDMRG calculations, we fix the parameters of our system, according to Ref. [60]. Specifically, we choose: $\Omega = 2\pi \times 1.4 \times 10^6$ Hz, $\vartheta = 0$, $R_b = 2.4a$ and $R_{\text{trunc}} = \sqrt{7}a$, where a is the lattice spacing and R_{trunc} is the truncation distance for the numerical calculations. The only free parameter will be the detuning Δ, which we will vary within the range $(1, 6)$ in order to identify the different phases of matter.

The expectation value of a $\boldsymbol{Z}$ string operator for a given ground state can be deduced, using TenPy packages, as each local Z_j operator of the non-local $\boldsymbol{Z}$ string can be written as $\mathbb{I} - 2n_j$. On the other hand, the evaluation of a $\boldsymbol{X}$ string operator is a bit more tedious and is given by the following procedure. Given the ground state $|\psi_0\rangle$, we find the time evolved state $|\psi_\tau\rangle = U_\tau |\psi_0\rangle$, where $\tau = \frac{4\pi}{3\sqrt{3}\Omega}$, and the time evolution operator is given by

$$U_\tau = e^{-i\tau H'} \tag{6.8}$$

and the prime Hamiltonian is derived from Eq. (6.1) by setting $\Delta = 0$ and $\vartheta = -\frac{i\pi}{2}$ as follows

$$H = i\frac{\Omega}{2}\sum_j (b_j - b_j^\dagger) + \frac{1}{2}\sum_{j,k} V(r_{jk}) n_j n_k \tag{6.9}$$

In this way, measuring the $\boldsymbol{X}$ string for the state $|\psi_0\rangle$ is equivalent to measuring the $\boldsymbol{Z}$ for the time-evolved state $|\psi_\tau\rangle$. This was realized in [59], by demonstrating that

$$e^{i\tau H'} \boldsymbol{Z} e^{-i\tau H'} = \boldsymbol{X} \tag{6.10}$$

This duality is explicitly shown in Figure 6.8. Finally, for the time evolution of the ground state, we changed the van der Waals interaction strength by reducing the blockade radius $R_b = 1.53a$ and the truncation distance $R_{\text{trunc}} = a$. By doing so, each atom would interact through H' only with its two closest neighbors. Thus, the time-evolution Hamiltonian is "local" and only contains interactions within each Kagome triangle.

6.4 Results

Our numerical calculations aim to verify the following three properties

1. Our system has a QSL phase even after we introduce a puncture
2. We get mixed boundaries with both e and m anyonic condensations
3. The states with anyons on the punctures, defined as $|e\rangle$ and $|m\rangle$, can be constructed

Upon evaluating the expectation value of the string operators $\boldsymbol{Z}$ and $\boldsymbol{X}$ for closed loops, we find a QSL phase emerging for detuning values between $\Delta = 3.25$ and $\Delta = 3.75$. As explained in the previous section, a QSL phase is stabilized when these string operators are both non-vanishing. This result is illustrated in Figure 6.9.

Next, we need to verify that the puncture has mixed boundaries. To do this, we have to measure $\boldsymbol{Z}$ and $\boldsymbol{X}$ string operators that begin and end on the same "part" of the boundary, as shown in Figure 6.6. We find that the component of the boundary with detuning $\Delta' = 0.4\Delta$ has vanishing $\boldsymbol{Z}$ and close to one $\boldsymbol{X}$ string, as expected for a e-condensate. Similarly, we find that the rest of the boundary, where the detuning is Δ, has $\boldsymbol{Z}$ value close to one and $\boldsymbol{X}$ close to zero, suggesting a m-condensate. The numerical results are summarized in Table 6.3.

Next, by executing the iDMRG multiple times with various initializations, we were able to find the $|e\rangle$ and $|m\rangle$ ground states that are described in Table 6.2. The $|e\rangle$ state is characterized by alternating positive and negative $\boldsymbol{Z}$ (of magnitude close to one) string operators across the puncture, while the $\boldsymbol{X}$ has a constant sign. The $|m\rangle$ is characterized by alternating positive and negative $\boldsymbol{X}$ (of magnitude close to one), while the $\boldsymbol{Z}$ has a constant sign. These numerical results are shown in Table 6.4. Finding the other two ground states, the $|\mathbb{I}\rangle$ and $|f\rangle$, that appear in the toric code is not relevant.

Finally, we normalize the expectation values of our non-local operators by calculating the joint expectation value of two strings. For example, the normalized expectation value of the string operator $\boldsymbol{Z}_S$ is obtained by averaging $\langle \boldsymbol{Z}_{S_i} \rangle / \sqrt{\langle \boldsymbol{Z}_{S_i} \boldsymbol{Z}_{S_j} \rangle}$ over the strings i and j.

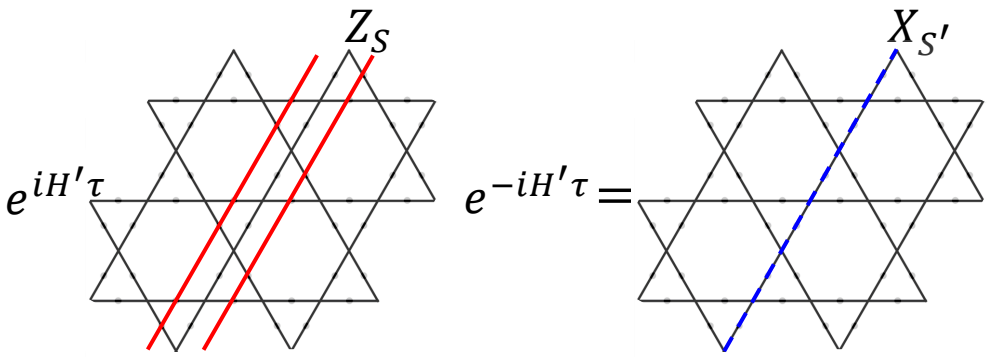

Figure 6.8: Example of the duality between the $\boldsymbol{Z}$ and $\boldsymbol{X}$ operators defined along the S and S' paths, as explained in Eq. (6.10).

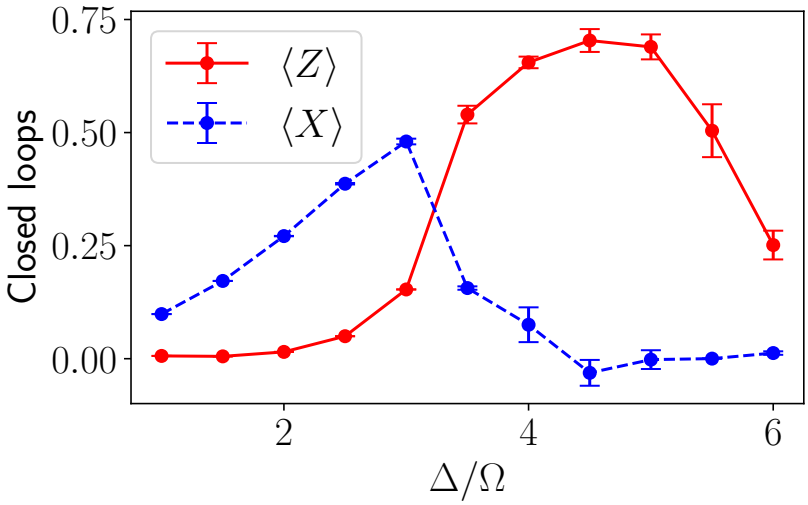

Figure 6.9: Expectation values of closed $\boldsymbol{Z}$ and $\boldsymbol{X}$ strings as a function of Δ/Ω, obtained using iDMRG averaged over all single-hexagon loops in a 6×4 infinite cylinder system.

Table 6.3: Numerical results for normalized expectation values for the string operators shown in Figure 6.7.

Operator	Expectation Value
$\boldsymbol{Z}_1$	0.0259 ± 0.0129
$\boldsymbol{X}_1$	1.086 ± 0.0612
$\boldsymbol{Z}_2$	0.974 ± 0.196
$\boldsymbol{X}_2$	0.300 ± 0.0496

Table 6.4: Numerical results for normalized expectation values for the string operators shown in Figure 6.6. Note that the values for $\langle \boldsymbol{Z}_S \rangle$ should be 0 but have high standard error values, such that they are consistent with 0 with 2 standard errors. The high standard error can be attributed to the small bond dimension in iDMRG simulations.

Operator	$\|e\rangle$	$\|m\rangle$
$\boldsymbol{Z}_{C_1}$	1.007 ± 0.0487	-1.154 ± 0.0990
$\boldsymbol{Z}_{C_2}$	-1.0266 ± 0.0523	-0.931 ± 0.000849
$\boldsymbol{Z}_{C_3}$	1.015 ± 0.0543	-0.999 ± 0.0633
$\boldsymbol{X}_{C_1'}$	0.826 ± 0.136	1.261 ± 0.0313
$\boldsymbol{X}_{C_2'}$	1.111 ± 0.0994	-0.811 ± 0.312
$\boldsymbol{X}_{C_3'}$	1.072 ± 0.0224	1.097 ± 0.0535
$\boldsymbol{Z}_S$	-0.309 ± 0.301	-0.495 ± 0.329
$\boldsymbol{X}_{S'}$	-0.000183 ± 0.000113	-0.0132 ± 0.00648

6.5 Quantum Computation using Rydberg Atoms

In order to realize non-Abelian anyons, we need to consider a system with four mixed-boundary punctures, p_1, p_2, p_3, and p_4. The punctures p_1 and p_2 can be in any of the following states: $|\mathbb{I}\rangle_{12}$, $|e\rangle_{12}$, $|m\rangle_{12}$, $|f\rangle_{12} = |e \otimes m\rangle_{12}$. It's pedagogical to review the physical meaning of these states. The first state in which no anyons can be found in the boundary of each puncture. The second and third corresponds to the state with an e and m anyon at each boundary boundary[†], respectively. Finally, the remaining state has both types of anyons in each boundary. Similar definitions can be made for p_3 and p_4 punctures. This is critical in order to construct the superposition states $|\pm\rangle_{12}$ and $|\pm\rangle_{34}$, defined in Eq. (6.7).

In the system with four punctures, we will focus on a two-dimensional subspace of the entire Hilbert space, spanned by the states $|+\rangle_{12}|+\rangle_{34}$ and $|-\rangle_{12}|-\rangle_{34}$. These superposition states can also be written as

$$|\pm\rangle_{12}|\pm\rangle_{34} = \frac{1}{\sqrt{2}}\left(|\mathbb{I}\rangle_{1234} \pm |f\rangle_{1234}\right) \tag{6.11}$$

where the four-puncture logical states corresponding to $\mathbb{I}$ and f are given by

$$|\mathbb{I}\rangle_{1234} = \frac{1}{\sqrt{2}}\left(|e\rangle_{12}|e\rangle_{34} + |m\rangle_{12}|m\rangle_{34}\right) \tag{6.12}$$

$$|f\rangle_{1234} = \frac{1}{\sqrt{2}}\left(|e\rangle_{12}|m\rangle_{34} + |m\rangle_{12}|e\rangle_{34}\right) \tag{6.13}$$

It follows that the transformation matrix for the two basis sets $\{|+\rangle_{12}|+\rangle_{34}, |-\rangle_{12}|-\rangle_{34}\}$ and $\{|\mathbb{I}\rangle_{1234}, |f\rangle_{1234}\}$ is the fusion matrix of the Ising anyon mode

$$\mathrm{F} = \frac{1}{\sqrt{2}}\begin{pmatrix} 1 & 1 \\ 1 & -1 \end{pmatrix} \tag{6.14}$$

[†]An alternative interpretation is the following: if the system is given by the state $|e\rangle$, then an e anyon can be found in the boundary of one puncture. This anyon will travel to the second puncture and annihilate into the condensation.

These states, which are relevant for quantum computation, can be constructed by applying the string operators $\boldsymbol{Z}_S$ and $\boldsymbol{X}_S$ via additional ancilla atoms[†], introduced in Ref. [157]. These ancillary atoms have to be different than Rubidium so that they can be moved around by a laser without affecting the Ruby lattice atoms. For example, we can choose ^{23}Na, but this choice is not unique. Using the ancillary atom as a control qubit and the Rydberg atom at site j as the target, we can define the controlled-Z gate

$$CZ_j^a = |0\rangle_a \langle 0| \otimes \mathbb{I} + |1\rangle_a \langle 1| \otimes Z_j \tag{6.15}$$

where the physical implementation of the CZ_i^a gate have studied in [158, 159, 160, 161]. The Eq. (6.15) gives Z_j whenever the ancilla is projected into the state $|1\rangle_a$. We can repeat this method by moving the ancilla along the string S in order to obtain

$$C\boldsymbol{Z}_S^a = \prod_{j\in S} CZ_j^a = |0\rangle_a \langle 0| \otimes \mathbb{I} + |1\rangle_a \langle 1| \otimes \boldsymbol{Z}_S \tag{6.16}$$

The $\boldsymbol{X}_{S'}$ operator can be obtained via the Eq. (6.10), upon finding the S string conjugate to S' as shown in Figure 6.8, as follows

$$C\boldsymbol{X}_{S'}^a = e^{i\tau H'} \cdot C\boldsymbol{Z}_S^a \cdot e^{-i\tau H'} \tag{6.17}$$

By defining the ancilla paths S and S', as explained in Figure 6.6, this method enables us to obtain the states $|e\rangle_{12}$ and $|m\rangle_{12}$, given the initial state $|\mathbb{I}\rangle_{12}$. Furthermore, we can create the superposition states in Eq. (6.7) by using two ancilla qubits. The first ancilla implements the $C\boldsymbol{Z}_{S_1}^{a_1}$ string between the m-condensed boundaries, whereas the second ancilla gives $C\boldsymbol{X}_{S_1'}^{a_2}$ string between the e-condensed boundaries. The product of these two controlled

[†]The ancilla atoms are a two-level quantum system, hence a qubit.

gates gives

$$C\boldsymbol{Z}_S^{a_1} C\boldsymbol{X}_{S'}^{a_2} = |00\rangle_{a_1a_2}\langle 00|\otimes\mathbb{I} + |10\rangle_{a_1a_2}\langle 10|\otimes\boldsymbol{Z}_S + |01\rangle_{a_1a_2}\langle 01|\otimes\boldsymbol{X}_{S'} + |11\rangle_{a_1a_2}\langle 11|\otimes\boldsymbol{Z}_S\boldsymbol{X}_{S'} \tag{6.18}$$

which creates a superposition of the $\boldsymbol{X}$ and $\boldsymbol{Z}$ strings, upon projecting the ancilla states onto $\frac{1}{\sqrt{2}}(|01\rangle \pm |10\rangle)$. It is instructive to review the preparation of the superposition state by an explicit example. Consider the two mixed-boundary punctures system prepared in trivial ground state $|\mathbb{I}\rangle$, coupled with two ancilla qubits initialized in the state $|\psi^{(2)}\rangle_{a_1a_2}$. Then, by applying the $\boldsymbol{X}$ and $\boldsymbol{Z}$ strings we get

$$|\Phi^{(2)}\rangle = C\boldsymbol{X}_{S_1}^{a_1} \cdot C\boldsymbol{Z}_{S_2}^{a_2} |\psi^{(2)}\rangle_{a_1a_2} |\mathbb{I}\rangle_{12} \tag{6.19}$$

where $|\psi^{(2)}\rangle_{a_1a_2}$ is an arbitrary state of the two ancillary qubits. It is evident from Eq. (6.18) that $|\Phi^{(2)}\rangle$ is, in general, a superposition of all four ancilla states $\{|00\rangle, |10\rangle, |01\rangle, |11\rangle\}$. To retrieve the $|\pm\rangle_{12}$ states, we perform measurements on the ancilla qubits that project onto the Bell states

$$|\Psi^{\pm}\rangle = \frac{1}{\sqrt{2}}(|01\rangle \pm |10\rangle) \tag{6.20}$$

then the state in Eq. (6.19) becomes

$$|\Phi^{(2)}\rangle = \sum_{\sigma=\pm} c_\sigma |\Psi^\sigma\rangle_{a_1a_2} |\sigma\rangle_{12} \tag{6.21}$$

where the coefficients $c_\pm$ depend on the choice of the initial state $|\psi^{(2)}\rangle$ of the ancilla qubits.

Next, we consider a system with four mixed-boundary punctures p_1, p_2, p_3 and p_4, prepared in the topologically trivial ground state $|\mathbb{I}\rangle$. In order to create a state in the two-dimensional Hilbert subspace spanned by the basis $\{|+\rangle_{12}|+\rangle_{34}, |-\rangle_{12}|-\rangle_{34}\}$, we need to introduce four ancilla qubits initialized into $|\psi^{(4)}\rangle_{a_1a_2a_3a_4}$. Following the previous procedure, we can apply the string operators $\boldsymbol{X}_{S'_{12}}$, $\boldsymbol{Z}_{S_{12}}$, $\boldsymbol{X}_{S'_{34}}$, $\boldsymbol{Z}_{S_{34}}$, where the strings S_{12} (S_{34}) connect

the punctures p_1, p_2 (p_3, p_4). We obtain the state

$$|\Phi^{(4)}\rangle = C\boldsymbol{X}_{S_1}^{a_1} \cdot C\boldsymbol{Z}_{S_2}^{a_2} \cdot C\boldsymbol{X}_{S_3}^{a_3} \cdot C\boldsymbol{Z}_{S_4}^{a_4} |\psi^{(4)}\rangle_{a_1a_2a_3a_4} |\mathbb{I}\rangle_{1234} \tag{6.22}$$

where $|\psi^{(4)}\rangle$ is an arbitrary state. We select the superposition states $|\pm\rangle_{12} |\pm\rangle_{34}$, by performing measurements on the ancilla qubits that project onto a state in the span of $\{|\Psi^+\rangle_{a_1a_2} |\Psi^+\rangle_{a_3a_4}, |\Psi^-\rangle_{a_1a_2} |\Psi^-\rangle_{a_3a_4}\}$. Thus, getting

$$|\Phi^{(4)}\rangle = \sum_{\sigma=\pm} c_\sigma |\Psi^\sigma\rangle_{a_1a_2} |\Psi^\sigma\rangle_{a_3a_4} |\sigma\rangle_{12} |\sigma\rangle_{34} \tag{6.23}$$

Similarly, we can obtain the $|\mathbb{I}\rangle_{1234}$ and $|f\rangle_{1234}$ states, introduced in Eqs. (6.12) and (6.13), by projecting into the space spanned by the states $|\Psi^+\rangle_{a_1a_2} |\Psi^+\rangle_{a_3a_4} \pm |\Psi^-\rangle_{a_1a_2} |\Psi^-\rangle_{a_3a_4}$.

As highlighted in Chapter 1, the process of quantum computation requires the following: state preparation, application of unitary gates, and then measurement. In this quantum computing scheme, we initialize the quantum state by performing measurements on the ancillary qubits; thus causing the Eq. (6.23) to collapse[†] into $|\sigma\rangle_{12} |\sigma\rangle_{34}$, with $\sigma = \pm$. However, by measuring the ancilla, they decouple and can no longer be used to apply quantum gates. To remedy this, instead of fixing the initial state by an ancilla measurement, we first apply the quantum gates and then measure all ancilla qubits. This can be understood in the following way. Let's assume that we initialize the system into the state $|\sigma\rangle_{12} |\sigma\rangle_{34}$ and then apply the unitary gate U. The final state is a superposition

$$\sum_{\sigma'=\pm} U^{\sigma\sigma'} |\sigma'\rangle_{12} |\sigma'\rangle_{34} \tag{6.24}$$

where $U^{\sigma\sigma'}$ is a 2×2 matrix. It turns out that we can implement U (acting on the Rydberg system with four-punctures) by acting on the ancilla qubits with a dual unitary $\widetilde{U}$ such that

$$\widetilde{U} |\Psi^\sigma\rangle_{a_1a_2} |\Psi^\sigma\rangle_{a_3a_4} = \sum_{\sigma'=\pm} \widetilde{U}^{\sigma\sigma'} |\Psi^{\sigma'}\rangle_{a_1a_2} |\Psi^{\sigma'}\rangle_{a_3a_4} \tag{6.25}$$

[†]The states that collapse into the other $|\Phi^\pm\rangle$ Bell states, are discarded

where the 2×2 matrix $\widetilde{U}^{\sigma\sigma'}$ is the transpose of $U^{\sigma\sigma'}$. Finally, by applying the unitary gate $\widetilde{U}$ on the state $|\Phi^{(4)}\rangle$ and then measuring the ancilla qubits with outcome σ, the state of the system can collapse to the desired final state. To be more precise, for the system collapses into the Eq. (6.24), we need to prepare the initial state of the ancilla so that all c_σ coefficients are equal.

To implement the braid group of the Ising anyon model, we apply the dual exchange matrices

$$\widetilde{R}_{12} = e^{i\frac{\pi}{4}X_{a_1}X_{a_2}} \quad , \quad \widetilde{R}_{23} = e^{-i\frac{\pi}{4}Z_{a_2}Z_{a_3}} \quad , \quad \widetilde{R}_{34} = e^{i\frac{\pi}{4}X_{a_3}X_{a_4}} \quad , \quad \widetilde{R}_{41} = e^{-i\frac{\pi}{4}Z_{a_4}Z_{a_1}} \tag{6.25}$$

on the ancilla qubits. Then by measuring the ancillary qubits, we realize the exchange matrices R_{ij}, acting on the four-puncture system of Ising anyons. The Ising fusion matrix F (Eq. (6.14)) is similarly implemented via its dual

$$\widetilde{F} = \widetilde{R}_{12}^{-1}\widetilde{R}_{23}\widetilde{R}_{12}^{-1} \tag{6.26}$$

acting on the ancilla qubits.

In order to define two logical qubits and construct entangling gates (e.g., CZ, CNOT), we need to add two more mixed-boundary punctures into the lattice and two ancillary qubits. In general, we observe that to create N logical qubits, we need to consider a system of $2N + 2$ mixed-boundary punctures $p_1, \ldots, p_{2N+2}$, and an equal number of ancilla qubits, $a_1, \ldots, a_{2N+2}$.

Chapter 7

Conclusion and Outlook

In this thesis, we studied and developed schemes for fault-tolerant quantum computation via braiding non-Abelian anyons in two ways: by constructing mathematically consistent CFT wavefunctions and by numerically simulating Rydberg atoms with mixed boundary lattice punctures. Regarding the former, conformal field theories have been extremely useful in building trial energy-gapped wavefunctions with anyonic excitations in the fractional quantum Hall effect. This approach was motivated by the description of FQHE using a low-energy effective Chern-Simons theory in three spacetime dimensions [41, 42] and the duality between CS and CFTs theories [43]. Of course, not every CFT can describe systems in topological phases of matter; a key ingredient is the existence of an Abelian field operator with a conformal dimension $h < 1$.

Several CFT wavefunctions have been proposed in the literature in order to describe fractional quantum Hall states and their anyonic excitations at different filling fractions. In the early-1980s, Laughlin introduced a wavefunction corresponding to a free boson CFT in order to explain FQHE at filling $\nu = \frac{1}{\Lambda}$. Experimental results suggest that these states exhibit Abelian anyonic excitations [32, 33]. However, for quantum computation, we are interested in non-Abelian anyons whose braid group suffices for the implementation of non-trivial quantum gates. A quantum Hall state supporting Ising anyons was later proposed by Moore and Read [44], with a ground state characterized by including a Pfaffian term onto

the Laughlin ground state. In particular, this state was constructed by using the conformal blocks of the critical Ising CFT $\mathcal{M}(4,3)$. To this day, one of the promising candidates for the experimental observation [34, 35] of this state is the FQHE at filling $\nu = \frac{5}{2}$. This state is also related to the Majorana zero modes (MZMs) that are predicted at the edges of $p + ip$ superconductors [162, 163], which follow the Ising braiding statistics. Several different wavefunctions such as the Read-Rezayi, Halperin, and non-Abelian spin-singlet (NASS) state [49, 50, 51] can be found in the literature. The Read-Rezayi wavefunction is a generalization based on the parafermionic $\mathbb{Z}_3$ CFT which supports Fibonacci anyons and offers the possibility for universal topological quantum computation. On the other hand, the Halperin and NASS differ from the Moore-Read state as they describe unpolarized-spin systems.

In Chapters 4 and 5, we constructed an energy-gapped wavefunction based on the coset CFT $SU(2)_1^{\otimes k}/SU(2)_k$. This was motivated by the Moore-Read wavefunction that was based on the Minimal Model $\mathcal{M}(4,3)$ and exhibits excitations with Ising statistics. We showed that the coset CFT $SU(2)_1^{\otimes k}/SU(2)_k$ contains a primary field of the same conformal weight, fusion rules, and correlators as $\sigma \equiv \Phi_{(1,2)}$ in the Minimal Models. Additionally, the coset CFT contains a field ψ of conformal weight $h = \frac{1}{2}$ and Abelian fusion rules, which aren't present in Minimal Models with $k > 2$. Finding a primary with conformal dimension less than one is critical in order to obtain a gapped state that can give fault-tolerant quantum computation. These properties allowed us to use correlators of the coset CFT to generalize the quantum statistics of the Moore-Read wavefunction for $k \geq 3$ in a way that leads to fault-tolerant universal quantum computing. Explicit calculations for the braiding and fusion matrices involving six anyonic excitations were calculated in detail in Chapter 4. Additionally, we "sketched" the generalization to an arbitrary number of anyons for every k.

In more recent years, two different approaches have gained a lot of interest in the scientific community. The first method regards the search for anyons in lattice models of neutral Rydberg atoms. In Refs. [59, 60, 164], the authors suggested that the $\mathbb{Z}_2$ topological order, which includes the e and m Abelian anyons, can be found by properly fine-tuning the

dynamics of the Rydberg atoms in Ryby and Kagome lattices. Further, research supports the existence of this topological phase of matter in different lattices, such as the honeycomb lattice [165]. In Chapter 6, we introduced four mixed boundary punctures in a Ruby lattice with Rydberg atoms. We verified that the system has a quantum spin liquid phase for intermediate values of Δ/Ω and the existence of both smooth and rough boundaries across the punctures. We showed how to construct the superposition states $|\pm\rangle$ (defined in Eq. (6.7)) by introducing ancillary qubits. By doing so, we constructed quantum gates that realize the Ising braiding group.

The second method involves the simulation of Abelian and non-Abelian anyonic statistics using the current NISQ devices. This paradigm is better understood in terms of quantum error-correcting codes. A toric code-like degenerate ground state is prepared corresponding to no anyonic excitations at all. Then, anyons and their braiding can be implemented via unitary gates that mimic the effects of the non-local Pauli string operators. Error protection is guaranteed by measuring the stabilizers during the process of quantum computation. More specifically, the $\mathbb{Z}_{\not 2}$ topological order of a surface code was realized using superconducting qubits [69]. Different topologically ordered states corresponding to non-Abelian states were simulated using superconducting quantum hardware [70, 166]. To simulate non-Abelian braiding and fusion matrices lattice twists were implemented, as described in [63], effectively by deforming the stabilizer operators. Similar results have been found using different platforms, such as ion-traps (D_4 topological order) [71], photonics (D_3 topological order) [167], and Rydberg atoms (Fibonacci anyons) [168].

A possible future extension of the work presented in this dissertation would be to simulate the wavefunction based on the $SU(2)_1^{\otimes k}/SU(2)_k$ coset CFT via NISQ hardware. In particular, the simulation of theories with $k = 3$ and $k \geq 5$ can lead to surface codes with Fibonacci or different non-Abelian braiding matrices that could offer universal topological quantum computation. In this framework, the wavefunction of four anyons would be mapped into a qubit, whereas a higher number of anyons would lead qudits.

It would be interesting to find a system that will provide a physical realization of the coset wavefunction. Existing CFT wavefunctions such as the Pfaffian Moore-Read [44], the anti-Pfaffian [47], the Read-Rezayi [49], and several others have all been proposed to describe states in the fractional quantum Hall effect. For example, non-conclusive data support the existence of the Moore-Read state (Isign anyonic excitations) in the FQHE at filling $\nu = \frac{5}{2}$ [34, 35] and the Read-Rezayi (Fibonacci anyonic excitations) in the FQHE at filling $\nu = \frac{13}{5}$ [36]. Motivated by that, we would like to understand if the coset wavefunctions with $k \geq 3$ could also be realized in FQHE with different fillings and what would be the experimental signatures of these states (e.g., expected thermal Hall conductance). Another idea would be to better understand the connection of these coset quantum Hall states to two-dimensional superconductors. Similar works for the Moore-Read and Read-Rezayi states can be found in [162, 169]. This would offer more avenues for the experimental detection of non-Abelian anyons, which are required in order to build a universal topological quantum computer.

Furthermore, it would be instructive to explore connections of the coset wavefunction to different states, such as the non-Abelian spin-singlet (NASS) state. This is motivated by the observation that the coset $SU(2)_1^{\otimes k}/SU(2)_k$ is isomorphic to $SU(k)_2/U(1)^{\otimes(k-1)}$. Thus, for $k = 3$, the coset CFT introduced in this thesis can be understood in terms of two free bosons and the $SU(3)_2$ theory. As the latter has been proposed to emerge in fast-rotating cold atoms [53] and two-dimensional coupled multi-component quantum wires [54], this could suggest new experimental directions.

Finally, it was recently proposed that a generalized Ising model could be realized in the Rydberg atom platform by introducing a second excited energy state [170]. As discussed in Ref. [170], different quantum spin models including the Potts model can be mapped into this generalized Ising model. Motivated by the connections of the 3-state Potts model to the $\mathbb{Z}_3$ and the $\mathcal{M}(6,5)$ CFT, it would be interesting to explore similar connections between Rydberg atoms and the coset $SU(2)_1^{\otimes k}/SU(2)_k$.

Bibliography

[1] G. E. Moore, "Cramming more components onto integrated circuits, Reprinted from Electronics (1965)," *IEEE Solid-State Circuits Society Newsletter*, vol. 11, pp. 33–35, 2006. 1

[2] J. R. Powell, "The Quantum Limit to Moore's Law," *Proceedings of the IEEE*, vol. 96, pp. 1247–1248, 2008. 1

[3] R. P. Feynman, "Simulating physics with computers," *International Journal of Theoretical Physics*, vol. 21, pp. 467–488, 1982. 1

[4] D. Deutsch, "Quantum theory, the Church–Turing principle and the universal quantum computer," *Proceedings of the Royal Society A*, vol. 400, pp. 97–117, 1985. 1

[5] S. W. Peter, "Algorithms for quantum computation: discrete logarithms and factoring," *Proceedings 35th Annual Symposium on Foundations of Computer Science*, pp. 124–134, 1994. 1

[6] G. K. Lov, "A fast quantum mechanical algorithm for database search," *Proceedings of the Twenty-Eighth Annual ACM Symposium on Theory of Computing*, p. 212–219, 1996. 2

[7] C. H. Bennett, G. Brassard, and A. K. Ekert, "Quantum cryptography," *Scientific American*, vol. 267, no. 4, pp. 50–57, 1992. 2

[8] N. S. Blunt, J. Camps, O. Crawford, R. Izsak, S. Leontica, A. Mirani, A. E. Moylett, S. A. Scivier, C. Suenderhauf, P. Schopf, *et al.*, "Perspective on the current state-of-the-art of quantum computing for drug discovery applications," *Journal of Chemical Theory and Computation*, vol. 18, no. 12, pp. 7001–7023, 2022. 2

[9] D. P. DiVincenzo, "The Physical Implementation of Quantum Computation," *Fortschritte der Physik*, vol. 48, pp. 771–783, 2000. 2

[10] T. D. Ladd, F. Jelezko, R. Laflamme, Y. Nakamura, C. Monroe, and J. L. O'Brien, "Quantum computers," *nature*, vol. 464, no. 7285, pp. 45–53, 2010. 2

[11] R. W. Hamming, "Error detecting and error correcting codes," *The Bell System Technical Journal*, vol. 29, pp. 147–160, 1950. 3

[12] W. K. Wootters and W. H. Zurek, "A single quantum cannot be cloned," *Nature*, vol. 299, pp. 802–803, 1982. 3

[13] J. von Neumann, "Mathematical Foundations of Quantum Mechanics: New Edition," *Princeton University Press*, 2018. 3

[14] P. W. Shor, "Scheme for reducing decoherence in quantum computer memory," *Physical Review A*, vol. 52, pp. 2493–2496, 1995. 3

[15] J. Preskill, "Quantum Computing in the NISQ era and beyond," *Quantum*, vol. 2, p. 79, 2018. 3

[16] E. Knill, R. Laflamme, and W. H. Zurek, "Resilient quantum computation," *Science*, vol. 279, pp. 342–345, 1998. 3

[17] A. Y. Kitaev, "Fault-tolerant quantum computation by anyons," *Annals of Physics*, vol. 303, pp. 2–30, 2003. 3, 4, 7, 14

[18] A. Y. Kitaev, "Anyons in an exactly solved model and beyond," *Annals of Physics*, vol. 321, pp. 2–111, 2006. 3, 4, 7, 14, 15, 75

[19] R. O. Walter and J. Preskill, "Topological quantum computation," *NASA International Conference on Quantum Computing and Quantum Communications*, p. 341–356, 1998. 3

[20] M. H. Freedman, A. Kitaev, and Z. Wang, "Simulation of topological field theories by quantum computers," *Communications in Mathematical Physics*, vol. 227, pp. 587–603, 2002. 3

[21] M. H. Freedman, M. Larsen, and Z. Wang, "A modular functor which is universal for quantum computation," *Communications in Mathematical Physics*, vol. 227, p. 605–622, 2002. 3

[22] M. H. Freedman, A. Kitaev, M. J. Larsen, and W. Zhenghan, "Topological quantum computations," *Bulletin of the American Mathematical Society*, vol. 40, pp. 31–38, 2003. 3

[23] S. H. Simon, "Topological quantum: Lecture notes and proto-book," 2020. 3

[24] Z. Wang, *Topological quantum computation*. No. 112, American Mathematical Soc., 2010. 3

[25] F. Wilczek, "Quantum Mechanics of Fractional-Spin Particles," *Physical Review Letters*, vol. 49, pp. 957–959, 1982. 4, 10

[26] V. Lahtinen and J. K. Pachos, "A Short Introduction to Topological Quantum Computation," *SciPost Physics*, vol. 3, p. 21, 2017. 4, 15

[27] S. Trebst, M. Troyer, Z. Wang, and A. W. W. Ludwig, "A short introduction to fibonacci anyon models," *Progress of Theoretical Physics Supplement*, vol. 176, pp. 384–407, 06 2008. 4, 20

[28] W. M. Witzel and S. Das Sarma, "Quantum theory for electron spin decoherence induced by nuclear spin dynamics in semiconductor quantum computer architectures:

Spectral diffusion of localized electron spins in the nuclear solid-state environment," *Physical Review B*, vol. 74, pp. 035322–035346, 2006. 4, 14

[29] S. D. Sarma, M. Freedman, and C. Nayak, "Topologically protected qubits from a possible non-abelian fractional quantum hall state," *Physical review letters*, vol. 94, no. 16, p. 166802, 2005. 4, 14

[30] A. Y. Kitaev, "Unpaired Majorana fermions in quantum wires," *Physics-Uspekhi*, vol. 44, p. 131, 2001. 4

[31] S. D. Sarma, M. Freedman, and C. Nayak, "Majorana zero modes and topological quantum computation," *npj Quantum Information*, vol. 1, no. 1, pp. 1–13, 2015. 4

[32] J. Nakamura, S. Liang, G. C. Gardner, and M. J. Manfra, "Direct observation of anyonic braiding statistics," *Nature Physics*, vol. 16, no. 9, pp. 931–936, 2020. 4, 22, 24, 92

[33] J.-M. Berroir, Q. Dong, *et al.*, "Fractional statistics in anyon collisions," *Science*, vol. 368, no. 6487, pp. 173–177, 2020. 4, 22, 92

[34] M. Banerjee, M. Heiblum, V. Umansky, D. E. Feldman, Y. Oreg, and A. Stern, "Observation of half-integer thermal hall conductance," *Nature*, vol. 559, no. 7713, pp. 205–210, 2018. 4, 93, 95

[35] B. Dutta, W. Yang, R. A. Melcer, H. K. Kundu, M. Heiblum, V. I. Umansky, Y. Oreg, A. Stern, and D. F. Mross, "Novel method distinguishing between competing topological orders," 2021. 4, 93, 95

[36] R. S. Mong, M. P. Zaletel, F. Pollmann, and Z. Papic, "Fibonacci anyons and charge density order in the 12/5 and 13/5 quantum hall plateaus," *Physical Review B*, vol. 95, p. 115136, 2015. 4, 95

[37] D. C. Tsui, H. L. Stormer, and A. C. Gossard, "Two-dimensional magnetotransport in the extreme quantum limit," *Physical Review Letters*, vol. 48, pp. 1559–1562, 1982. 5

[38] K. von Klitzing, G. Dorda, and M. Pepper, "New method for high-accuracy determination of the fine-structure constant based on quantized hall resistance," *Physical Review Letters*, vol. 45, pp. 494–497, 1980. 5

[39] R. B. Laughlin, "Anomalous Quantum Hall Effect: An Incompressible Quantum Fluid with Fractionally Charged Excitations," *Physical Review Letters*, vol. 50, pp. 1395–1398, 1983. 5, 14, 54

[40] D. Tong, "Lectures on the quantum hall effect," *arXiv preprint arXiv:1606.06687*, 2016. 5, 6

[41] Zhang, Hansson, and Kivelson, "Effective-field-theory model for the fractional quantum hall effect.," *Physical review letters*, vol. 62 1, pp. 82–85, 1989. 6, 92

[42] A. Lopez and E. Fradkin, "Fractional quantum Hall effect and Chern-Simons gauge theories," *Physical Review B*, vol. 44, pp. 5246–5262, 1991. 6, 92

[43] E. Witten, "Quantum field theory and the Jones polynomial," *Communications in Mathematical Physics*, vol. 121, pp. 351–399, 1989. 6, 92

[44] G. Moore and N. Read, "Nonabelions in the fractional quantum hall effect," *Nuclear Physics B*, vol. 360, pp. 362–396, 1991. 6, 8, 54, 61, 66, 68, 92, 95

[45] C. Nayak and F. Wilczek, "2n-quasihole states realize 2n1-dimensional spinor braiding statistics in paired quantum hall states," *Nuclear Physics*, vol. 479, pp. 529–553, 1996. 6

[46] P. Bonderson, V. Gurarie, and C. Nayak, "Plasma analogy and non-abelian statistics for ising-type quantum hall states," *Physical Review B*, vol. 83, p. 075303, 2010. 6, 53, 54, 55

[47] M. Levin, B. I. Halperin, and B. Rosenow, "Particle-hole symmetry and the pfaffian state.," *Physical review letters*, vol. 99 23, 2007. 6, 95

[48] S.-S. Lee, S. Ryu, C. Nayak, and M. P. A. Fisher, "Particle-hole symmetry and the nu=5/2 quantum hall state.," *Physical review letters*, vol. 99 23, 2007. 6

[49] N. Read and E. Rezayi, "Quasiholes and fermionic zero modes of paired fractional quantum Hall states: The mechanism for non-Abelian statistics," *Physical Review B*, vol. 54, pp. 16864–16887, 1996. 6, 54, 68, 93, 95

[50] B. I. Halperin, "Theory of the quantized hall conductance," *Helvetica Physica Acta*, vol. 56, no. 75, 1983. 7, 93

[51] E. Ardonne and K. Schoutens, "New class of non-abelian spin-singlet quantum hall states," *Physical review letters*, vol. 82, no. 25, p. 5096, 1999. 7, 93

[52] E. Ardonne and G. Sierra, "Chiral correlators of the ising conformal field theory," *Journal of Physics A: Mathematical and Theoretical*, vol. 43, no. 50, p. 505402, 2010. 7, 54

[53] J. W. Reijnders, F. Van Lankvelt, K. Schoutens, and N. Read, "Quantum hall states and boson triplet condensate for rotating spin-1 bosons," *Physical review letters*, vol. 89, no. 12, p. 120401, 2002. 7, 95

[54] Y. Fuji and P. Lecheminant, "Non-abelian s u (n- 1)-singlet fractional quantum hall states from coupled wires," *Physical Review B*, vol. 95, no. 12, p. 125130, 2017. 7, 95

[55] S. Bravyi and A. Y. Kitaev, "Quantum codes on a lattice with boundary," *arXiv: Quantum Physics*, 1998. 7, 75

[56] A. G. Fowler, M. Mariantoni, J. M. Martinis, and A. N. Cleland, "Surface codes: Towards practical large-scale quantum computation," *Physical Review A*, vol. 86, no. 3, p. 032324, 2012. 7, 75

[57] Jaksch, Cirac, Zoller, Rolston, Côté, and Lukin, "Fast quantum gates for neutral atoms," *Physical review letters*, vol. 85 10, pp. 2208–11, 2000. 7

[58] R. Samajdar, W. W. Ho, H. Pichler, M. D. Lukin, and S. Sachdev, "Quantum phases of rydberg atoms on a kagome lattice," *Proceedings of the National Academy of Sciences*, vol. 118, 2020. 7

[59] R. Verresen, M. D. Lukin, and A. Vishwanath, "Prediction of toric code topological order from rydberg blockade," *Physical Review X*, vol. 11, no. 3, p. 031005, 2021. 7, 8, 14, 72, 75, 82, 93

[60] G. Semeghini, H. Levine, A. Keesling, S. Ebadi, T. T. Wang, D. Bluvstein, R. Verresen, H. Pichler, M. Kalinowski, R. Samajdar, *et al.*, "Probing topological spin liquids on a programmable quantum simulator," *Science*, vol. 374, no. 6572, pp. 1242–1247, 2021. 7, 14, 72, 75, 82, 93

[61] E. Urban, T. A. Johnson, T. Henage, L. Isenhower, D. Yavuz, T. Walker, and M. Saffman, "Observation of rydberg blockade between two atoms," *Nature Physics*, vol. 5, no. 2, pp. 110–114, 2009. 7, 71

[62] A. Gaëtan, Y. Miroshnychenko, T. Wilk, A. Chotia, M. Viteau, D. Comparat, P. Pillet, A. Browaeys, and P. Grangier, "Observation of collective excitation of two individual atoms in the rydberg blockade regime," *Nature Physics*, vol. 5, no. 2, pp. 115–118, 2009. 7

[63] H. Bombín, "Topological order with a twist: Ising anyons from an abelian model," *Physical review letters*, vol. 105, no. 3, p. 030403, 2010. 8, 94

[64] M. Barkeshli, C.-M. Jian, and X.-L. Qi, "Twist defects and projective non-abelian braiding statistics," *Physical Review B*, vol. 87, no. 4, p. 045130, 2013. 8

[65] H. Zheng, A. Dua, and L. Jiang, "Demonstrating non-abelian statistics of majorana fermions using twist defects," *Physical Review B*, vol. 92, no. 24, p. 245139, 2015. 8

[66] T. Scruby and D. E. Browne, "A hierarchy of anyon models realised by twists in stacked surface codes," *Quantum*, vol. 4, p. 251, 2020. 8

[67] B. J. Brown, K. Laubscher, M. S. Kesselring, and J. R. Wootton, "Poking holes and cutting corners to achieve clifford gates with the surface code," *Physical Review X*, vol. 7, no. 2, p. 021029, 2017. 8, 72

[68] A. Benhemou, J. K. Pachos, and D. E. Browne, "Non-abelian statistics with mixed-boundary punctures on the toric code," *Physical Review A*, vol. 105, no. 4, p. 042417, 2022. 8, 9, 72, 77

[69] K. Satzinger, Y.-J. Liu, A. Smith, C. Knapp, M. Newman, C. Jones, Z. Chen, C. Quintana, X. Mi, A. Dunsworth, *et al.*, "Realizing topologically ordered states on a quantum processor," *Science*, vol. 374, no. 6572, pp. 1237–1241, 2021. 8, 94

[70] T. I. Andersen, Y. D. Lensky, K. Kechedzhi, I. Drozdov, A. Bengtsson, S. Hong, A. Morvan, X. Mi, A. Opremcak, R. Acharya, *et al.*, "Observation of non-abelian exchange statistics on a superconducting processor," *arXiv preprint arXiv:2210.10255*, 2022. 8, 94

[71] M. Iqbal, N. Tantivasadakarn, R. Verresen, S. L. Campbell, J. M. Dreiling, C. Figgatt, J. P. Gaebler, J. Johansen, M. Mills, S. A. Moses, *et al.*, "Creation of non-abelian topological order and anyons on a trapped-ion processor," *arXiv preprint arXiv:2305.03766*, 2023. 8, 94

[72] E. Artin, "Theory of braids," *Annals of Mathematics*, vol. 48, no. 1, pp. 101–126, 1947. 11

[73] J. K. Pachos, *Introduction to Topological Quantum Computation*. Cambridge University Press, 2012. 13, 16

[74] L. D. Landau, "On the theory of phase transitions," *Pergamon*, pp. 193–216, 1965. 14

[75] V. Ginzburg and L. D. Landau, "On the theory of superconductivity," *Pergamon*, pp. 217–225, 1965. 14

[76] X.-G. Wen, "Topological orders in rigid states," *International Journal of Modern Physics B*, vol. 4, no. 02, pp. 239–271, 1990. 14

[77] C. Nayak, S. H. Simon, A. Stern, M. Freedman, and S. D. Sarma, "Non-abelian anyons and topological quantum computation," *Reviews of Modern Physics*, vol. 80, no. 3, p. 1083, 2008. 15

[78] L. S. Georgiev, "Topologically protected gates for quantum computation with non-abelian anyons in the pfaffian quantum hall state," *Physical Review B*, vol. 74, no. 23, p. 235112, 2006. 19, 44, 48

[79] A. Ahlbrecht, L. S. Georgiev, and R. F. Werner, "Implementation of clifford gates in the ising-anyon topological quantum computer," *Physical Review A*, vol. 79, no. 3, p. 032311, 2009. 19, 44, 48

[80] N. E. Bonesteel, L. Hormozi, G. Zikos, and S. H. Simon, "Braid topologies for quantum computation," *Physical review letters*, vol. 95, no. 14, p. 140503, 2005. 22, 45, 50

[81] M. A. Nielsen and I. Chuang, "Quantum computation and quantum information," 2002. 22

[82] L. Hormozi, G. Zikos, N. E. Bonesteel, and S. H. Simon, "Topological quantum compiling," *Physical Review B*, vol. 75, no. 16, p. 165310, 2007. 22, 45

[83] B. Field and T. Simula, "Introduction to topological quantum computation with non-abelian anyons," *Quantum Science and Technology*, vol. 3, no. 4, p. 045004, 2018. 22, 45

[84] N. Bonesteel, L. Hormozi, G. Zikos, and S. Simon, "Quantum computing with non-abelian quasiparticles," *International Journal of Modern Physics B*, vol. 21, no. 08n09, pp. 1372–1378, 2007. 22

[85] C. d. C. Chamon, D. Freed, S. Kivelson, S. Sondhi, and X. Wen, "Two point-contact interferometer for quantum hall systems," *Physical Review B*, vol. 55, no. 4, p. 2331, 1997. 24

[86] V. Goldman, J. Liu, and A. Zaslavsky, "Fractional statistics of laughlin quasiparticles in quantum antidots," *Physical Review B*, vol. 71, no. 15, p. 153303, 2005. 24

[87] F. Camino, W. Zhou, and V. Goldman, "e/3 laughlin quasiparticle primary-filling ν= 1/3 interferometer," *Physical review letters*, vol. 98, no. 7, p. 076805, 2007. 24

[88] F. Camino, W. Zhou, and V. Goldman, "Aharonov-bohm superperiod in a laughlin quasiparticle interferometer," *Physical review letters*, vol. 95, no. 24, p. 246802, 2005. 24

[89] S. D. Sarma, M. Freedman, and C. Nayak, "Topologically protected qubits from a possible non-abelian fractional quantum hall state," *Physical review letters*, vol. 94, no. 16, p. 166802, 2005. 24

[90] P. Bonderson, A. Kitaev, and K. Shtengel, "Detecting non-abelian statistics in the ν= 5/2 fractional quantum hall state," *Physical review letters*, vol. 96, no. 1, p. 016803, 2006. 24

[91] A. Stern and B. I. Halperin, "Proposed experiments to probe the non-abelian ν= 5/2 quantum hall state," *Physical review letters*, vol. 96, no. 1, p. 016802, 2006. 24

[92] S. An, P. Jiang, H. Choi, W. Kang, S. Simon, L. Pfeiffer, K. West, and K. Baldwin, "Braiding of abelian and non-abelian anyons in the fractional quantum hall effect," *arXiv preprint arXiv:1112.3400*, 2011. 24

[93] R. Willett, K. Shtengel, C. Nayak, L. Pfeiffer, Y. Chung, M. Peabody, K. Baldwin, and K. West, "Interference measurements of non-abelian e/4 & abelian e/2 quasiparticle braiding," *Physical Review X*, vol. 13, no. 1, p. 011028, 2023. 24

[94] P. Di Francesco, P. Mathieu, and D. Senechal, *Conformal Field Theory*. Graduate Texts in Contemporary Physics, New York: Springer-Verlag, 1997. 25, 27, 42, 122

[95] A. Schellekens, "Introduction to conformal field theory," *Fortschritte der Physik/Progress of Physics*, vol. 44, no. 8, pp. 605–705, 1996. 25

[96] A. A. Belavin, "Infinite conformal symmetry of critical fluctuations in two dimensions," *Journal of Statistical Physics*, vol. 34, pp. 763–774, 1984. 25

[97] J. L. Cardy, "Conformal Invariance and Surface Critical Behavior," *Nucl. Phys. B*, vol. 240, pp. 514–532, 1984. 25

[98] D. Friedan, Z.-a. Qiu, and S. H. Shenker, "Conformal Invariance, Unitarity and Two-Dimensional Critical Exponents," *Phys. Rev. Lett.*, vol. 52, pp. 1575–1578, 1984. 25

[99] A. A. Belavin, A. M. Polyakov, and A. B. Zamolodchikov, "Infinite Conformal Symmetry in Two-Dimensional Quantum Field Theory," *Nucl. Phys. B*, vol. 241, pp. 333–380, 1984. 25, 27

[100] D. Friedan, Z.-a. Qiu, and S. H. Shenker, "Superconformal Invariance in Two-Dimensions and the Tricritical Ising Model," *Phys. Lett. B*, vol. 151, pp. 37–43, 1985. 25

[101] V. S. Dotsenko, "Critical Behavior and Associated Conformal Algebra of the Z(3) Potts Model," *Nucl. Phys. B*, vol. 235, pp. 54–74, 1984. 25

[102] N. Seiberg and E. Witten, "String theory and noncommutative geometry," *Journal of High Energy Physics*, vol. 1999, no. 09, p. 032, 1999. 25

[103] E. Witten, "Anti de sitter space and holography," *Advances in Theoretical and Mathematical Physics*, vol. 2, no. 2, pp. 253–291, 1998. 25

[104] J. Maldacena, "The large-n limit of superconformal field theories and supergravity," *International journal of theoretical physics*, vol. 38, no. 4, pp. 1113–1133, 1999. 25

[105] M. A. Virasoro, "Subsidiary conditions and ghosts in dual resonance models," *Phys. Rev. D*, vol. 1, pp. 2933–2936, 1970. 30

[106] R. Brower and C. Thorn, "Eliminating spurious states from the dual resonance model," *Nuclear Physics B*, vol. 31, no. 1, pp. 163–182, 1971. 30

[107] A. B. Zamolodchikov, "Irreversibility of the Flux of the Renormalization Group in a 2D Field Theory," *JETP Lett.*, vol. 43, pp. 730–732, 1986. 30

[108] V. G. Kac, "Contravariant form for infinite-dimensional lie algebras and superalgebras," in *Group Theoretical Methods in Physics* (W. Beiglböck, A. Böhm, and E. Takasugi, eds.), (Berlin, Heidelberg), pp. 441–445, Springer Berlin Heidelberg, 1979. 31

[109] B. L. Feigin and D. B. Fuks, "Invariant skew symmetric differential operators on the line and verma modules over the Virasoro algebra," *Funct. Anal. Appl.*, vol. 16, pp. 114–126, 1982. 31

[110] D. Friedan, S. H. Shenker, and Z.-a. Qiu, "Details of the Nonunitarity Proof for Highest Weight Representations of the Virasoro Algebra," *Commun. Math. Phys.*, vol. 107, p. 535, 1986. 31

[111] V. S. Dotsenko and V. A. Fateev, "Conformal Algebra and Multipoint Correlation Functions in Two-Dimensional Statistical Models," *Nucl. Phys. B*, vol. 240, p. 312, 1984. 31

[112] V. S. Dotsenko and V. A. Fateev, "Four Point Correlation Functions and the Operator Algebra in the Two-Dimensional Conformal Invariant Theories with the Central Charge c < 1," *Nucl. Phys. B*, vol. 251, pp. 691–734, 1985. 31

[113] V. S. Dotsenko and V. A. Fateev, "Operator Algebra of Two-Dimensional Conformal Theories with Central Charge C <= 1," *Phys. Lett. B*, vol. 154, pp. 291–295, 1985. 31

[114] G. Felder, "BRST Approach to Minimal Models," *Nucl. Phys. B*, vol. 317, p. 215, 1989. [Erratum: Nucl.Phys.B 324, 548 (1989)]. 32

[115] E. P. Verlinde, "Fusion rules and modular transformations in 2d conformal field theory," *Nuclear Physics*, vol. 300, pp. 360–376, 1988. 34

[116] S. D. Mathur, "Quantum kac-moody symmetry in integrable field theories," *Nuclear Physics B*, vol. 369, no. 1, pp. 433–460, 1992. 35

[117] E. Kokkas, A. Bagheri, Z. Wang, and G. Siopsis, "Quantum computing with two-dimensional conformal field theories," *arXiv preprint arXiv:2112.06144*, 2021. 38, 52

[118] G. W. Moore and N. Seiberg, "Classical and Quantum Conformal Field Theory," *Commun. Math. Phys.*, vol. 123, p. 177, 1989. 39

[119] G. Moore and N. Seiberg, *Lectures on RCFT*, pp. 263–361. Boston, MA: Springer US, 1990. 39

[120] E. Schrödinger, "An undulatory theory of the mechanics of atoms and molecules," *Phys. Rev.*, vol. 28, pp. 1049–1070, Dec 1926. 52

[121] L. S. Georgiev, "Towards a universal set of topologically protected gates for quantum computation with pfaffian qubits," *Nuclear Physics B*, vol. 789, no. 3, pp. 552–590, 2008. 54

[122] V. Gurarie and C. Nayak, "A plasma analogy and berry matrices for non-abelian quantum hall states," *Nuclear Physics*, vol. 506, pp. 685–694, 1997. 54

[123] P. Goodard, A. Kent, and D. Olive, "Virasoro algebras and coset space models," *Physics Letters B*, vol. 152, no. 1, pp. 88–92, 1985. 55

[124] P. Goddard, A. Kent, and D. I. Olive, "Unitary representations of the virasoro and super-virasoro algebras," *Communications in Mathematical Physics*, vol. 103, pp. 105–119, 1986. 55, 57

[125] M. Y. Lashkevich, "Coset construction of minimal models," *Int. J. Mod. Phys. A*, vol. 8, pp. 5673–5700, 1993. 55

[126] N. Chair and E. H. Saidi, "On the WZW fields realization of critical models of the minimal series," 8 1995. 55

[127] T. S. Choi, I. G. Koh, B. C. Park, and H. J. Shin, "DYNAMICS OF THE COSET CONFORMAL FIELD THEORY: BPZ EQUATION FROM KZ EQUATION IN GKO CONSTRUCTION," *Phys. Lett. B*, vol. 233, pp. 163–168, 1989. 55

[128] D. C. Dunbar and K. G. Joshi, "Characters for coset conformal field theories and maverick examples," *International Journal of Modern Physics A*, vol. 8, no. 23, pp. 4103–4121, 1993. 55

[129] K. Gawedzki and A. Kupiainen, "G/h Conformal Field Theory from Gauged WZW Model," *Phys. Lett. B*, vol. 215, pp. 119–123, 1988. 55, 58

[130] J. Isidro, J. Labastida, and A. Ramallo, "Coset constructions in chern-simons gauge theory," *Physics Letters B*, vol. 282, no. 1-2, pp. 63–72, 1992. 55

[131] K. Gawedzki and A. Kupiainen, "Coset Construction from Functional Integrals," *Nucl. Phys. B*, vol. 320, pp. 625–668, 1989. 55, 58

[132] D. Karabali and H. J. Schnitzer, "Brst quantization of the gauged wzw action and coset conformal field theories," *Nuclear Physics B*, vol. 329, no. 3, pp. 649–666, 1990. 55

[133] Z. Jaskólski and P. Suchanek, "Non-rational su (2) cosets and liouville field theory," *arXiv preprint arXiv:1510.01773*, 2015. 55

[134] A. Cappelli, L. S. Georgiev, and I. T. Todorov, "Parafermion hall states from coset projections of abelian conformal theories," *Nuclear Physics B*, vol. 599, no. 3, pp. 499–530, 2001. 55

[135] E. Witten, "Nonabelian Bosonization in Two-Dimensions," *Commun. Math. Phys.*, vol. 92, pp. 455–472, 1984. 56

[136] V. G. Kac, *Infinite-dimensional Lie algebras*. Cambridge university press, 1990. 56

[137] M. R. Gaberdiel and R. Gopakumar, "Minimal model holography," *Journal of Physics A: Mathematical and Theoretical*, vol. 46, no. 21, p. 214002, 2013. 56

[138] I. I. Kogan, A. Lewis, and O. A. Soloviev, "Knizhnik-zamolodchikov type equations for gauged wznw models," *International Journal of Modern Physics*, vol. 13, pp. 1345–1367, 1997. 56, 58, 125

[139] V. G. Knizhnik and A. B. Zamolodchikov, "Current Algebra and Wess-Zumino Model in Two-Dimensions," *Nucl. Phys. B*, vol. 247, pp. 83–103, 1984. 58

[140] V. S. Dotsenko, "The Free Field Representation of the SU(2) Conformal Field Theory," *Nucl. Phys. B*, vol. 338, pp. 747–758, 1990. 58

[141] G. Sierra, "Conformal field theory and the exact solution of the bcs hamiltonian," *Nuclear Physics B*, vol. 572, no. 3, pp. 517–534, 2000. 58, 123

[142] N. M. Bauer, E. Kokkas, V. Ale, and G. Siopsis, "Non-Abelian anyons with Rydberg atoms," *Phys. Rev. A*, vol. 107, no. 6, p. 062407, 2023. 71

[143] I. H. Deutsch, G. K. Brennen, and P. S. Jessen, "Quantum computing with neutral atoms in an optical lattice," *Fortschritte der Physik: Progress of Physics*, vol. 48, no. 9-11, pp. 925–943, 2000. 71

[144] M. Anderlini, P. J. Lee, B. L. Brown, J. Sebby-Strabley, W. D. Phillips, and J. V. Porto, "Controlled exchange interaction between pairs of neutral atoms in an optical lattice," *Nature*, vol. 448, no. 7152, pp. 452–456, 2007. 71

[145] H.-J. Briegel, T. Calarco, D. Jaksch, J. I. Cirac, and P. Zoller, "Quantum computing with neutral atoms," *Journal of modern optics*, vol. 47, no. 2-3, pp. 415–451, 2000. 71

[146] I. I. Ryabtsev, D. B. Tretyakov, and I. I. Beterov, "Applicability of rydberg atoms to quantum computers," *Journal of Physics B: Atomic, Molecular and Optical Physics*, vol. 38, no. 2, p. S421, 2005. 71

[147] M. Saffman, T. G. Walker, and K. Mølmer, "Quantum information with rydberg atoms," *Reviews of modern physics*, vol. 82, no. 3, p. 2313, 2010. 71

[148] H. Bernien, S. Schwartz, A. Keesling, H. Levine, A. Omran, H. Pichler, S. Choi, A. S. Zibrov, M. Endres, M. Greiner, *et al.*, "Probing many-body dynamics on a 51-atom quantum simulator," *Nature*, vol. 551, no. 7682, pp. 579–584, 2017. 71

[149] M. Endres, H. Bernien, A. Keesling, H. Levine, E. R. Anschuetz, A. Krajenbrink, C. Senko, V. Vuletić, M. Greiner, and M. D. Lukin, "Atom-by-atom assembly of defect-free one-dimensional cold atom arrays," *Science*, vol. 354, pp. 1024 – 1027, 2016. 71

[150] A. Keesling, A. Omran, H. Levine, H. Bernien, H. Pichler, S. Choi, R. Samajdar, S. Schwartz, P. Silvi, S. Sachdev, *et al.*, "Quantum kibble–zurek mechanism and critical dynamics on a programmable rydberg simulator," *Nature*, vol. 568, no. 7751, pp. 207–211, 2019. 71

[151] H. Levine, A. Keesling, A. Omran, H. Bernien, S. Schwartz, A. S. Zibrov, M. Endres, M. Greiner, V. Vuletić, and M. D. Lukin, "High-fidelity control and entanglement of rydberg-atom qubits," *Physical review letters*, vol. 121, no. 12, p. 123603, 2018. 71

[152] H. Levine, A. Keesling, G. Semeghini, A. Omran, T. T. Wang, S. Ebadi, H. Bernien, M. Greiner, V. Vuletić, H. Pichler, *et al.*, "Parallel implementation of high-fidelity multiqubit gates with neutral atoms," *Physical review letters*, vol. 123, no. 17, p. 170503, 2019. 71

[153] D. Bluvstein, H. Levine, G. Semeghini, T. T. Wang, S. Ebadi, M. Kalinowski, A. Keesling, N. Maskara, H. Pichler, M. Greiner, *et al.*, "A quantum processor based on coherent transport of entangled atom arrays," *Nature*, vol. 604, no. 7906, pp. 451–456, 2022. 71

[154] I. Cong, H. Levine, A. Keesling, D. Bluvstein, S.-T. Wang, and M. D. Lukin, "Hardware-efficient, fault-tolerant quantum computation with rydberg atoms," *Physical Review X*, vol. 12, no. 2, p. 021049, 2022. 71

[155] G. Torlai, B. Timar, E. P. Van Nieuwenburg, H. Levine, A. Omran, A. Keesling, H. Bernien, M. Greiner, V. Vuletić, M. D. Lukin, *et al.*, "Integrating neural networks with a quantum simulator for state reconstruction," *Physical review letters*, vol. 123, no. 23, p. 230504, 2019. 71

[156] J. Hauschild and F. Pollmann, "Efficient numerical simulations with tensor networks: Tensor network python (tenpy)," *SciPost Physics Lecture Notes*, p. 005, 2018. 80

[157] M. Aguado, G. Brennen, F. Verstraete, and J. I. Cirac, "Creation, manipulation, and detection of abelian and non-abelian anyons in optical lattices," *Physical review letters*, vol. 101, no. 26, p. 260501, 2008. 88

[158] D. Jaksch, H. J. Briegel, J. I. Cirac, C. W. Gardiner, and P. Zoller, "Entanglement of atoms via cold controlled collisions," *Phys. Rev. Lett.*, vol. 82, pp. 1975–1978, 1999. 88

[159] M. P. Jones, J. Beugnon, A. Gaëtan, J. Zhang, G. Messin, A. Browaeys, and P. Grangier, "Fast quantum state control of a single trapped neutral atom," *Physical Review A*, vol. 75, no. 4, p. 040301, 2007. 88

[160] G. K. Brennen, C. M. Caves, P. S. Jessen, and I. H. Deutsch, "Quantum logic gates in optical lattices," *Physical Review Letters*, vol. 82, no. 5, p. 1060, 1999. 88

[161] M. D. Lukin, M. Fleischhauer, R. Cote, L. Duan, D. Jaksch, J. I. Cirac, and P. Zoller, "Dipole blockade and quantum information processing in mesoscopic atomic ensembles," *Physical review letters*, vol. 87, no. 3, p. 037901, 2001. 88

[162] N. Read and D. Green, "Paired states of fermions in two dimensions with breaking of parity and time-reversal symmetries and the fractional quantum hall effect," *Physical Review B*, vol. 61, no. 15, p. 10267, 2000. 93, 95

[163] P. Fendley, M. P. Fisher, and C. Nayak, "Edge states and tunneling of non-abelian quasiparticles in the ν= 5/ 2 quantum hall state and p+ i p superconductors," *Physical Review B*, vol. 75, no. 4, p. 045317, 2007. 93

[164] R. Sahay, A. Vishwanath, and R. Verresen, "Quantum spin puddles and lakes: Nisq-era spin liquids from non-equilibrium dynamics," *arXiv preprint arXiv:2211.01381*, 2022. 93

[165] M. Kornjača, R. Samajdar, T. Macrì, N. Gemelke, S.-T. Wang, and F. Liu, "Trimer quantum spin liquid in a honeycomb array of rydberg atoms," *arXiv preprint arXiv:2211.00653*, 2022. 94

[166] S. Xu, Z.-Z. Sun, K. Wang, L. Xiang, Z. Bao, Z. Zhu, F. Shen, Z. Song, P. Zhang, W. Ren, *et al.*, "Digital simulation of non-abelian anyons with 68 programmable superconducting qubits," *arXiv preprint arXiv:2211.09802*, 2022. 94

[167] S. Goel, M. Reynolds, M. Girling, W. McCutcheon, S. Leedumrongwatthanakun, V. Srivastav, D. Jennings, M. Malik, and J. K. Pachos, "Unveiling the non-abelian statistics of $d(s\_3)$ anyons via photonic simulation," *arXiv preprint arXiv:2304.05286*, 2023. 94

[168] A. Benhemou, T. Angkhanawin, C. S. Adams, D. E. Browne, and J. K. Pachos, "Universality of z 3 parafermions via edge-mode interaction and quantum simulation of topological space evolution with rydberg atoms," *Physical Review Research*, vol. 5, no. 2, p. 023076, 2023. 94

[169] R. S. Mong, D. J. Clarke, J. Alicea, N. H. Lindner, P. Fendley, C. Nayak, Y. Oreg, A. Stern, E. Berg, K. Shtengel, *et al.*, "Universal topological quantum computation from a superconductor-abelian quantum hall heterostructure," *Physical Review X*, vol. 4, no. 1, p. 011036, 2014. 95

[170] R. Verresen, "Everything is a quantum ising model," *arXiv preprint arXiv:2301.11917*, 2023. 95

[171] "On the einstein podolsky rosen paradox," *Physics Physique Fizika*, vol. 1, no. 3, p. 195, 1964. 116

[172] L. Eberhardt, "Wess-zumino-witten models," *YRISW PhD School in Vienna*, vol. 2, 2019. 122

Appendices

Appendix A

Quantum Computation Preliminaries

As discussed in Chapter 1, the basic unit of information in the field of quantum computation is the qubit $|\psi\rangle = a\,|0\rangle + b\,|1\rangle$, as defined in Eq. (1.1). The coefficients a and b are complex numbers that are normalized by the condition $|a|^2 + |b|^2 = 1$. The states $|0\rangle$ and $|1\rangle$ form the basis of the two-dimensional Hilbert space. This is not a unique basis choice. By choosing $a = \frac{1}{\sqrt{2}}$ and $b = \pm\frac{1}{\sqrt{2}}$, we can write

$$|\pm\rangle = \frac{1}{\sqrt{2}}(|0\rangle \pm |1\rangle) \tag{A.1}$$

which defines a second set that spans the two-dimensional Hilbert space. More generally, if both coefficients a and b are non-zero, then the qubit is in a superposition state.

Similarly, a system with two qubits can be written, in terms of the basis $\{|00\rangle, |01\rangle, |10\rangle, |11\rangle\}$, as the linear superposition

$$|\psi\rangle = a\,|00\rangle + b\,|01\rangle + c\,|10\rangle + d\,|11\rangle \tag{A.2}$$

with the normalization condition $|a|^2 + |b|^2 + |c|^2 + |d|^2 = 1$. These states are even richer, as the two qubits can be correlated via quantum entanglement. Such quantum correlations are, in fact, stronger than classical correlations [171]. A commonly used set of entangled states

are the four Bell states

$$|\Phi^{\pm}\rangle = \frac{1}{\sqrt{2}}(|00\rangle \pm |11\rangle)) \tag{A.3}$$

$$|\Psi^{\pm}\rangle = \frac{1}{\sqrt{2}}(|01\rangle \pm |10\rangle) \tag{A.4}$$

which form a second basis for the four-dimensional Hilbert space of the two-qubit system.

Having defined the qubit, in order to perform quantum computation, we need to act with a unitary quantum gate. In order to apply any arbitrary computation, a universal set of quantum gates is required. A convenient universal set includes the Hadamard, T-phase, and S-phase gates

$$H = \frac{1}{\sqrt{2}} \begin{pmatrix} 1 & 1 \\ 1 & -1 \end{pmatrix} \quad , \quad S = \begin{pmatrix} 1 & 0 \\ 0 & i \end{pmatrix} \quad , \quad T = \begin{pmatrix} 1 & 0 \\ 0 & e^{i\frac{\pi}{4}} \end{pmatrix} \tag{A.5}$$

which are three single-qubit gates and a two-qubit (entangling) gate with matrix representation

$$CNOT = \begin{pmatrix} 1 & 0 & 0 & 0 \\ 0 & 1 & 0 & 0 \\ 0 & 0 & 0 & 1 \\ 0 & 0 & 1 & 0 \end{pmatrix} \tag{A.6}$$

A quantum algorithm can be designed by appropriately using these quantum gates and by introducing additional qubits, if necessary. After processing the quantum information, we recover information about the final state of the system via a measurement.

Appendix B

Details of calculations for the 2N-point amplitudes

Details of the five-point amplitude

In the mimimal model $\mathcal{M}(k+2,k+1)$ with $k \geq 3$, the five-point correlator $\langle \sigma_1 \sigma_2 \sigma_3 \sigma_4 \varepsilon_5 \rangle$ (Eq. (4.19)) has three conformal blocks shown in Figure 4.4. The calculation of the exchange matrices involving the points η_1, η_2, and η_3 can be simplified by working in the $\eta_5 \to \eta_4$ limit. To this end, we need to change bases so that σ_4 and ε_5 fuse together. A suitable change of basis is shown in Figure B.1. It involves four-point amplitudes that can be found explicitly. The first correlator $\mathcal{K}_1$ transforms trivially. The other two correlators, $\mathcal{K}_2$ and $\mathcal{K}_3$, tranform to $\mathcal{K}_2'$ and $\mathcal{K}_3'$ via a matrix D, as shown. Working in the Coulomb gas formalism, after fixing three points, we obtain these four-point correlators in terms of Hypergeometric functions

$$\begin{aligned} \mathcal{K}_2(x) &= x^{-\frac{2k}{k+2}}(1-x)^{\frac{k+1}{k+2}} \int_1^\infty dw w^{\frac{2k}{k+2}}(w-x)^{-\frac{2k+2}{k+2}}(w-1)^{-\frac{k+1}{k+2}} \\ &= \frac{\Gamma\left(\frac{1}{k+2}\right)^2}{\Gamma\left(\frac{2}{k+2}\right)}(1-x)^{-\frac{k}{k+2}} x^{-\frac{2k}{k+2}} {}_2F_1\left(\frac{1}{k+2}, -\frac{2k}{k+2}; \frac{2}{k+2}; x\right) \end{aligned} \tag{B.1}$$

$$\begin{aligned}\mathcal{K}_3(x) &= x^{-\frac{2k}{k+2}}(1-x)^{\frac{k+1}{k+2}}\int_0^x dw w^{\frac{2k}{k+2}}(x-w)^{-\frac{2k+2}{k+2}}(1-w)^{-\frac{k+1}{k+2}} \\ &= \frac{\Gamma\left(-\frac{k}{k+2}\right)\Gamma\left(\frac{3k+2}{k+2}\right)}{\Gamma\left(\frac{2(k+1)}{k+2}\right)}(1-x)^{\frac{k+1}{k+2}}x^{-\frac{k}{k+2}}{}_2F_1\left(\frac{k+1}{k+2},\frac{3k+2}{k+2};\frac{2(k+1)}{k+2};x\right) \quad \text{(B.2)}\end{aligned}$$

$$\begin{aligned}\mathcal{K}_2'(x) &= x^{-\frac{2k}{k+2}}(1-x)^{\frac{k+1}{k+2}}\int_x^1 dw w^{\frac{2k}{k+2}}(w-x)^{-\frac{2k+2}{k+2}}(1-w)^{-\frac{k+1}{k+2}} \\ &= \frac{\Gamma\left(\frac{1}{k+2}\right)\Gamma\left(-\frac{k}{k+2}\right)}{\Gamma\left(\frac{1-k}{k+2}\right)}(1-x)^{-\frac{k}{k+2}}x^{-\frac{k}{k+2}}{}_2F_1\left(-\frac{k}{k+2},\frac{k+1}{k+2};\frac{1-k}{k+2};1-x\right) \quad \text{(B.3)}\end{aligned}$$

$$\begin{aligned}\mathcal{K}_3'(x) &= x^{-\frac{2k}{k+2}}(1-x)^{-\frac{k}{k+2}}\int_x^1 dw w^{-\frac{2k+2}{k+2}}(w-x)^{\frac{2k}{k+2}}(1-w)^{-\frac{k+1}{k+2}} \\ &= \frac{\Gamma\left(\frac{1}{k+2}\right)\Gamma\left(\frac{3k+2}{k+2}\right)}{\Gamma\left(\frac{3(k+1)}{k+2}\right)}(1-x)^{\frac{k+1}{k+2}}x^{-\frac{2k}{k+2}}{}_2F_1\left(\frac{1}{k+2},\frac{2(k+1)}{k+2};\frac{3(k+1)}{k+2};1-x\right) \quad \text{(B.4)}\end{aligned}$$

After some algebra, we find the elements of the transformation matrix D. These are given by

$$D_{11} = \frac{\sin\frac{2\pi}{k+2}}{\sin\frac{3\pi}{k+2}} \quad , \quad D_{12} = \frac{\sin\frac{4\pi}{k+2}}{\sin\frac{3\pi}{k+2}} \quad , \quad D_{21} = D_{22} = -\frac{\sin\frac{\pi}{k+2}}{\sin\frac{3\pi}{k+2}} \quad \text{(B.5)}$$

After applying this basis change to the five-point correlators depicted in Figure 4.4, and using the OPE $\sigma(\eta_4)\varepsilon(\eta_5) \sim \eta_{45}^{-\frac{k}{(k+2)}}\sigma(\eta_4) + \eta_{45}^{\frac{k+1}{k+2}}\varepsilon'(\eta_4)$, we deduce in the limit $\eta_5 \to \eta_4$

$$\mathcal{F}_1^{(5)} \approx \eta_{45}^{-\frac{k}{k+2}}\mathcal{F}_1^{(4)} \quad \text{(B.6)}$$

$$\mathcal{F}_2^{(5)} \approx \eta_{45}^{-\frac{k}{k+2}}D_{11}\mathcal{F}_2^{(4)} + \eta_{45}^{\frac{k+1}{k+2}}D_{12}\mathcal{F}_3^{(4)} \quad \text{(B.7)}$$

$$\mathcal{F}_3^{(5)} \approx \eta_{45}^{-\frac{k}{k+2}}D_{21}\mathcal{F}_2^{(4)} + \eta_{45}^{\frac{k+1}{k+2}}D_{22}\mathcal{F}_3^{(4)} \quad \text{(B.8)}$$

where the four-point correlators $\mathcal{F}_1^{(4)}$, $\mathcal{F}_2^{(4)}$ are depicted in Figure 4.2 and $\mathcal{F}_3^{(4)}$ is depicted in Figure B.2.

Since this correlator does not require screening charges, we readily deduce the algebraic expression

$$\mathcal{F}_3^{(4)} = \eta_{12}^{\frac{k}{2(k+2)}} (\eta_{13}\eta_{23})^{\frac{k+1}{2(k+2)}} (\eta_{14}\eta_{24}\eta_{34})^{-\frac{3k+1}{2(k+2)}} \ . \tag{B.9}$$

Using the explicit expressions in Eqs. (B.6) - (B.8), involving four-point amplitudes, we easily obtain the exchange matrices of the five-point amplitudes depicted in Figure 4.4 corresponding to exchanges between the positions η_1, η_2, and η_3.

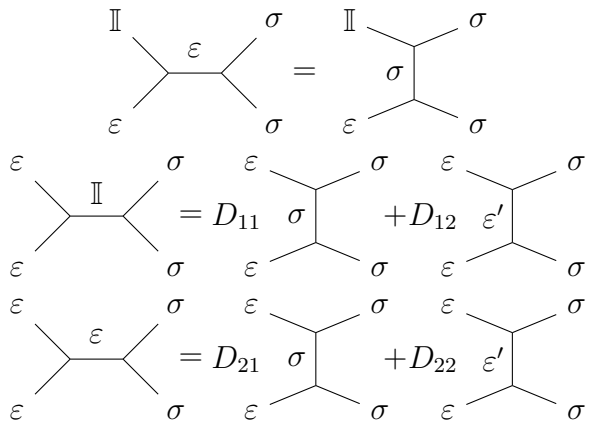

Figure B.1: Basis change for the mixed four-point correlators. The LHS of the first, second and third line are denoted as $\mathcal{K}_1$, $\mathcal{K}_2$ and $\mathcal{K}_3$ respectively. On the RHS we have the correlators $\mathcal{K}'_1$, $\mathcal{K}'_2$ and $\mathcal{K}'_3$.

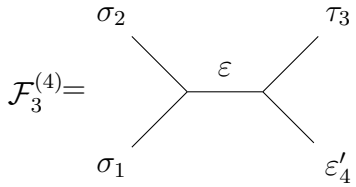

Figure B.2: The four-point function $\langle\sigma_1\sigma_2\sigma_3\varepsilon'_4\rangle$

Appendix C

Wess-Zumino-Witten Models

The classical action of the WZW models is given by

$$S = \frac{k}{16\pi}\int d^2x \mathrm{Tr}[\partial^\mu g^{-1}\partial_\mu g] + k\,\Gamma \tag{C.1}$$

with

$$\Gamma = -\frac{i}{24\pi}\int d^3y \epsilon_{\alpha\beta\gamma}\mathrm{Tr}[\tilde{g}^{-1}\partial^\alpha\tilde{g}\tilde{g}^{-1}\partial^\beta\tilde{g}\tilde{g}^{-1}\partial^\gamma\tilde{g}^{-1}] \tag{C.2}$$

where $g(x)$ is a matrix bosonic field associated with a Lie algebra g. It should be clarified here, that $g(x)$ lives in a two-dimensional manifold with a Lie group G, whereas $\tilde{g}(x)$ is an extension into a three-dimensional manifold. As explained in [94, 172], the quantum theory of Eq. (5.7) requires k to be an integer.

A straightforward way to evaluate correlators in the $SU(2)_k$ WZW model is through the Wakimoto free-field representation in which the WZW model is expressed in terms of a free boson field φ and a ghost system consisting of boson β and γ fields. The central charge c of the theory and background charge α_0 are given in terms of the level k of the WZW model as

$$c = 3 - 12\alpha_0^2 = \frac{3k}{k+2} \tag{C.3}$$

The primary fields $\Phi^j_m(z)$ depend on two parameters taking the values $j = 0, \frac{1}{2}, \ldots, \frac{k}{2}$ and $m = -j, \ldots, j$. In the free-field representation,

$$\Phi^j_m(z) = \gamma^{j-m}(z) e^{-2ij\alpha_0\varphi(z)} \tag{C.4}$$

To compute correlators, we also need the conjugate fields $\tilde{\Phi}^j_m(z)$ and screening charges Q_+. Following the Ref. [141], the conjugate of the highest-weight field is given by

$$\tilde{\Phi}^j_j(z) = \beta^{2j-q-1}(z) e^{2i(j-q-1)\alpha_0\varphi(z)} \tag{C.5}$$

The other fields can also be expressed in terms of boson fields, but we will not need explicit expressions. In general, there are two possible screening charges. For our purposes, we only need to introduce the positive screening charge

$$Q_+ = \int dw \beta(w) e^{2i\alpha_0\varphi(w)} \tag{C.6}$$

Here, we will concentrate on amplitudes involving primary fields with $j = \frac{1}{2}$. To simplify the notation, we will define these fields by $\Phi_\pm \equiv \Phi^{\frac{1}{2}}_{\pm\frac{1}{2}}$.

The four-point correlators of fields $Y_{\mu,m_1m_2m_3m_4}$ with $j = \frac{1}{2}$ and $m_i = \pm$ $(i = 1, 2, 3, 4)$, have two conformal blocks labeled by the parameter $\mu = 1, 2$ We obtain the non-vanishing amplitudes

$$\begin{aligned}
Y_{1,+--+} &= \langle \Phi_+(\eta_1) Q_+ \Phi_-(\eta_2) \Phi_-(\eta_3) \tilde{\Phi}_+(\eta_4) \rangle \\
&= -\left[x(1-x)\right]^{\frac{1}{2(k+2)}} \int_0^x dw \frac{\left[w(x-w)(1-w)\right]^{-\frac{1}{k+2}}}{x-w} \\
&\quad -\left[x(1-x)\right]^{\frac{1}{2(k+2)}} \int_0^x dw \frac{\left[w(x-w)(1-w)\right]^{-\frac{1}{k+2}}}{1-w} \\
&= -\frac{\Gamma\left(-\frac{1}{k+2}\right)\Gamma\left(\frac{k+1}{k+2}\right)}{\Gamma\left(\frac{k}{k+2}\right)} (1-x)^{\frac{1}{2k+4}} x^{-\frac{3}{2k+4}} {}_2F_1\left(-\frac{1}{k+2}, \frac{1}{k+2}; \frac{k}{k+2}; x\right)
\end{aligned} \tag{C.7}$$

$$
\begin{aligned}
Y_{1,--++} &= \langle \Phi_-(\eta_1) Q_+ \Phi_-(\eta_2) \Phi_+(\eta_3) \tilde{\Phi}_+(\eta_4) \rangle \\
&= [x(1-x)]^{\frac{1}{2(k+2)}} \int_0^x dw \frac{[w(x-w)(1-w)]^{-\frac{1}{k+2}}}{w} \\
&\quad - [x(1-x)]^{\frac{1}{2(k+2)}} \int_0^x dw \frac{[w(x-w)(1-w)]^{-\frac{1}{k+2}}}{x-w} \\
&= -\frac{\Gamma\left(-\frac{1}{k+2}\right)\Gamma\left(\frac{k+1}{k+2}\right)}{q\Gamma\left(\frac{k}{k+2}\right)} (1-x)^{\frac{1}{2k+4}} x^{\frac{2k+1}{2k+4}} {}_2F_1\left(\frac{k+1}{k+2}, \frac{k+3}{k+2}; \frac{2k+2}{k+2}; x\right) \quad \text{(C.8)}
\end{aligned}
$$

$$
\begin{aligned}
Y_{1,-+-+} &= \langle \Phi_-(\eta_1) Q_+ \Phi_+(\eta_2) \Phi_-(\eta_3) \tilde{\Phi}_+(\eta_4) \rangle \\
&= [x(1-x)]^{\frac{1}{2(k+2)}} \int_0^x dw \frac{[w(x-w)(1-w)]^{-\frac{1}{k+2}}}{w} \\
&\quad - [x(1-x)]^{\frac{1}{2(k+2)}} \int_0^x dw \frac{[w(x-w)(1-w)]^{-\frac{1}{k+2}}}{1-w} \\
&= \frac{\Gamma\left(-\frac{1}{k+2}\right)\Gamma\left(\frac{k+1}{k+2}\right)}{\Gamma\left(\frac{k}{k+2}\right)} (1-x)^{\frac{1}{2k+4}} x^{-\frac{3}{2k+4}} {}_2F_1\left(\frac{1}{k+2}, \frac{k+1}{k+2}; \frac{k}{k+2}; x\right) \quad \text{(C.9)}
\end{aligned}
$$

$$
\begin{aligned}
Y_{2,+--+} &= \langle \Phi_+(\eta_1) \Phi_-(\eta_2) \Phi_-(\eta_3) Q_+ \tilde{\Phi}_+(\eta_4) \rangle \\
&= [x(1-x)]^{\frac{1}{2(k+2)}} \int_1^\infty dw \frac{[w(w-x)(w-1)]^{-\frac{1}{k+2}}}{w-x} \\
&\quad + [x(1-x)]^{\frac{1}{2(k+2)}} \int_1^\infty dw \frac{[w(w-x)(w-1)]^{-\frac{1}{k+2}}}{w-1} \\
&= \frac{\Gamma\left(-\frac{1}{k+2}\right)\Gamma\left(\frac{3}{k+2}\right)}{2\Gamma\left(\frac{2}{k+2}\right)} (1-x)^{\frac{1}{2k+4}} x^{\frac{1}{2k+4}} {}_2F_1\left(\frac{1}{k+2}, \frac{3}{k+2}; \frac{k+4}{k+2}; x\right) \quad \text{(C.10)}
\end{aligned}
$$

$$
\begin{aligned}
Y_{2,--++} &= \langle \Phi_-(\eta_1) \Phi_-(\eta_2) \Phi_+(\eta_3) Q_+ \tilde{\Phi}_+(\eta_4) \rangle \\
&= [x(1-x)]^{\frac{1}{2(k+2)}} \int_1^\infty dw \frac{[w(w-x)(w-1)]^{-\frac{1}{k+2}}}{w} \\
&\quad + [x(1-x)]^{\frac{1}{2(k+2)}} \int_1^\infty dw \frac{[w(w-x)(w-1)]^{-\frac{1}{k+2}}}{w-x} \\
&= -\frac{\Gamma\left(-\frac{1}{k+2}\right)\Gamma\left(\frac{3}{k+2}\right)}{\Gamma\left(\frac{2}{k+2}\right)} (1-x)^{\frac{1}{2k+4}} x^{\frac{1}{2k+4}} {}_2F_1\left(\frac{1}{k+2}, \frac{3}{k+2}; \frac{2}{k+2}; x\right) \quad \text{(C.11)}
\end{aligned}
$$

$$
\begin{aligned}
Y_{2,-+-+} &= \langle \Phi_-(\eta_1)\Phi_+(\eta_2)\Phi_-(\eta_3)Q_+\tilde{\Phi}_+(\eta_4)\rangle \\
&= [x(1-x)]^{\frac{1}{2(k+2)}} \int_1^\infty dw \frac{[w(w-x)(w-1)]^{-\frac{1}{k+2}}}{w} \\
&\quad + [x(1-x)]^{\frac{1}{2(k+2)}} \int_1^\infty dw \frac{[w(w-x)(w-1)]^{-\frac{1}{k+2}}}{w-1} \\
&= \frac{\Gamma\left(-\frac{1}{k+2}\right)\Gamma\left(\frac{3}{k+2}\right)}{2\Gamma\left(\frac{2}{k+2}\right)} (1-x)^{-\frac{3}{2(k+2)}} x^{\frac{1}{2k+4}} {}_2F_1\left(\frac{1}{k+2}, \frac{k+1}{k+2}; \frac{k+4}{k+2}; x\right) \qquad \text{(C.12)}
\end{aligned}
$$

Notice that only two of these functions are independent for each conformal block, because of the constraints

$$
Y_{\mu,+--+} + Y_{\mu,--++} + Y_{\mu,-+-+} = 0 \ , \quad \mu = 1, 2 \qquad \text{(C.13)}
$$

We obtain the expressions (Eq. (5.19)) from the corresponding $X_{1,m_1m_2m_3m_4}$ for $k = 1$. The second conformal block does not contribute in $SU(2)_1$ [138].

Vita

Elias Kokkas was born in 1992 in Warwick, NY, and raised in the city of Larissa, Greece. In 2011, he enrolled in the Aristotle University of Thessaloniki to study physics. He received a B.S. in physics with a concentration in theoretical physics in 2016. In the same year, he joined the University of Tennessee to pursue a Ph.D. in physics. In 2018, he joined Prof. Siopsis's group and started working in the field of topological quantum computation.